

https://dspace.org/

Design and construction criteria for domes in low-cost housing

Talocchino, Gianfranco

2007-02-15T11:49:30Z
http://hdl.handle.net/10539/2005

Downloaded from a DSpace repository. https://dspace.org/

DESIGN & CONSTRUCTION CRITERIA FOR DOMES IN LOW-COST HOUSING

G. Talocchino

A dissertation submitted to the Faculty of Engineering and the Built Environment, University of the Witwatersrand, in fulfillment of the requirements for the degree of Master of Science in Engineering.

Johannesburg, 2005

TABLE OF CONTENTS

TABLE OF CONTENTS II
DECLARATION I
ABSTRACT II
ACKNOWLEDGEMENTS III
LIST OF FIGURES IV
LIST OF TABLES IX
LIST OF SYMBOLS XI

1. INTRODUCTION 1

1.1 STATEMENT OF THE PROBLEM 1
1.2 AIMS OF THE INVESTIGATION 2
1.3 METHOD OF INVESTIGATION 2
1.4 A BRIEF HISTORY OF THE DOME 5
1.5 RECENT DEVELOPMENTS IN COMPRESSED EARTH & DOME 7
CONSTRUCTION 7
1.5.1 FIBRE REINFORCED SOIL CRETE BLOCKS FOR THE CONSTRUCTION OF LOW-COST HOUSING – RODRIGO FERNANDEZ (UNIVERSITY OF THE WITWATERSRAND, 2003) 7
1.5.2 DOMES IN LOW-COST HOUSING – S.J. MAGAIA (UNIVERSITY OF THE WITWATERSRAND, SEPTEMBER 2003) 8
1.5.3 THE MONOLITHIC DOME SOLUTION 9
1.5.4 THE DOME SPACE SOLUTION 9
1.5.5 THE TLHOLEGO ECO-VILLAGE 10
1.6 ARCHITECTURAL CONSIDERATIONS 10
1.6.1 SHAPE 11
1.6.2 STRUCTURAL STRENGTH 13
1.6.3 RAIN PENETRATION & DAMP PROOFING 13
1.6.4 THERMAL PERFORMANCE 15
1.6.5 LIGHTING 16
1.6.6 INTERNAL ARRANGEMENT 16

2. SHAPE INVESTIGATION 18

2.1 METHODS OF SHAPE INVESTIGATION 18
2.2 CLASSICAL THIN SHELL THEORY 18
2.2.1 THE STRUCTURAL ELEMENTS 18
2.2.2 FORCES AND MOMENTS IN THE STRUCTURE 19
2.2.3 CLASSICAL DOME THEORY 20
2.2.4 CLASSICAL DOME/RING THEORY 22
DOME/RING THEORY IS THE THEORY APPLIED TO DOME STRUCTURES WITH A RING BEAM AT THE BASE OF THE STRUCTURE. THE STRUCTURE DOES NOT BEHAVE AS IF IT WERE FIXED OR PINNED, BUT SOMEWHERE BETWEEN THESE TWO CONDITIONS. 22

THE RING BEAM WILL ALLOW A CERTAIN AMOUNT OF ROTATION AND OUTWARD DISPLACEMENT AT THE BASE, WHICH A FIXED BASE WOULD NOT. THEREFORE, TWO NEW ERRORS ARE INTRODUCED AND THESE ARE ADDED TO THE DOME MEMBRANE ERRORS TO OBTAIN THE TOTAL DOME/RING ERRORS. 22

$$D_{10}^{R} = (\cos\alpha + \frac{12y_0 e}{d^2})\frac{r^2 N'_{\alpha}}{Ebd} \quad (2.11)$$ 22

2.3 BASIC FINITE ELEMENT ANALYSIS (FEA) THEORY 23
2.3.1 TYPES OF ELEMENTS USED 24
2.3.2 METHODS OF IMPROVING FEA ACCURACY 25
2.4 SENSITIVITY ANALYSIS 25
2.4.1 DESCRIPTION OF THE ANALYSIS 25
2.4.2 SENSITIVITY ANALYSIS RESULTS 27
2.4.3 EFFECT OF VARYING THE STIFFNESS OF THE STRUCTURE 29
2.4.4 SUMMARY OF SENSITIVITY ANALYSIS FINDINGS 32

2.5 SHAPE ANALYSIS 33

2.5.1 DESCRIPTION OF THE ANALYSIS 33
2.5.2 SHAPE EVALUATION CRITERIA 35
2.5.3 PRESENTATION OF THE ANALYSIS RESULTS 35
2.6 SHAPE ANALYSIS RESULTS (STRUCTURE TYPES A & C) 37
2.6.1 THE CATENARY 37
2.6.2 SECTIONS THROUGH THE HEMISPHERE 42
2.6.3 SECTIONS THROUGH THE PARABOLA 45
2.6.4 THE ELLIPSE 49
2.7 SHAPE ANALYSIS RESULTS (STRUCTURE TYPE B) 52
2.8 SUMMARY OF THE RESULTS 54
2.8.1 TABULATED SUMMARY 54
2.8.2 SUMMARY DISCUSSION 56

3. MATERIALS INVESTIGATION 57

3.1 LITERATURE INVESTIGATION 57
3.1.1 CEMENT STABILIZED EARTH BLOCKS (CEB'S) 57
3.2 LABORATORY TESTING 59
3.2.1 FIBRE REINFORCED PLASTER TESTS 59
3.2.2 BRICKFORCE, WIRE WRAPPING & WIRE MESH TESTS 65
3.2.3 PLASTIC DAMP PROOF COURSE (DPC) FRICTION TESTS 68

4. STRUCTURAL ANALYSIS 75

4.1 THE MODEL 76
4.1.1 THE DIMENSIONS OF THE STRUCTURE 76
4.1.2 THE FINITE ELEMENT ANALYSIS (FEA) MODEL 76
4.2 LOADING CALCULATIONS 77

4.2.1 DEAD LOAD (SELF WEIGHT) 77
4.2.2 LIVE LOAD 78
4.2.3 WIND LOAD 78
4.2.4 TEMPERATURE LOAD 80
4.3 LOAD COMBINATIONS 83
4.4 FINITE ELEMENT ANALYSIS RESULTS 83
4.4.1 THE EFFECTS OF THE SKYLIGHT OPENINGS AND POINT LOADING 84
4.4.2 THE EFFECTS OF WINDOW AND DOOR OPENINGS 86
4.4.3 THE EFFECTS OF TEMPERATURE LOADING 90
4.4.4 FINAL DESIGN RESULTS 93

.5. DESIGN OF STRUCTURAL ELEMENTS 103

5.1 DESIGN THEORY 103
5.1.1 MASONRY DESIGN 103
5.1.2 FOUNDATION DESIGN 112
5.2 DESIGN CALCULATION RESULTS 113
5.2.1 THE DOME 113
5.2.2 THE CYLINDER WALL 120
5.2.3 THE FOUNDATION DESIGN RESULTS 124
5.2.5 OVERALL STABILITY 125

6. CONSTRUCTION AND COST ANALYSIS 126

6.1 REINFORCED CONCRETE DOME CONSTRUCTION 126
6.2 BRICK DOME AND VAULT CONSTRUCTION 127
6.3 CONSTRUCTION PROCEDURE OF THE PROTOTYPE 28M^2 DOME 129
6.3.1 SITE PREPARATION & SETTING OUT 129
6.3.2 THE FOUNDATION 130
6.3.3 THE CYLINDER WALL 132
6.3.4 THE INFLATABLE FORMWORK 133
6.3.5 THE DOME CONSTRUCTION 134
6.3.6 THE ARCHES AND SKYLIGHT CONSTRUCTION 135
6.3.7 WIRE WRAPPING AROUND THE OPENINGS 137
6.3.8 PLASTERING, PAINTING & FINISHING OF THE DOME 138
6.4 CONSTRUCTION MATERIALS INVESTIGATION 139
6.4.1 MORTAR STRENGTH TESTS 139
6.4.2 FOUNDATION AND FLOOR SLAB TESTS 141
6.5 COST ANALYSIS 143

7. CONCLUSIONS & RECOMMENDATIONS 146

APPENDIX A (SELECTED ABAQUS™ OUTPUT) 151

APPENDIX B (ALTERNATIVE STRUCTURE) 154

REFERENCES..... 158

DECLARATION

I declare that this dissertation is my own, unaided work. It is being submitted for the Degree of Master of Science in Engineering in the University of the Witwatersrand, Johannesburg. It has not been submitted before for any degree or examination in any other University.

Signature _____

Date: 8th day of December 2005

ABSTRACT

This dissertation investigates the different design and construction considerations involved when building a masonry dome. A detailed shape investigation was undertaken in order to summarize the best shaped dome structures. General recommendations are given for the shapes that produce the least tension and the most useable space.

The effects of openings, temperature loading and wind loading were considered and a finite element analysis of the final structure was undertaken. It was found that regions of high tension exist around openings, especially under temperature loading, and materials suitable to resisting this tension were investigated (fibre plaster, chicken wire mesh and wire wrapping around openings).

The final structure was built using an inflatable formwork. The construction procedure was well documented and a study of alternative methods of construction is presented.

This dissertation shows that a durable, architecturally and structurally efficient low-cost masonry dome can be built if proper attention is given to minimizing and resisting tension within the structure.

Acknowledgements

I would like to thank Prof. M. Gohnert for his invaluable support and encouragement which made this dissertation possible. I am also grateful to HydraForm South Africa who supplied the cement stabilized earth blocks used in the construction of the dome, as well as the Central Johannesburg College who provided a site for the dome. The final dome structure was constructed by Dome Space South Africa. I would like to thank them for their involvement.

Gianfranco Talocchino

List of Figures

CHAPTER 1

Figure 1.1 – Distribution of South African Houses (RSA Census, 2001) pg1
Figure 1.2 – Flow Diagram of the Investigation pg4
Figure 1.3 - Zulu Hut (KwaZulu-Natal) pg5
Figure 1.4 - Musgum Farmstead pg5
Figure 1.5 - The Ramesseum Storage Vaults, Gourna, Egypt pg6
Figure 1.6 - Low-Cost Dome built by S.J. Magaia(2003) pg8
Figure 1.7 – EcoShells in Haiti. (www.monolithic.com) pg9
Figure 1.8 – Dome Homes built by Dome Space pg9
Figure 1.9 – Dome Cookhouse – Tlholego Eco-Village pg10
Figure 1.10 – Useable Space within Possible Low-Cost Dome Structures pg12
Figure 1.11 - Hoop and Meridian Directions pg13
Figure 1.12 – Plaster Coatings & Shrinkage (Houben, Guillaud, 1994) pg14
Figures 1.13– Possible Internal Arrangements for Low-Cost Houses pg17

CHAPTER 2

Figure 2.1 – The Basic Structural Elements pg19
Figure 2.2 – Forces and Moments in Shell Structures pg19
Figure 2.3 – Dome/Ring Equations' Parameters pg23
Figure 2.4 – Sensitivity Analysis Dome Dimensions pg26
Figure 2.5 – Graph of Meridian Forces - Sensitivity Analysis pg27
Figure 2.6 – Graph of Hoop Forces - Sensitivity Analysis pg28
Figure 2.7 – Graph of Meridian Moments - Sensitivity Analysis pg28
Figure 2.8 – Effect of Varying the Shell Thickness - Sensitivity Analysis pg30
Figure 2.9 – Graph of N_θ - Effect of Varying Ring Dimensions - Sensitivity Analysis pg31
Figure 2.10 – Graph of M_φ - Effect of Varying Ring Dimensions - Sensitivity Analysis pg32
Figure 2.11 – Y/L Ratio Parameters pg36
Figure 2.12 – Fixed Base Reaction Forces pg37
Figure 2.13 – The Ideal Shape of a Dome Structure pg38
Figure 2.14 –The Catenary Equation Variables pg38
Figure 2.15 – Graph of Maximum Hoop Force vs. Y/L – Catenary pg39
Figure 2.16 – Graph of Maximum Meridian Moments vs. Y/L – Catenary pg39
Figure 2.17 – Graph of Hoop Stresses – Catenary Y = 4.92m pg40
Figure 2.18 – Graph of Meridian Stresses – Catenary Y = 4.92m pg40

Figure 2.19 – Graph of Maximum Hoop Force vs. Y/L – Hemisphere pg43
Figure 2.20 – Graph of Maximum Meridian Moments vs. Y/L – Hemisphere pg43
Figure 2.21 – Graph of Hoop Stresses – Sectioned Hemisphere r = 3.5 pg43
Figure 2.22 – Graph of Meridian Stresses – Sectioned Hemisphere r = 3.5 pg44
Figure 2.23 – Graph of Maximum Hoop Force vs. Y/L – Parabola pg46
Figure 2.24 – Graph of Maximum Meridian Moment vs. Y/L – Parabola pg46
Figure 2.25 – Graph of Hoop Stresses – Parabola (y = 8m) pg47
Figure 2.26 – Graph of Meridian Stresses – Parabola (y = 8m) pg47
Figure 2.27 – Graph of Maximum Hoop Force vs. Y/L – Ellipse pg50
Figure 2.28 – Maximum Meridian Moment vs. Y/L – Ellipse pg50
Figure 2.29 – Graph of Hoop Stresses – Ellipse (B = 3.2m; Y = 3.2m) pg51
Figure 2.30 – Graph of Meridian Stresses – Ellipse (B = 3.2m; Y = 3.2m) pg51
Figure 2.31 – Graph of N(θ) – Shells with 1m Cylinder Walls – Structure Type B pg53
Figure 2.32 – Graph of M(Φ) – Shells with 1m Cylinder Walls – Structure Type B pg53
Figure 2.33 – Useable Space Parameters pg55

CHAPTER 3
Figure 3.1 – Stress-strain behavior of FRC (Fulton 2001:253) pg61
Figure 3.2 – Stress-Strain Curve Parameters pg66
Figure 3.3 – Graph of Brickforce Yield Stress pg67
Figure 3.4 – Graph of Wire Wrapping Yield Stress pg67
Figure 3.5 – Graph of Chicken Mesh Yield Stress pg68
Figure 3.6 – Line Diagram of the Inclined Plane Method pg70
Figure 3.7 – Inclined Plane Friction Test Apparatus pg70

CHAPTER 4
Figure 4.1 – Prototype 28m^2 (Structure type (B)) pg75
Figure 4.2 – Dimensions of the Final Structure (Prototype 28m^2 Dome) pg76
Figure 4.3 – 3D FEA Model (Final Structure) pg77
Figure 4.4 – Wind Pressure on a Dome and a Cylinder (Billington, 1965:74) pg78
Figure 4.5 – Partitioned Model (Wind Load- Patch load) pg80
Figure 4.6 – Two Examples of Cracking Induced by Volume Changes pg81
Figure 4.7 – Sections along Which Results are Presented pg83
Figure 4.8 – Concentrated Load around a Skylight Opening (Billington, 1965:45) pg84
Figure 4.9 – Graph of the Effect of Skylight Opening on Hoop Force pg85
Figure 4.10 – Graph of the Effect of Skylight Opening on Meridian Moments pg85

Figure 4.11 – Stress (Von Mises) around Supported and Unsupported Dome Openings pg86
Figure 4.12 – Cracks Patterns around Openings at the Sparrow Aids Village pg87
Figure 4.13 – Graph of Hoop Forces around Window Openings pg88
Figure 4.14 – Graph of Meridian Moments around Window Openings pg89
Figure 4.15 – Cracking on the inside face of a Window pg89
Figure 4.16 – Graph of Hoop Force (1.2TL+0.9DL) pg90
Figure 4.17 – Graph of Meridian Moment (1.2TL+0.9DL) pg91
Figure 4.18 – Graph of Hoop Force (1.2TL+0.9DL – Half Structure) pg92
Figure 4.19 – Graph of Meridian Moment (1.2TL+0.9DL– Half Structure) pg92
Figure 4.20 – Graph of Hoop Forces (ULS) – Centre Section pg94
Figure 4.21 – Graph of Meridian Moments (ULS) – Centre Section pg94
Figure 4.22 – Graph of Hoop Forces (ULS) – Door Section pg95
Figure 4.23 – Graph of Meridian Moments (ULS) – Door Section pg95
Figure 4.24 – Graph of Hoop Forces (ULS) – Window Section pg96
Figure 4.25 – Graph of Meridian Moments (ULS) – Window Section pg96
Figure 4.26 – Graph of Hoop Stresses – Centre Section pg97
Figure 4.27 – Graph of Meridian Stresses – Centre Section pg98
Figure 4.28 – Graph of Hoop Stresses – Window Section pg99
Figure 4.29 – Graph of Hoop Stresses – Door Section pg99
Figure 4.30 – Graph of Meridian Stresses – Window Section pg100
Figure 4.31 – Graph of Meridian Stresses – Door Section pg101
Figure 4.32 – Serviceability Deflections – U2 pg102
Figure 4.33 – Serviceability Deflections – U1 pg102

CHAPTER 5

Figure 5.1 – Stresses in a Masonry Wall (Curtin, 1985:60) pg105
Figure 5.2 – Masonry Flexural Failure Planes (Curtin, 1985:61) pg107
Figure 5.3 – Cracked Section Stress Block (Crofts & Lane, 2000:154) pg107
Figure 5.4 – Design Stress Block, Compressive Stress pg108
Figure 5.5 – Design Stress Blocks – Compressive and Tensile Stress pg109
Figure 5.6 – Design Stress Blocks - Tensile Stress pg110
Figure 5.7 – HydraForm Splitter Block pg113
Figure 5.8 – Graph of Hoop Moment & Resistance – Centre Section (Dome) pg114
Figure 5.9 – Graph of Hoop Stresses & Resistances – Centre Section (Dome) pg115
Figure 5.10 – Final Structure - Concrete Lintel pg116
Figure 5.11 – Graph of Meridian Moment & Resistance – Centre Section (Dome) pg116

Figure 5.12 – Graph of Meridian Stresses & Resistances – Centre Section (Dome) pg117
Figure 5.13 – Wire Wrapping Detail pg118
Figure 5.14 – Graph of Hoop Moments & Resistances –
Centre Section (Cylinder Wall) pg121
Figure 5.15 – Graph of Hoop Stresses & Resistances –
Centre Section (Cylinder Wall) pg122
Figure 5.16 – Graph of Meridian Moment & Resistance –
Centre Section (Cylinder Wall) pg122
Figure 5.17 – Graph of Meridian Stresses & Resistances –
Centre Section (Cylinder Wall) pg123
Figure 5.18 – Graph of Shear Stress in the Structure pg123
Figure 5.19 – Foundation Detail (adapted from Dome Space drawing) pg125

CHAPTER 6
Figure 6.1 – EcoShell Dome Construction Method (www.monolithic.com) pg127
Figure 6.2 – Nubian Method of Dome Construction (Auroville Institute) pg128
Figure 6.3 – Setting Out Equipment for the Foundation pg130
Figure 6.4 – Setting Out of the Foundation pg130
Figure 6.5 – Digging the Foundation pg131
Figure 6.6 – Short Foundation Walls pg131
Figure 6.7 – Placing of Foundation Reinforcing & Concrete pg132
Figure 6.8 – Splitting the Splitter Blocks pg132
Figure 6.9 – Construction of the Cylinder Wall pg133
Figure 6.10 – The Inflatable Formwork pg134
Figure 6.11 – Dome Construction pg135
Figure 6.12 – Construction of the Arches pg136
Figure 6.13 – Door Arch pg136
Figure 6.14 – Un-plastered Dome pg137
Figure 6.15 – Wire Wrapping around Door Opening pg137
Figure 6.16 – Concrete Lintel pg138
Figure 6.17 – The Completed 28m^2 Dome pg138
Figure 6.18 – Graph of the Strength of the Mortar pg140
Figure 6.19 – The Schmidt Hammer pg141
Figure 6.20 – Schmidt Hammer Results (Schmidt, 1950) pg142

APPENDIX B

Figure B1 – Alternative Structure – Structure Type C pg154
Figure B2 – Meridian Forces (Dome) – Structure Type C pg155
Figure B3 – Hoop Forces (Dome) - Structure Type C pg155
Figure B4 – Meridian Moments (Dome) – Structure Type C pg156
Figure B5 – Meridian Forces (Cylinder) – Structure Type C pg156
Figure B6 – Hoop Forces (Cylinder) – Structure Type C pg157
Figure B7 – Meridian Moments (Cylinder) – Structure Type C pg157

List of Tables

CHAPTER 1

Table 1.1 – Thermal Conductivity tests on Earth blocks (Lamb, 1998) pg16

CHAPTER 2

Table 2.1– Fixed Base Reaction Forces – Catenary pg41

Table 2.2– Fixed Base Reaction Forces – Sectioned Hemisphere pg44

Table 2.3 – Parabola – Fixed Base Reaction Forces pg48

Table 2.4– Fixed Base Reaction Forces – Ellipse pg52

Table 2.5 – Summary of the Best Shapes pg55

CHAPTER 3

Table 3.1 – Basic Soil Requirements for CEB Production (Uzoegbo, 2003) pg58

Table 3.2 – Properties of Cement Stabilized Earth Blocks pg58

Table 3.3 – Mortar Compressive Strengths (SABS 0164: Part 1 Table 1) pg61

Table 3.4 – Compressive Strength Tests Results pg62

Table 3.5 – Tension Test Results – Fibre Plaster pg64

Table 3.6 - Concrete Block Sliding Down Mortar Surface pg72

Table 3.7 - One Layer of DPC Wrapped around Concrete Block pg73

Table 3.8 - Two Layers of DPC Wrapped around Concrete Block and Mortar Surface pg74

CHAPTER 4

Table 4.1 – Load Combinations According to SABS 0160 – 1989 pg83

CHAPTER 5

Table 5.1 – Wire Wrapping Calculation – Door Section pg119

Table 5.2 – Wire Wrapping Calculation – Window Section pg119

Table 5.3 – Foundation Loading pg124

CHAPTER 6

Table 6.1 – Requirements for Mortar (SABS 0164:1 Table 1) pg139

Table 6.2 – Mix Proportions for Mortar (SABS 0249 Table 5) pg139

Table 6.3 – Foundation and Floor Slab Compressive Strengths pg142

Table 6.4 – Cost Comparisons of Low-Cost Housing Schemes pg144

APPENDIX A

Table A1 – 1.5DL – Centre Section Results pg152

Table A2 – 0.9DL+1.3WL (Suction side) – Centre Section Results pg153

List of Symbols

DESCRIPTION	SYMBOL
Radius of the dome	a
Cross-sectional area	A
Area of Steel	A_s
Height of the ring beam	b
Compressive Force	C
External Pressure Coefficient	C_p
Ring compression induced @ skylight opening	$C_{\varphi 0}$
Thickness of the ring beam	d
Horizontal displacement of the dome @ the base	D_{10}^{D}
Horizontal displacement of the ring beam	D_{10}^{R}
Rotation of the dome @ the base	D_{20}^{D}
Rotation of the ring beam	D_{20}^{R}
Compatibility Matrix Variable	D_{11}
Compatibility Matrix Variable	D_{12}
Compatibility Matrix Variable	D_{21}
Compatibility Matrix Variable	D_{22}
Dead Load	DL
Young's Modulus	E
Characteristic compressive strength	f_k
Yield Strength of Steel	f_y
Force	F
Design vertical load	g_a
Design vertical stress	g_d
Shell Thickness	h
Horizontal thrust @ base of dome	H
Horizontal thrust caused by skylight opening	$H_{\varphi 0}$
Moment of inertia	I
Constant depending on altitude	k_p
Base diameter of the dome	L
Live Load	LL
Moment	M
Allowable moment	M_{allow}

DESCRIPTION	SYMBOL
Applied moment	M_{appl}
Moment @ base of dome	M_{α}
Hoop moment	M_{θ}
Meridian moment	M_{φ}
Hoop force	N_{θ}
Meridian force	N_{φ}
Hoop membrane force	N'_{θ}
Meridian membrane force	N'_{φ}
Free stream velocity	p
Wind pressure	p_z
Point load @ skylight opening	P
Uniformly distributed load	q
Radius of ring beam	r
Thickness of fibre plaster	t
Tensile force	T
Characteristic wind speed	v_z
Volume	V
Weight	W
Wind Load	WL
Cartesian x – coordinate	x
Cartesian y – coordinate	y
Half of the ring beam height	y_0
Height of the dome	Y
Cartesian z – coordinate	z
Capacity reduction factor	β
Horizontal displacement @ base of dome	Δ_H
Rotation @ base of dome	Δ_{φ}
Strain	ε
Angle in the vertical plane of the dome	φ
Material safety factor	γ_m
Friction coefficient	μ
Stress	σ
Poisson's ratio	υ

1. Introduction

1.1 Statement of the Problem

There is a large demand for low cost housing in South Africa. The 2001 South African Census showed that approximately 1.9 million households are informal and approximately 1.7 million are classified as traditional dwellings (Figure 1.1).

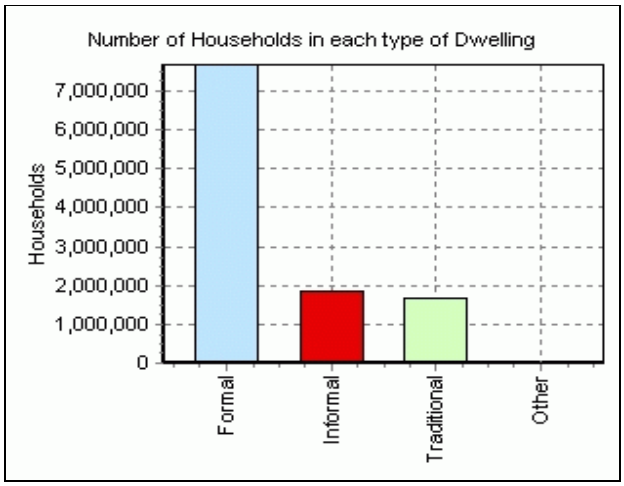

Figure 1.1 – Distribution of South African Houses (RSA Census, 2001)

The people living in traditional houses live mainly in the rural areas of South Africa. These houses could be improved on, making them more durable. The number of informal houses is a concern, as a large proportion of these houses are located in squatter camps (shanty towns) in urban areas. The living conditions in these areas are poor. There is a great need for a more formal type of housing that would provide improved thermal properties during winter, as well as a greater resistance to the elements.

Current mass housing solutions focus on conventional methods of construction (i.e. rectangular brick structures with roof trusses).

Innovative and cost effective materials and construction procedures are needed in order to improve the growing housing shortage. Dome structures have been used effectively, in studies done at The University of the Witwatersrand, as an alternative housing form. This dissertation seeks to investigate the dome structure as a low cost housing alternative. The problem of cost effective materials is addressed by using cement stabilized earth blocks (CEB's) in the construction of the dome.

1.2 Aims of the Investigation

The main objectives of this dissertation are:

- To identify the optimal shaped dome structure that can be used in low cost housing
- To investigate the important design criteria with regard to domes
- To utilize affordable materials (compressed earth blocks) that can be acquired in remote areas
- To investigate different methods of dome construction
- To construct a durable, architecturally and structurally efficient low cost dome house

1.3 Method of Investigation

The method of the investigation is shown in Figure 1.2 (pg. 4).
This investigation was design orientated and therefore the solution procedure was iterative. Many different shapes can be used in the design of shell structures, and therefore the most important step in any shell analysis is determining the best shape for the structures given function. A shape investigation was undertaken in order to determine the optimum shape of the structure. In order to perform this investigation the material properties needed to be defined. This was done through a literature investigation. Once an optimum shape was found the design of the structural elements (masonry, ring

beam) was performed. Through investigation it was found that a masonry dome solution for low-cost housing already existed (Dome Space solution). The shape of this dome was optimal from an architectural point of view (i.e. maximum useable space). However, specific problems were identified with this solution (e.g. lack of ductility allowing thermal cracking and cracking induced in regions of high stress), and therefore some engineering of the solution was required. The construction technique used to build the dome was well documented. This was done in order to check the quality of the materials on site, and to compare the construction procedure used to traditional dome construction techniques (e.g. Nubian method of construction used by Magaia (2003)).

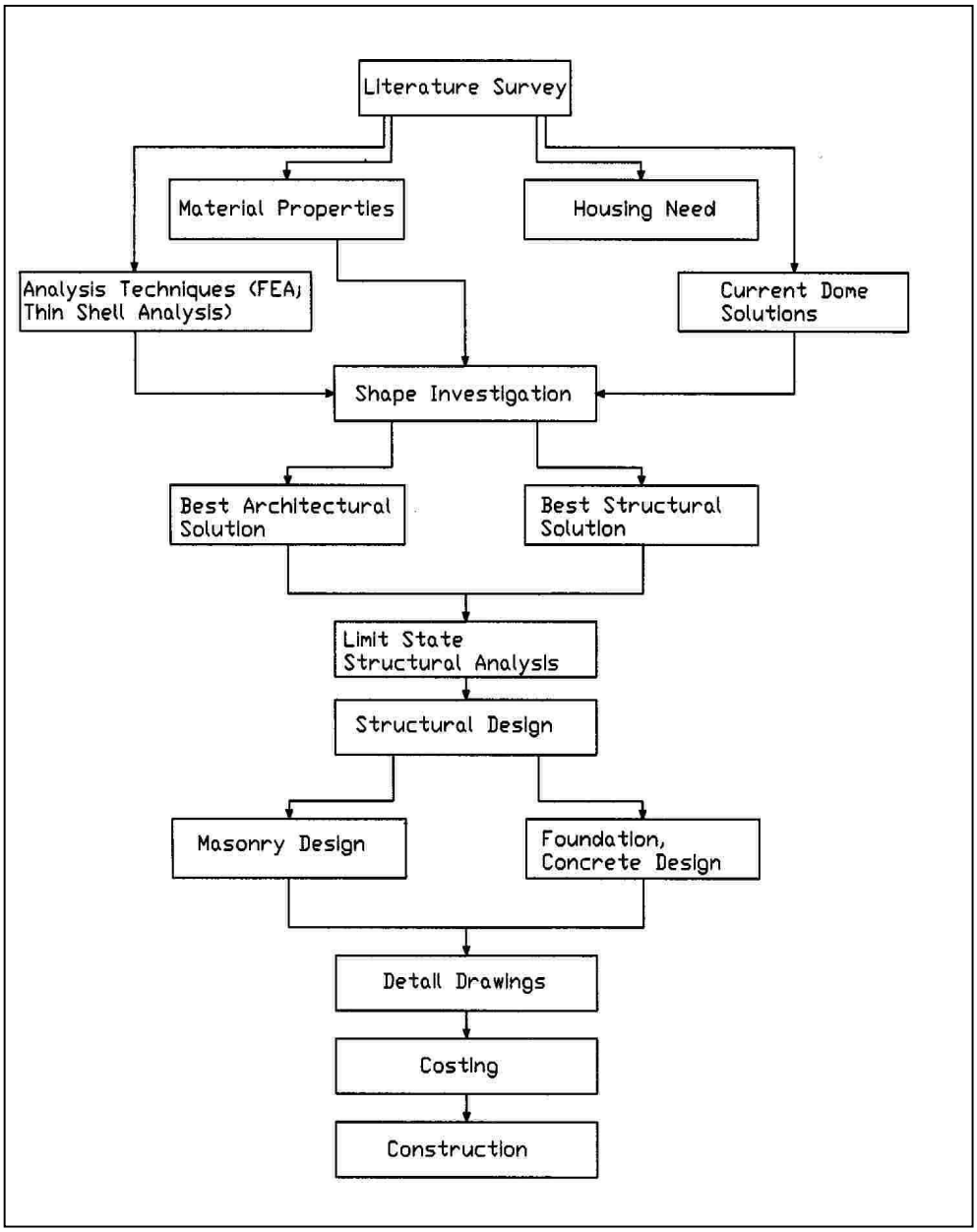

Figure 1.2 – Flow Diagram of the Investigation

1.4 A Brief History of the Dome

Domes have been used throughout the ages as a housing form, or an element of a housing form (roof structure). African and aboriginal societies built domes by planting branches in the ground and weaving the dome shape (Kirchner, 1988). Figure 1.3 shows a typical Zulu hut in Kwazulu-Natal, South Africa.



Figure 1.3 - Zulu Hut (KwaZulu-Natal)

The dome was also used by the Musgum tribe of Cameroon (Gardi, 1973). This parabolic dome consists of a highly cohesive earth shell, 15-20cm (5.9-7.9 inches) thick at its base, 5cm (1.97 inches) thick at the top and 7-8m (23-26 ft) high. Figure 1.4 shows a typical Musgum dome.

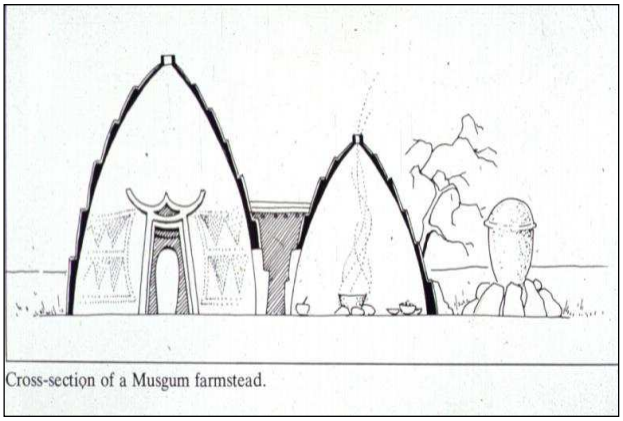

Figure 1.4 - Musgum Farmstead

The dome shape has also been used historically to span large distances, as reinforced concrete and steel have been relatively recent developments on the historical scale. The Moguls, Egyptians, Byzantines and Romans used domes and vaults extensively. Examples of these are The Shrine of the Living King (Samarkand) built by the Moguls, The Pantheon in Rome and The Temple of Ramses II (near Aswan). The Temple of Ramses II was constructed out of earth bricks in 1290BC and parts of the structure, such as the vaults where the priests stored grain, are still standing (Melaragno, 1991). This illustrates the great potential of earth as a durable construction material.



Figure 1.5 - The Ramesseum Storage Vaults, Gourna, Egypt

.

1.5 Recent Developments in Compressed Earth & Dome Construction

This section introduces some of the work that has been done in the field of earth and dome construction. The first two reports were done at The University of the Witwatersrand, and they provided some of the parameters used in this dissertation.

1.5.1 Fibre Reinforced Soil Crete Blocks for the Construction of Low-Cost Housing – Rodrigo Fernandez (University of the Witwatersrand, 2003)

This investigation focused on the production of fibre reinforced cement stabilized blocks. The objective was to study different types of soil, curing processes and reinforcements, in order to identify the most important parameters in the production of strong, durable blocks. The project was undertaken by the University of the Witwatersrand and the Lausanne Federal Institute of Technology (EPFL) (Fernandez, 2003). This report was useful to this project as it provided design information about the HydraForm earth block. Tests were performed to determine dry compressive strength, flexural strength, tensile strength and the modulus of elasticity of the blocks.

Scanning electron microscope analysis was also used in this investigation. It was found that the nature of the soil, particularly the clay content and plasticity index were important. These variables could be optimized to improve the mechanical properties of the blocks. It is important to note that fibres did not always contribute to strength, and in some cases actually reduced the strength of the blocks (Fernandez, 2003).

1.5.2 Domes in Low-Cost Housing – S.J. Magaia (University of the Witwatersrand, September 2003)

This investigation involved the construction of a dome shaped low-cost house in a rural area close to Maputo, Mozambique. Figure 1.6 shows the final product of this investigation. The study sought to prove the viability of this type of structure for the use of low-cost housing. Furthermore, the study was aimed at achieving a self-construction solution, using local materials to construct the dome. The concept was proved to be viable (Magaia, 2003). However, architectural issues were not adequately considered. Wasted space around the perimeter of the dome, lack of internal light and the unpleasant appearance of the dome were issues that were not sufficiently explored.

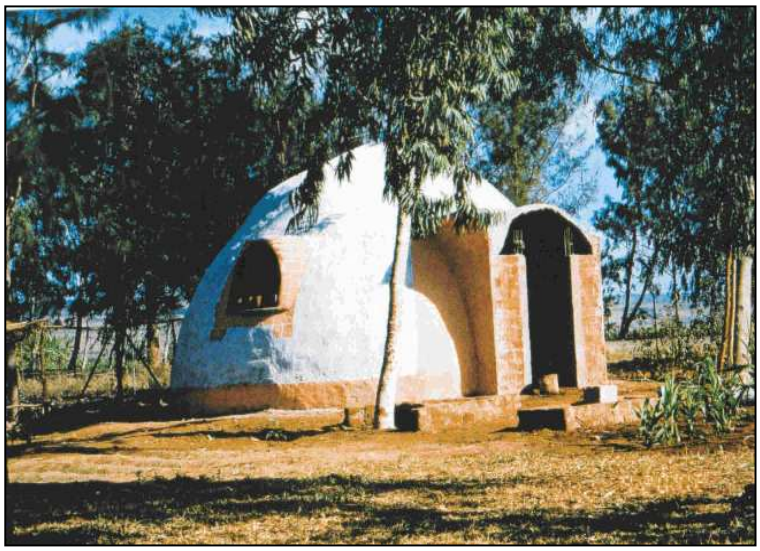

Figure 1.6 - Low-Cost Dome built by S.J. Magaia(2003)

1.5.3 The Monolithic Dome Solution



Figure 1.7 – EcoShells in Haiti. (www.monolithic.com)

The EcoShell is a dome home designed by Monolithic Dome of Texas. The above figure shows an EcoShell constructed in Haiti as a form of low-cost housing. The dome is constructed by spraying concrete onto an inflated formwork that has reinforcing bars attached to it. The EcoShell is hemispherical in shape. The benefit of this type of construction is the speed at which the structure can be erected (Garrison, 2004). However, the materials and equipment needed to construct sprayed concrete domes are relatively complex and costly. In a rural environment this type of construction may be difficult to implement.

1.5.4 The Dome Space Solution



Figure 1.8 – Dome Homes built by Dome Space

Figure 1.8 shows two masonry domes built by Dome Space, South Africa. The domes are hemispherical in shape and were built using inflatable formworks. The dome on the left was built for the Sparrow Aids Village and the dome on the right for a village in the same area. Extensive cracking was observed on the Sparrow Aids Village Dome. The cause of cracking in brick domes was a primary concern in this investigation, and is discussed further in sections 4.4.2 and 4.4.3.

1.5.5 The Tlholego Eco-Village

The Thholego Eco-Village is situated in the North West Province of South Africa. A masonry dome was built above a cylinder wall (to eaves height), and the structure was used as a kitchen for the local community. Cracking was also observed. Poor waterproofing, shrinkage and thermal cracking was postulated as the cause of cracking. Figure 1.9 shows the Tlholego Eco-Village Dome kitchen.



Figure 1.9 – Dome Kitchen – Tlholego Eco-Village

1.6 Architectural Considerations

This section deals with a few key architectural issues which need to be addressed when building any structure. The issues discussed can be summarized under the following headings:

- Shape
- Structural Strength
- Rain Penetration & Damp Proofing

- Thermal Performance
- Lighting
- Internal Arrangement of Walls
- Overall Aesthetics

1.6.1 Shape

The shape of the dome structure is perhaps the most important variable that needs to be investigated when designing a brick dome. Three types of dome structure were investigated (see figure 1.10). These were:

- A dome structure from ground level - Type (A)
- A dome placed on a short cylinder wall - Type (B)
- A section through a dome placed on a vertical cylinder wall (with a ring beam) - Type (C)

In this dissertation emphasis is placed on attaining the most efficiently shaped dome. The efficiency of the structure was measured in two ways: First, the shape and second, useable space. The dome curves in two directions making it very difficult to fit furniture into the home. Floor space is wasted when walls slope to the base of the structure. Figure 1.10 shows the three types of domes investigated in this report, as well as the concept of useable space. The units are given in metric millimeters.

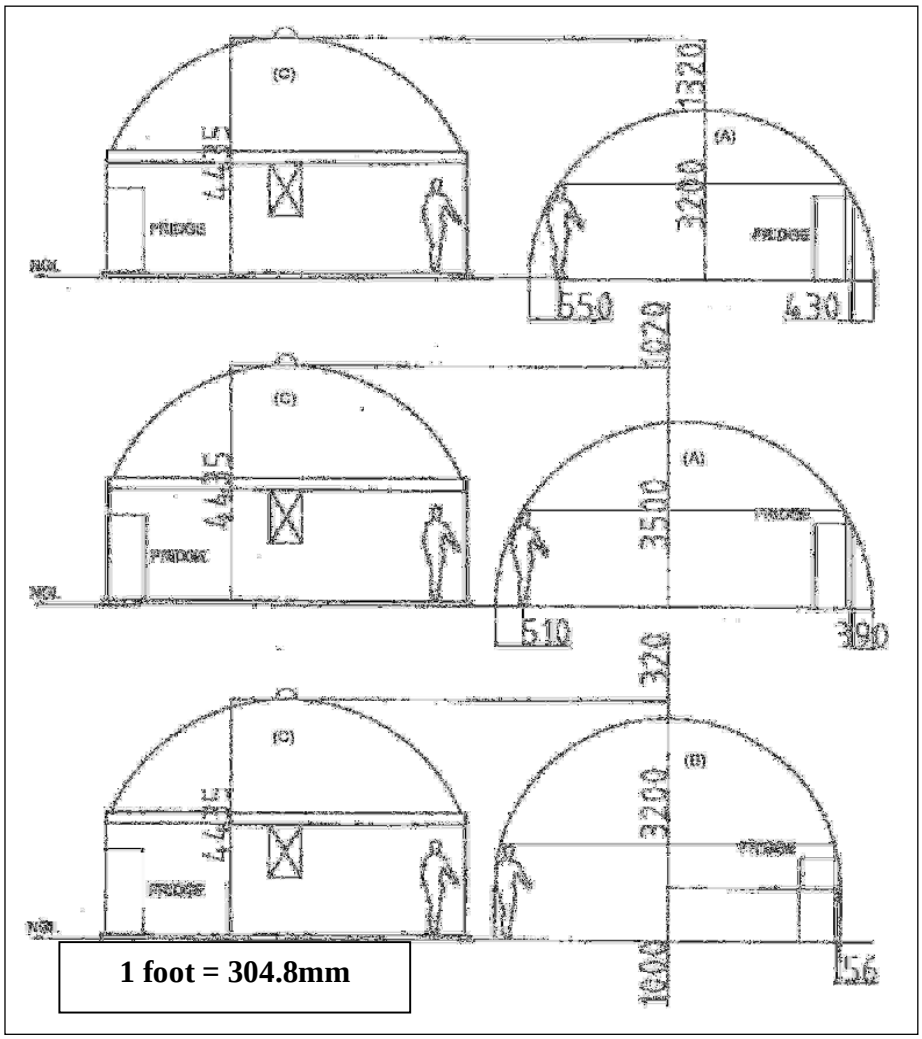

Figure 1.10 – Useable Space within Possible Low-Cost Dome Structures

In order to improve the amount of useable space within a dome the diameter of the dome needs to be increased so that items can be placed closer to the wall (structure type A). By doing this the floor area is increased, but space is still wasted around the edges of the dome. The two alternative shapes (B & C) in figure 1.10 incorporate a straight cylinder wall. Structure (B) comprises of a full dome roof and a short cylinder wall 1m high. Structure (C) comprises of a sectioned dome roof with a concrete ring beam resting on a cylinder wall to door height. Figure 1.10 shows that structures (B) and (C) are more desirable than structure (A) from a useable space point of view.

1.6.2 Structural Strength

The dome element of the structure was chosen for its structural strength as well as the savings envisaged by replacing a conventional roofing system with a monolithic element. The dome is defined as a doubly curved surface element. The dome's doubly curved surface allows it to carry loads (especially its dead weight) very effectively. The load is carried primarily by membrane action. Moments and shears are limited to the area around the base (or boundary) of the shell. Stiff horizontal rings around the shell limit the deformation in the meridian direction. Figure 1.11 shows the hoop and meridian directions in a shell.

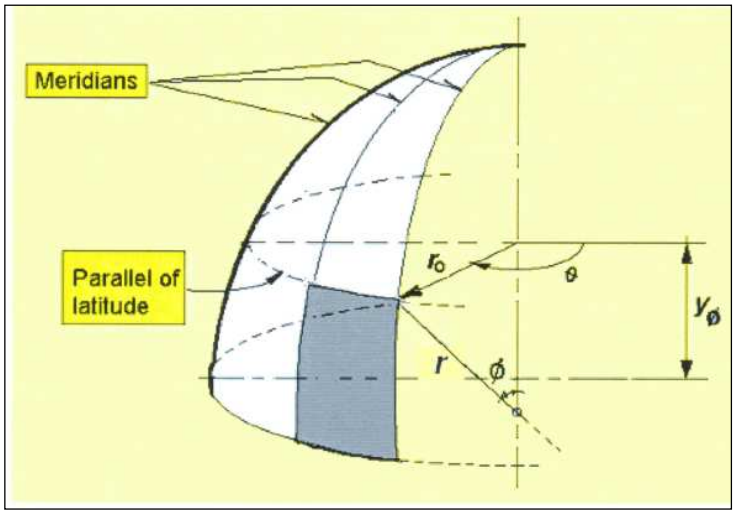

Figure 1.11 - Hoop and Meridian Directions (Magaia, 2003)

1.6.3 Rain Penetration & Damp Proofing

It is undesirable and unhealthy to have moisture within a living environment. Rain penetration can be prevented by careful detailing of the structure. The entire structure was plastered in order to prevent rain penetration. It is important to plaster the structure in stages in order to limit shrinkage. It is recommended (Doat, 1985) that plaster is applied in three coats to a vertical wall. It is very important that strong cement plasters are avoided. These form a

rigid surface above earth walls, and since the earth wall is not as rigid as the plaster the plaster tends to crack. Temperature and moisture cycles can cause further cracking. Moisture enters the wall and erodes parts of the wall away (Magaia, 2003). A possible solution to this is using fibre reinforcement or wire mesh in the plaster (William-Ellis, 1947)**.** These methods of reinforcing the plaster are explored to a greater extent in the materials investigation section. Figure 1.12 shows the shrinkage cycle of plaster on a vertical wall. For dome structures, the dome is very stiff owing to its shape. It is postulated that the stiffness of the shell prevents the contraction of the plaster (during shrinkage), causing the plaster to crack.

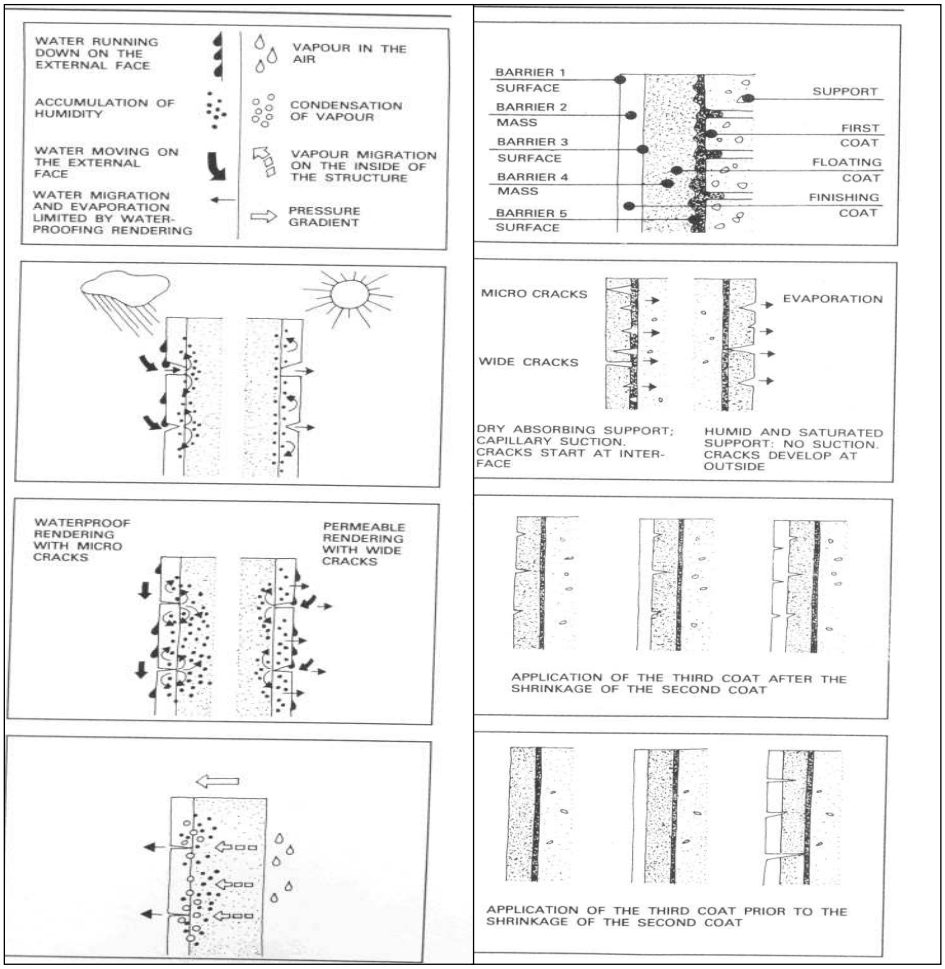

Figure 1.12 – Plaster Coatings & Shrinkage (Houben, Guillaud, 1994)

A reduction in the cement content in the plaster mix will help to reduce the stiffness of the plaster surface, and a reduction in the water content will limit the shrinkage of the plaster. It is important to note that plastering should take place on moderately warm and slightly humid days. Ten to twenty meter squared sections should be plastered at one time. All walls that are started should be finished on the same day, and the plastering should not extend to ground level due to capillary action which could cause moisture ingress.

1.6.4 Thermal Performance

The thermal performance of domed shaped houses is very favorable (Kirchner, 1988). Convection currents occur in well ventilated domes allowing more even temperatures during the summer months. The final structure chosen for construction had three windows and a door, at quarter points. There were no openings in the roof (except for very small vents in the skylight). The materials used to build the dome also contributed to the favorable thermal performance of the structure.

A good building material is one with a high heat capacity (it can store a fair amount of heat) and a low thermal conductivity (it retains the heat it stores). Thermal conductivity and heat capacity tests have been done on compressed earth blocks at The University of the Witwatersrand by Lamb (1998). The tests were performed on three types of earth blocks and a standard clay brick in order to compare their thermal conductivity and their heat capacity.
Table 1.1, overleaf, summarizes the relevant findings of Lambs' investigation.

TYPE OF BLOCK	THERMAL CONDUCTIVITY (K) [W/M˚C]	HEAT CAPACITY [KJ/KG˚C]	DENSITY [KG/M^3]
HydraForm Earth block • **Quaternary Sand (14% clay)** • **6% Cement**	0.578	0.853	1 780 (111 lb/ft^3)
Clay Fired Brick • **Standard according to SABS 1215**	0.82	0.8	1 826 (114 lb/ft^3)

Table 1.1 – Thermal Conductivity tests on Earth blocks (Lamb, 1998)

From table 1.1 we can see that the HydraForm Earth block[1] (used in this dissertation) has a lower thermal conductivity than the clay fired brick, which means it will retain more heat. It also has a greater heat capacity which means it will absorb more heat than clay fired bricks.

1.6.5 Lighting

The dome that was constructed was limited to three windows, a central skylight and a door. The skylight was positioned at the center of the dome as this is the most structurally efficient place to put it. It provides a central core of light within the house. A complaint with regard to low-cost domes built in the past was that they were very dark inside. The central skylight illuminates the inside of the structure and improves the lighting problem.

1.6.6 Internal Arrangement

This aspect of the design is of great importance and an architect may be needed to maximize the efficiency of the space. There are a large proportion of houses in both rural and urban areas that have four or more people living in one household (RSA Census 2001). This poses challenges to designers of low-cost houses as they need to be designed as small as possible and accommodate as

[1] HydraForm are a South African company who specialize in the production of cement stabilized earth blocks.

many people as possible. Figure 1.13 shows possible internal arrangements of low-cost dome houses. The arrangement will be dictated by the tenants' affluence. These internal arrangements were designed to accommodate between three to six people. Pit latrines on the outside of the house can be used to save space within the structure. Internal plumbing could be utilized with a service core supplying water to a basic kitchen and bathroom area. However, this solution would increase the costs. Figure 1.13 also shows an internal arrangement for a more affluent family (on the right). Cupboards and packing space can be installed around the perimeter of the house to save space.

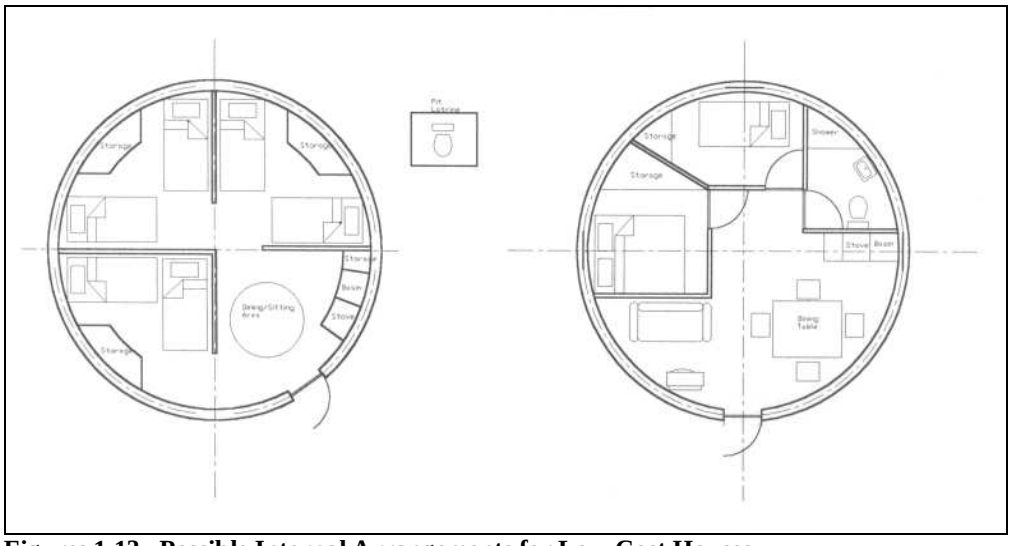

Figures 1.13– Possible Internal Arrangements for Low-Cost Houses

2. Shape Investigation

2.1 Methods of Shape Investigation

There are three main methods of designing shell structures. The first two involve the analysis of predetermined geometric shapes. These are classical thin shell theory and finite elements. The third method is an empirical method; this method involves scaled models of the structure. The Swiss engineer, Heinz Isler, used models to find funicular shapes by suspending materials so that they hung in pure tension. These models were then frozen and inverted, and a shape in perfect compression resulted. In this investigation classical shell theory and finite element analysis (FEA) are used to determine the best structural shapes. Three types of shape are presented:

- A dome structure from ground level - (Type A)
- A dome placed on a short cylinder wall - (Type B)
- A section through a dome placed on a vertical cylinder wall (with a ring beam) - (Type C)

2.2 Classical Thin Shell Theory

2.2.1 The Structural Elements

Figure 2.1 shows the basic structural elements of a dome home. The ring beam is an integral part of any dome as it prevents the dome from kicking out. It can be placed at ground level as a foundation or on a wall as shown in figure 2.1, overleaf.

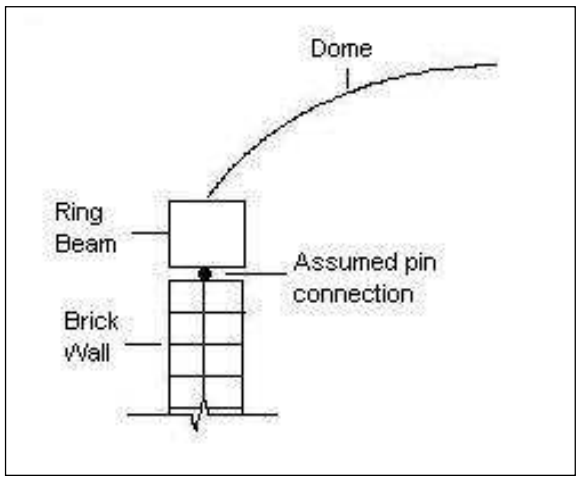

Figure 2.1 – The Basic Structural Elements

2.2.2 Forces and Moments in the Structure

This report assumes that the reader has a basic understanding of shell theory and therefore the equations have not been proven from first principles. The forces and moments that exist in a dome structure are summarized in figure 2.2.

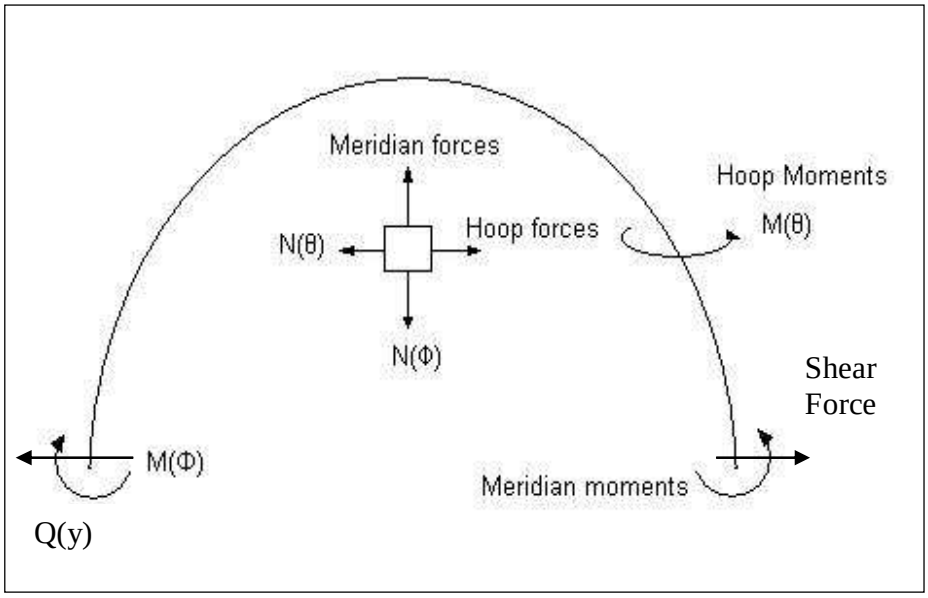

Figure 2.2 – Forces and Moments in Shell Structures

2.2.3 Classical Dome Theory

Classical dome theory was used to check the accuracy of the FEA analysis in the sensitivity analysis part of this chapter. This theory is well documented by Billington (1982). The solution procedure involves solving for the membrane forces and deformations without any restraints (supports at the edges) on the structure, and then correcting these results by applying a support restraint. Two sets of equations exist in this solution. They are the membrane equations and the boundary equations. According to Billington (1982), the solution can be broken up into four parts. The first part is called primary system. This system is based on membrane theory. The equations for the membrane forces with a uniformly distributed load (self weight load) applied to the shell surface are presented below.

$$N'_{\phi} = \frac{-aq}{(1+\cos\phi)} \qquad (2.1)$$

$$N'_{\theta} = aq\left(\frac{1}{1+\cos\phi} - \cos\phi\right) \qquad (2.2)$$

where,

a is the radius of a spherical dome

q is the uniformly distributed load

ϕ is the angle measured from the apex to the base of the dome

The second part of the solution involves calculating the errors. The errors are the deformations of the dome according to membrane theory. The equations presented are for a UDL load:

$$\Delta_H = \frac{a^2 q}{Eh}\left(\frac{1+\nu}{1+\cos\phi} - \cos\phi\right)\sin\phi = D_{10} \qquad (2.3)$$

$$\Delta_{\phi} = -\frac{aq}{Eh}(2+\nu)\sin\phi = D_{20} \qquad (2.4)$$

where,

D_{10} is equal to the horizontal membrane deformation

D_{20} is equal to the membrane rotation

E is equal to Young's Modulus

h is equal to the shell thickness

ν is equal to Poisson's ratio

The third part of the solution is to solve for the corrections.

$$\Delta_H = D_{11}H = \frac{2\beta a^2 H \sin^2\alpha}{Eh} \qquad (2.5)$$

$$\Delta_H = D_{12}M_{\alpha} = \frac{2\beta^2 a^2 M_{\alpha}\sin\alpha}{Eh} \qquad (2.6)$$

$$\Delta_{\alpha} = D_{21}H = \frac{2\beta^2 a^2 H \sin\alpha}{Eh} \qquad (2.7)$$

$$\Delta_{\alpha} = D_{22}M_{\alpha} = \frac{4\beta^3 a^2 M_{\alpha}}{Eh} \qquad (2.8)$$

where,

H and $\mathbf{M_{\alpha}}$ are the shear forces and moments respectively, applied at the base (edge) of the shell structure in order to correct the membrane displacements.

The fourth part of the solution is to determine H and M_{α}, using compatibility equations. The compatibility equations are

$$\sum\Delta_H = D_{10} + D_{11}H + D_{12}M_{\alpha} = 0 \qquad (2.9)$$

$$\sum\Delta_{\alpha} = D_{20} + D_{21}H + D_{22}M_{\alpha} = 0 \qquad (2.10)$$

The final steps in the solution are to calculate the shear forces, deformations and moments in the shell due to boundary effects. These equations can be seen in Billington (1982). The membrane forces are combined with the boundary effects.

2.2.4 Classical Dome/Ring Theory

Dome/Ring theory is the theory applied to dome structures with a ring beam at the base of the structure. The structure does not behave as if it were fixed or pinned, but somewhere between these two conditions.

The ring beam will allow a certain amount of rotation and outward displacement at the base, which a fixed base would not. Therefore, two new errors are introduced and these are added to the dome membrane errors to obtain the total dome/ring errors.

$$D_{10}^{R} = (\cos\alpha + \frac{12y_0 e}{d^2})\frac{r^2 N'_{\alpha}}{Ebd} \quad (2.11)$$

$$D_{20}^{R} = \frac{-N'_{\alpha} er^2}{EI_{R}} \quad (2.12)$$

$$D_{10} = D_{10}^{D} + D_{10}^{R} \quad (2.13)$$

$$D_{20} = D_{20}^{D} + D_{20}^{R} \quad (2.14)$$

The variables in the above equations are described in figure 2.3, overleaf.

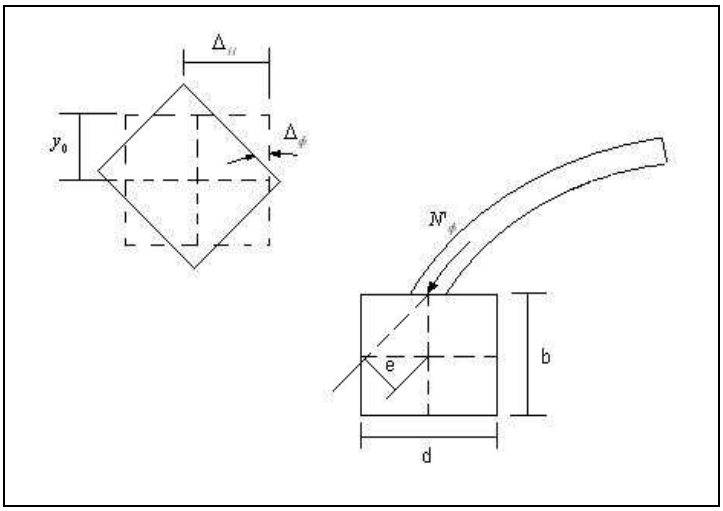

Figure 2.3 – Dome/Ring Equations' Parameters

The additional correction equations are:

$$\Delta_H = D_{11}^R H = (1 + \frac{12y_0^2}{d^2})\frac{r^2 H}{Ebd} \quad (2.15)$$

$$\Delta_\alpha = D_{21}^R H = \frac{-12r^2 y_0 H}{Ebd^3} \quad (2.16)$$

$$\Delta_H = D_{12}^R M_\alpha = \frac{-12r^2 y_0 M_\alpha}{Ebd^3} \quad (2.17)$$

$$\Delta_\alpha = D_{22}^R M_\alpha = \frac{12r^2 M_\alpha}{Ebd^3} \quad (2.18)$$

After this step the compatibility equations are compiled using equations 2.5 – 2.8 and 2.15 – 2.18. The rest of the equations are identical to the classical dome theory solution.

2.3 Basic Finite Element Analysis (FEA) Theory

Finite element analysis is used as an approximate solution to engineering problems. It is important to understand the limitations of this type of analysis, as well as the methods of assessing and improving the analysis when modeling

a structure. In this section a few practical issues regarding finite elements are discussed. The equations for the finite elements used are not presented.

2.3.1 Types of Elements Used

There are many shell elements that can be used to analyze a dome structure. This is due to the fact that shell elements are not fully compatible (the displacements are not always continuous along plate boundaries). Therefore errors can result in the analysis. For this reason a sensitivity analysis was done in order to check the accuracy of the FEA analysis against dome and dome/ring theory.

The final structure modeled in this report used three dimensional shell elements. The shape investigation used axi-symmetric finite elements owing to the symmetry of the problem. NAFEMS (National Agency for Finite Element Methods and Standards) suggests a few guidelines when choosing a shell element (Blitenthal, 2004). These are:

- Quadratic element types are more exact than linear elements.
- Linear elements are stiffer and produce lower displacements and stresses.
- Quadratic elements should be used for curved problems as they produce a better approximation. Linear elements will cause stress discontinuities along shell element boundaries.
- Shell elements are not accurate where there is a sharp change in geometry. This was one of the main concerns with the FEA analysis as there is a join between the ring beam and the dome structure. The sensitivity analysis proved that this was not a problem.

2.3.2 Methods of Improving FEA Accuracy

There are a few methods of improving the accuracy of the FEA analysis. The first is to use higher order elements (e.g. quadratic instead of linear). The majority of the other techniques involve the meshing of the model. These include:

- Using a structured mesh. A structured mesh comprises of square elements placed in a regular pattern. This type of mesh is not possible when modeling doubly curved surfaces. In this case, a triangular mesh, with triangles that are as close to equilateral as possible, or an irregular quadrilateral mesh, with quadrilaterals as close to square as possible, can be used.
- Using the mesh checking facilities provided by the FEA program to check aspect ratios (no greater than 3), free edges, angular distortion and internal element angles.
- Using second order elements if an automatic mesh generator is used.

Once the analysis has been completed the results should be evaluated and if necessary the mesh should be refined and the model reanalyzed. As mentioned earlier, a sensitivity analysis is important in checking the accuracy of the FEA model and can be used to find a suitable mesh.

2.4 Sensitivity Analysis

2.4.1 Description of the Analysis

It is extremely important when using finite element analysis to check whether the model is yielding accurate results. A sensitivity analysis was undertaken before the shape investigation in order to check the accuracy of the different types of finite elements that can be used to model the structure in Abaqus™. Two types of elements were investigated. These were the full 3D rotational shell element and the 2D axi-symmetric deformable shell element. Both

elements use a quadratic function to model their deflections. The results from these analyses were compared with a traditional shell analysis of the same structure. The sensitivity analysis was also used to check the influence of certain parameters on the results of the FEA analysis. Fixity at the base of the structure was investigated, as well as the effect of changing the thickness of the dome (stiffness) and changing the applied load on the structure.

A section through a hemisphere, with a radius of 3m (9.84 ft) and a height of 2.5m (8.2 ft) was used for this analysis. Three analyses were performed. In first analysis a fixed base was used, in the second a ring beam base was used (depth = 0.275m (11.2 inches), width = 0.29m (11.4 inches)), and in the third the dome was pinned. The properties of 30 MPa (4 351 psi) concrete were used in this analysis. A uniformly distributed load (UDL) of 4.69 kN/ m^2 (0.68 psi) was applied to the structure. This load included the dead load (self weight of the structure), as well as a live load of 0.5kN/ m^2 (0.07 psi).

The following figure shows the dome used for the sensitivity analysis:

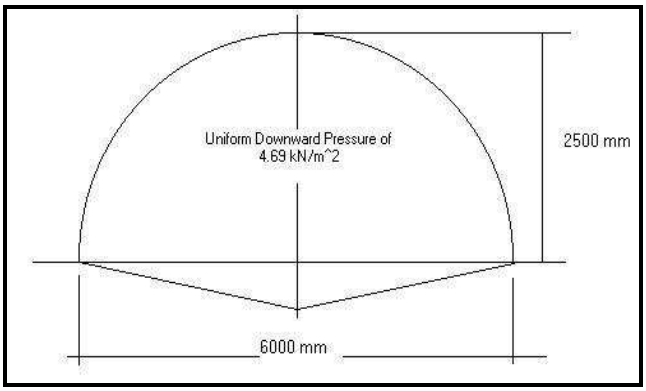

Figure 2.4 – Sensitivity Analysis Dome Dimensions

The results obtained from the three different analyses are presented below. They include the Meridian Force, the Hoop Force and the Meridian Moments. The Hoop Moments were excluded as they can be calculated by multiplying the meridian moments by Poisson's ratio. The accuracy of the finite element

analysis depends on the size of the elements chosen and the type of element chosen. Therefore, a fine mesh and elements with mid-side nodes were used in order to achieve good results.

2.4.2 Sensitivity Analysis Results

The results are presented along horizontal (x-direction) axis of the structure, from the centre of the dome to the dome base.

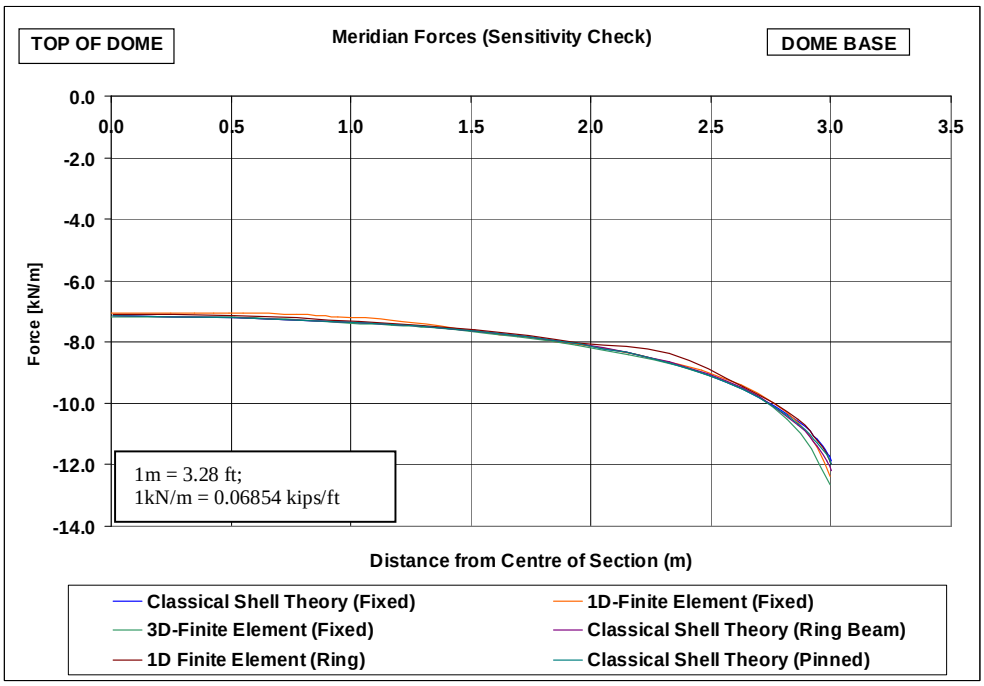

Figure 2.5 – Graph of Meridian Forces - Sensitivity Analysis

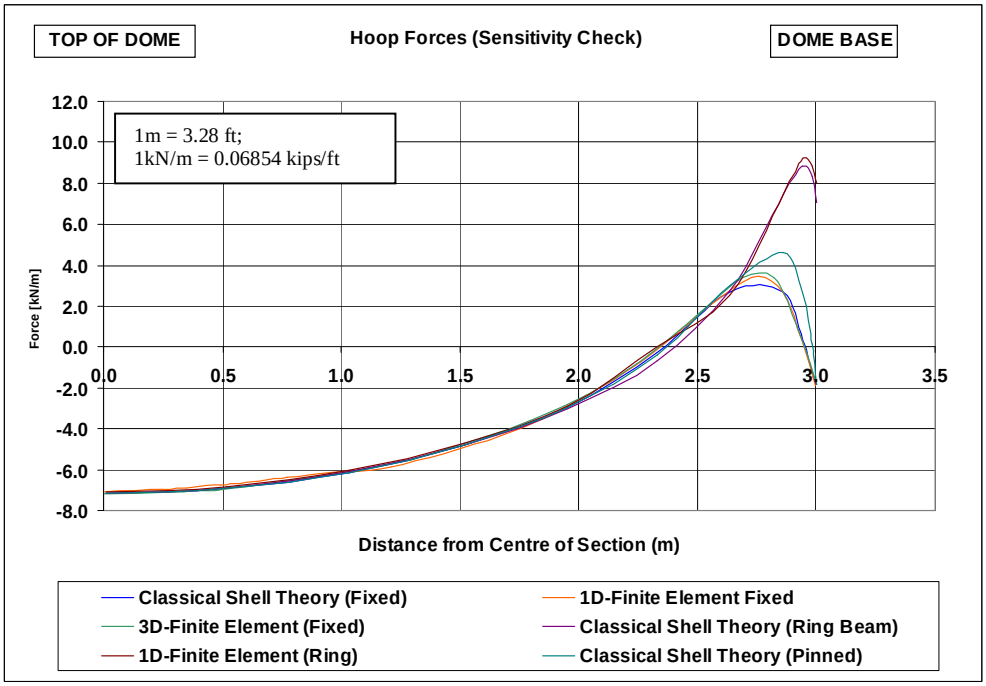

Figure 2.6 – Graph of Hoop Forces - Sensitivity Analysis

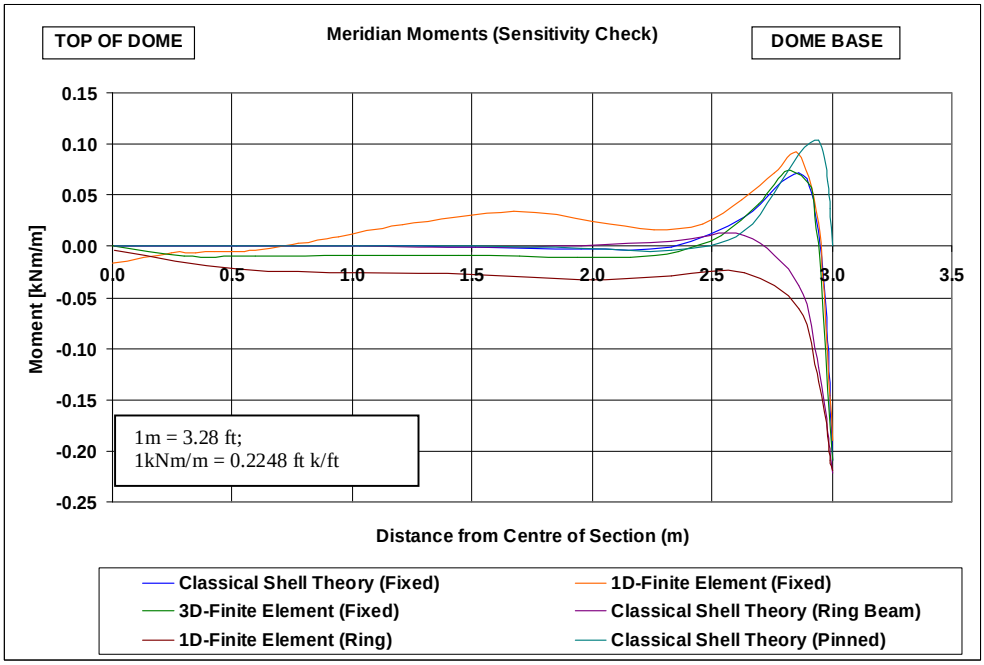

Figure 2.7 – Graph of Meridian Moments - Sensitivity Analysis

It can be seen from the above graphs that the Abaqus™ results follow classical shell theory results quite closely. It can also be noted that the 2D (axi-symmetric) method of analysis yielded results almost exactly the same as the shell theory results. This simplified the shape investigation as a 2D analysis could be done instead of a full 3D analysis.

The introduction of a ring beam at the base of the shell increased the hoop forces in the structure. The ring beam also affected the meridian moments**,** as seen in figure 2.7. In the ring beam analysis, the moments follow the same trend as the pinned base moments in the upper section of the dome. However, at the base of the dome the moments are closer to the values of the fixed base analysis.

2.4.3 Effect of Varying the Stiffness of the Structure

This section discusses the relationship between shell thickness (stiffness) and the forces in the dome, as well as the effect of varying the ring beam dimensions (stiffness at the base of the structure). This information is useful to determine a reasonably sized ring beam for the shape investigation.

Varying the Shell Thickness

The results presented are for a dome surface analyzed using shell theory. The self weight of the dome was increased according to its thickness. The graph overleaf shows the relationship between the shell thickness and the forces acting in the structure.

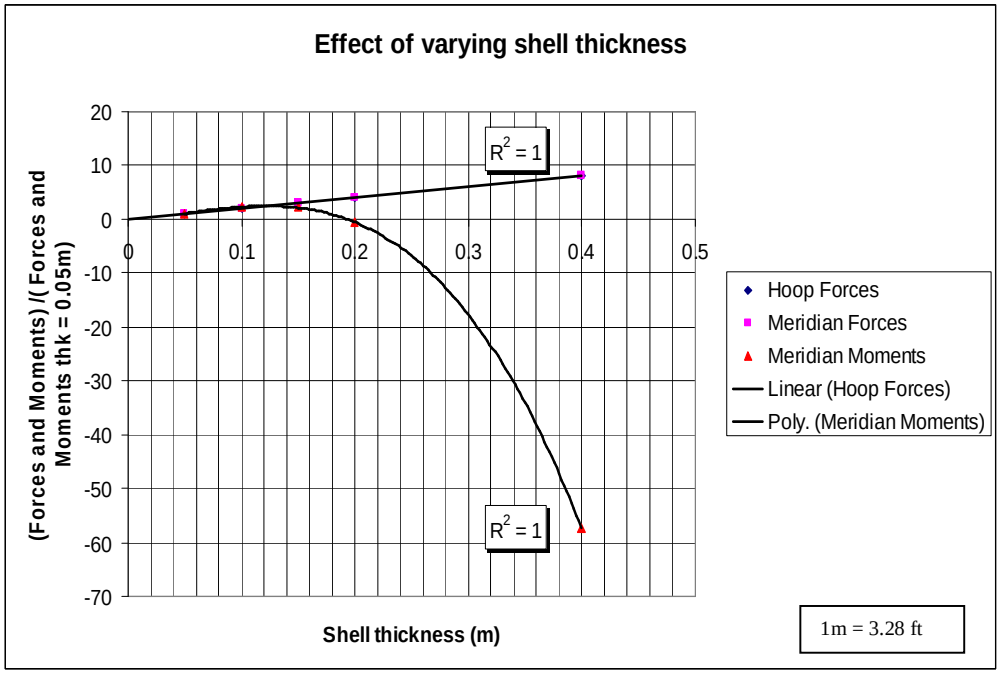

Figure 2.8 – Effect of Varying the Shell Thickness - Sensitivity Analysis

The relationship between the shell thickness and the forces is linear, whereas the relationship between the shell thickness and the moments is a polynomial of the 3rd order. It is therefore very important to select the thinnest possible shell section in order to minimize the forces and moments in the structure – stiffness attracts force. A thinner section will dissipate the forces quicker than a thicker sectioned thin shell. The moment region at the base of a thick shell (e.g. a concrete thin shell) is larger than the moment region at the base of a thinner shell (e.g. a thin steel shell). Young's Modulus (E) has no effect on the forces and moments as long as the same material is used throughout the shell. However, it does have an effect on the calculated deformations.

Varying the Ring Beam Dimensions

The following graphs show that as the ring dimensions are increased the forces and moments in the structure tend towards the fixed support case. It can also be seen that by including a ring beam the hoop forces in the structure are increased considerably. These findings prove the basic structural concept that stiffness attracts load. An infinitely stiff ring beam will attract the maximum amount of load (fixed base). If a smaller sized ring beam is used more load must be carried by the shell. Thus, the hoop forces in the shell are greater.

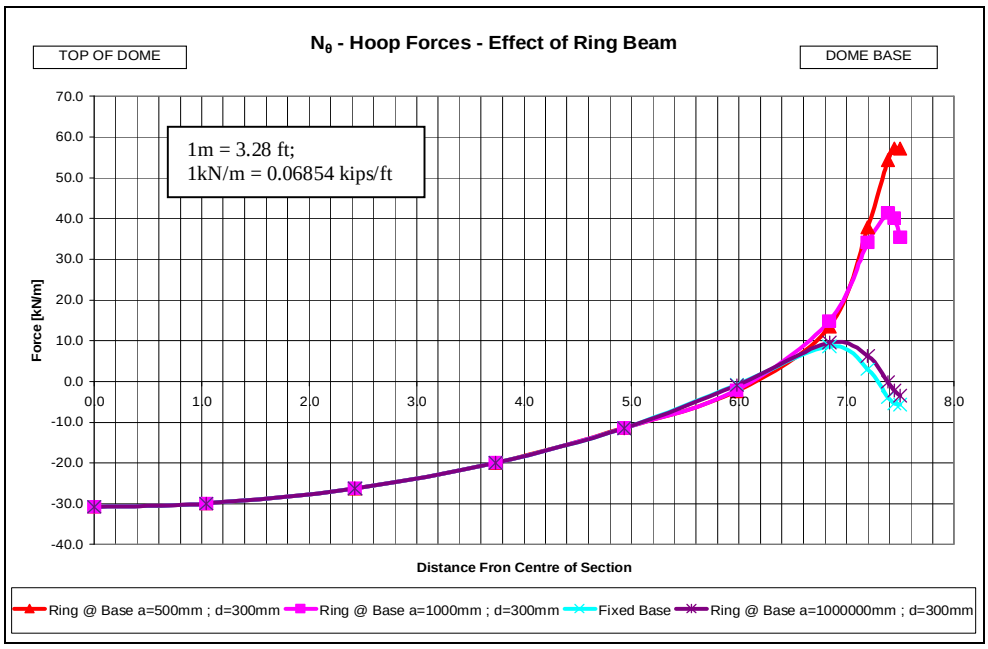

Figure 2.9 – Graph of N_θ - Effect of Varying Ring Dimensions - Sensitivity Analysis

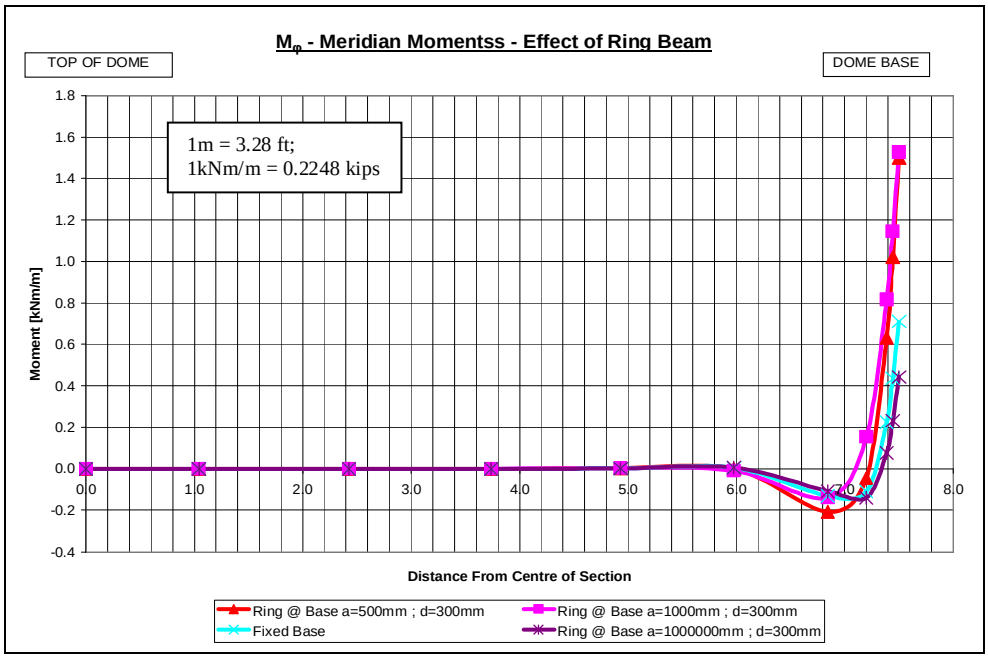

Figure 2.10 – Graph of M_{φ} - Effect of Varying Ring Dimensions - Sensitivity Analysis

2.4.4 Summary of Sensitivity Analysis Findings

The findings of the sensitivity analysis and their effect on the shape investigation were:

- An axi-symmetric finite element analysis could be used in the shape investigation, reducing computing and modeling time.
- The shell thickness and load on the shells were kept constant in the shape investigation in order to compare the forces in the different shapes.
- The hoop forces and meridian moments were found to be the main contributors to the tension stresses in the structure and therefore needed to be minimized. A fixed base analysis was performed in order to obtain accurate kicking out forces[2] at the bases of the dome shapes modeled from ground level.

[2] The kicking out force is the horizontal component of the meridian membrane force. This force acts at the base of the dome and pushes the dome support outward.

- A ring beam needed to be incorporated into the shape investigation, as the forces in the dome when a ring beam is used are somewhere between the fixed and pinned base forces. Therefore a reasonably sized ring beam was chosen in the shape investigation and the results of the analysis with a ring beam were compared to the fixed and pinned base results.

2.5 Shape Analysis

2.5.1 Description of the Analysis

This investigation was undertaken in order to obtain the most structurally efficient shape for the proposed low cost house. Three types of structure were investigated in the shape analysis. These were:

- **Type (A) - A dome structure from ground level**
- **Type (B) - A dome built directly onto a short cylinder wall**
- **Type (C) - A section through a dome placed on a vertical cylinder wall (with a ring beam)**

The shapes used in the above three structures were catenaries, parabolas, hemispheres and ellipses. The maximum height of the overall structure was limited to approximately four meters for building purposes. This constraint limited the shapes that could be used for the roof structure in option (C), above. The shapes were modeled in Abaqus^{TM} using axi-symmetric finite element analysis.

The material properties of the HydraForm (a South African earth brick manufacturer) earth blocks are given below:

- Density = 1 950kg/m^3 (121.7 lb/ft^3)
- Young's modulus = 3 500 MPa (507.6 ksi)
- Poisson's ratio = 0.2

- Shell thickness = 0.14 m (5.51 in.)

A standard ring beam was used to check the effect it has on the forces and moments in the structure. The dimensions of the ring beam for dome types (A) & (C) were assumed to be:

- Width (b) = 0.29m (11.4 in.)
- Depth (d) = 0.275m (10.8 in.)

A body force of 28, 7 kN/m^3 (0.105 lbf/in^3) was applied to the different shapes in this investigation. A body force was used as this the standard vertical load that can be used in Abaqus^{TM} (the FEA program). Using the same force enabled a direct comparison of the different shapes. The force was determined as follows:

Brick Density x Gravitational Constant

$$1950 kg/m^3 \times 9.81 = 19130 N/m^3$$

$$19130 N/m^3 \div 1000 = 19.13 kN/m^3$$

This load was then factored using the dead load factor of 1.5.

1.5 Dead Load

$$1.5 \times 19.13 = 28.7 kN/m^3 (0.105 \text{ lbf/in}^3)$$

The load factor of 1.5 DL was used in accordance with SABS 0160: Part1 (1989). This load factor yielded the maximum moments and forces within the final structure. It is important to note that the shape investigation is a comparative investigation and any reasonable load can be used to compare the effectiveness of the shapes.[3]

[3] The linear relationship between the applied force, and the resulting forces and moments in a dome structure can be seen in Figure 2.9.

2.5.2 Shape Evaluation Criteria

The important criteria for the evaluation of the different shapes can be summarized into four questions:

- Which shape yields the smallest tension forces (hoop forces) and moments?
- Where are the tension regions in the structure?
- Which dome shape produces the smallest kicking out forces?
- Which shape is the most suitable for low-cost housing (cost, useable space)?

The first three questions deal with tension in the structure. Tension stresses need to be minimized as they cannot be adequately resisted by the masonry and therefore, more expensive materials (e.g. reinforcing bars) are required to resist the stresses. The fourth question concerns the aesthetics and constructability of the structure.

2.5.3 Presentation of the Analysis Results

The results for each shape are summarized into three sections.

- The first section shows the maximum and minimum hoop forces and meridian moments in the different shapes. These forces are plotted against a Y/L (height/base diameter) ratio. The Y/L ratio is the ratio of the height of the structure to the diameter (figure 2.11). Moments are shown positive clockwise and positive forces are tensile.

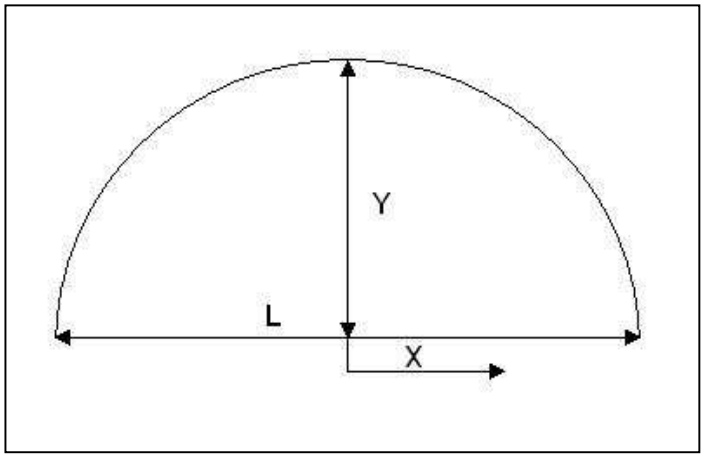

Figure 2.11 – Y/L Ratio Parameters

- In the second section, the stresses are plotted against the x-distance shown in figure 2.11. Basic elastic stress formulae are used to calculate the stresses. This formula is shown below:

$$\sigma = \frac{F}{A} \pm \frac{M}{Z} \quad (2.19)$$

where: F = force; N(θ) – hoop force ; N(φ) – meridian force

M = momen; M(θ) – hoop moment ; M(φ) – meridian moment

A = area [m^2]

Z = section modulus [m^3]

The elastic stress formula is applied to the hoop and meridian directions to check which regions of the best performing structures are in tension, and which faces (inside or outside) the tension stress is acting. It is important to note that positive values (in the stress plots) denote tension while negative values denote compression.

- The third section presents the kicking out forces at the base of the shape. The kicking out force is the horizontal component of the meridian membrane force. This force acts at the base of the dome and

pushes the dome support outward. This parameter is critical when designing domes supported at their bases with ring beams or walls (structure type C). The magnitude of the force, that pushes the dome outwards (RF1), determines the quantity of reinforcing in the ring beam. This force creates tension at the base of the structure, thus the need for reinforcing. In order to improve economy of the structure this force must be minimized. Figure 2.12 shows the Abaqus™ sign convention of the reaction forces at the base of the dome.

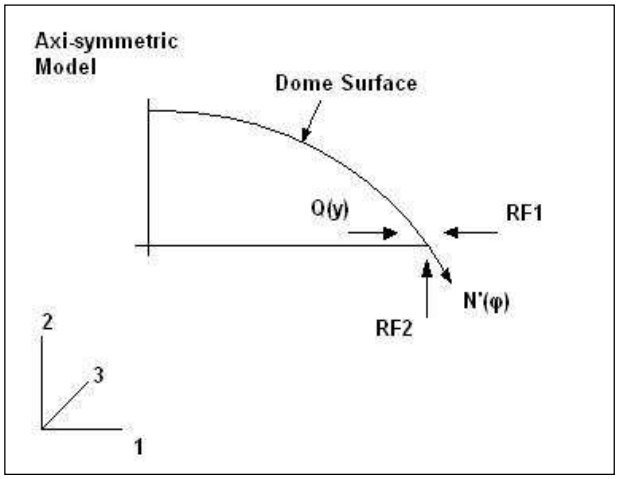

Figure 2.12 – Fixed Base Reaction Forces

2.6 Shape Analysis Results (Structure Types A & C)

2.6.1 The Catenary

A catenary shape is obtained when a chain is held at two ends and left to hang freely. This shape is in perfect tension when the only force acting on it is its self weight. If this shape is inverted it produces a structure in perfect compression. A catenary is the perfect shape for an arch or barrel vault structure. However, for a dome structure, experimental techniques are needed to find the optimum shape. Figure 2.13 illustrates why a catenary is the optimum shape for a barrel vault but not a dome.

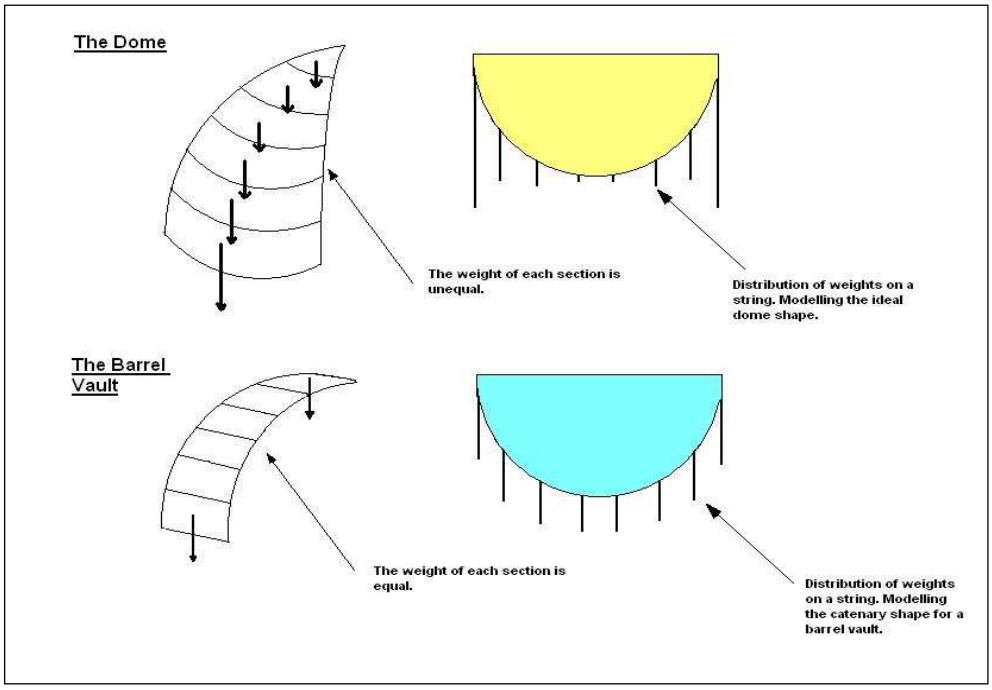

Figure 2.13 – The Ideal Shape of a Dome Structure

The equation of a catenary is:

$$y = a\cosh(\frac{x}{a}) \quad (2.20)$$

Y = Height of shape [m]

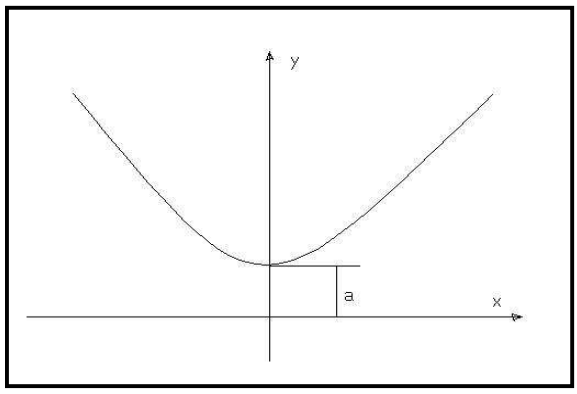

Figure 2.14 –The Catenary Equation Variables

The base diameter of the catenary was set at 6.4m (21 ft) in this investigation (the diameter of a reasonably sized low cost home). The y-value in the equation above is the variable that was changed in order to generate the different shapes. The following sections discuss the results of the catenary analysis.

Maximum & Minimum Forces & Moments

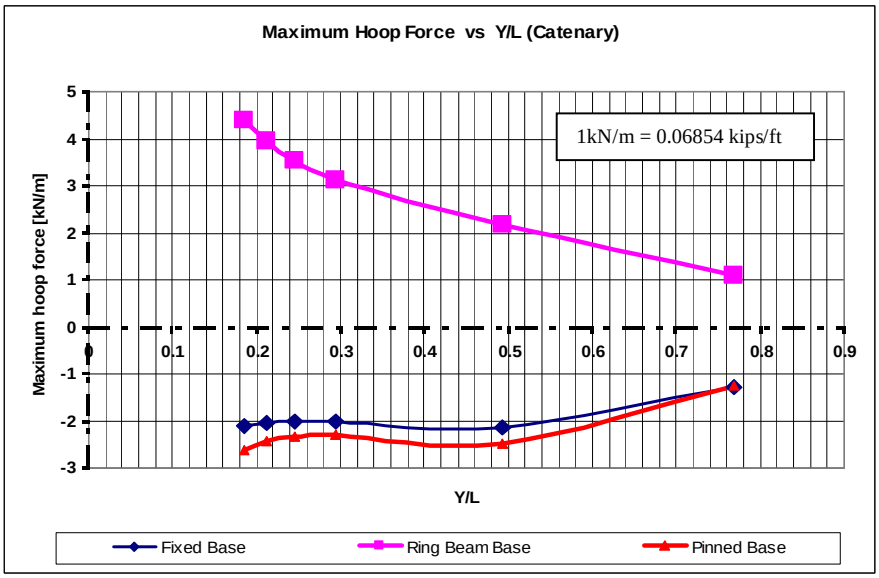

Figure 2.15 – Graph of Maximum Hoop Force vs. Y/L - Catenary

As seen in figure 2.15, the difference between the maximum hoop forces with a pinned base and a fixed base are very small, especially with higher values of Y/L. When a ring beam is used the hoop forces and moments increase considerably.

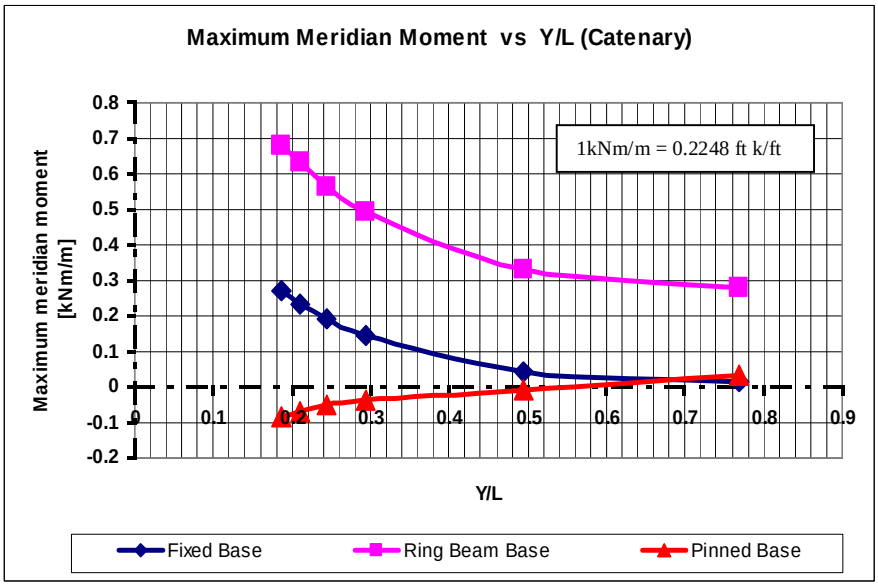

Figure 2.16 – Graph of Maximum Meridian Moments vs. Y/L - Catenary

The results show that as the height of the catenary decreases the base moments and the hoop tension forces increase. The Y = 4.92m (16.1 ft) catenary shape yields the best results for this criterion. This would be a reasonable shape from ground level (option (A)). Reasonably sized shapes for structure type (C) are the Y = 1.88m (6.2 ft) or y = 1.57m (5.1 ft) catenaries.

The Tension Region

The tensile stresses in the best catenary shape (Y/L = 0.77) are shown in figures 2.17 and 2.18.

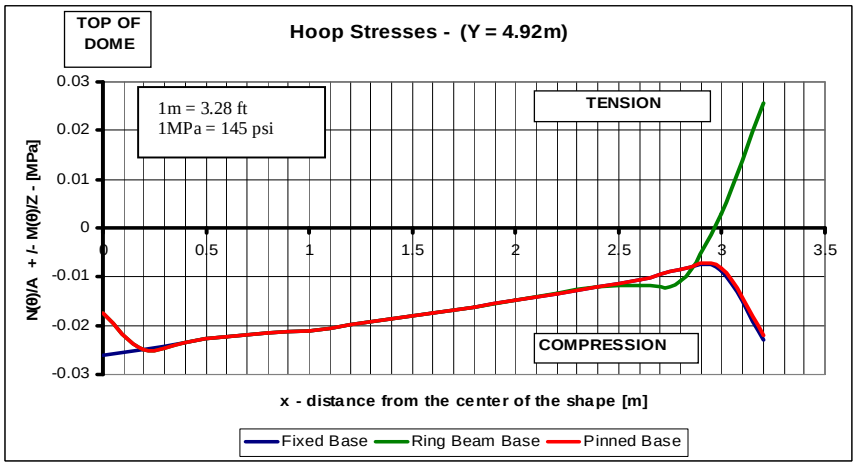

Figure 2.17 – Graph of Hoop Stresses – Catenary Y = 4.92m (16.1 ft)

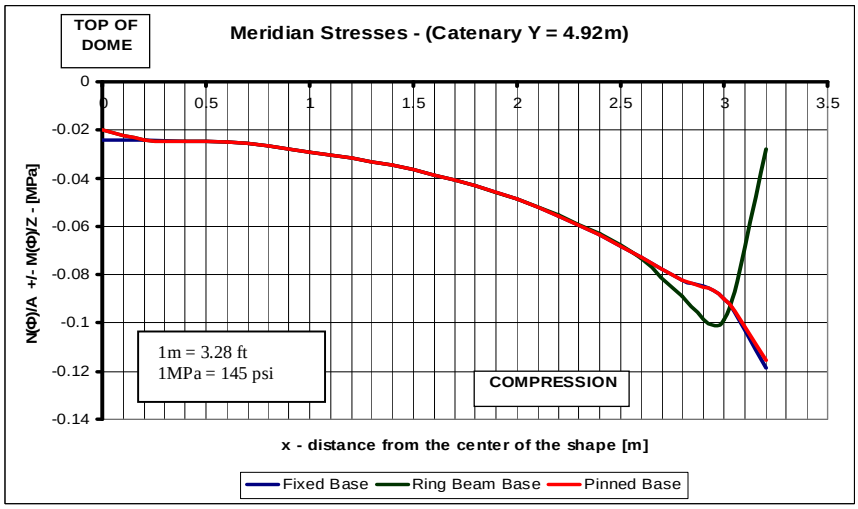

Figure 2.18 – Graph of Meridian Stresses – Catenary Y = 4.92m (16.1 ft)

The graphs shown on the previous page illustrate the effectiveness of the catenary shape under loading. In the meridian direction the entire structure is in compression. In the hoop direction, a very small portion of the structure is in tension when a ring beam is used.

Kicking Out Forces

These values were obtained from the fixed base analysis of the structure (refer to figure 2.12 for definition of the variables).

Height [m]	RF1 (kN/m)	RF2 (kN/m)
	Horizontal Reaction	Vertical Reaction
(Y = 4.92 m) (16.1 ft)	4.07 (0.28 kip/ft)	15.80 (1.08 kip/ft)
(Y = 3.16 m) (10.4 ft)	4.63 (0.32 kip/ft)	11.16 (0.76 kip/ft)
(Y = 1.88 m) (6.2 ft)	5.95 (0.41 kip/ft)	8.37 (0.57 kip/ft)
(Y = 1.57 m) (5.1 ft)	6.63 (0.45 kip/ft)	7.83 (0.54 kip/ft)
(Y = 1.35 m) (4.4 ft)	7.32 (0.50 kip/ft)	7.49 (0.51 kip/ft)
(Y = 1.19 m) (3.9 ft)	8.00 (0.55 kip/ft)	7.26 (0.5 kip/ft)

Table 2.1– Fixed Base Reaction Forces – Catenary

It can be seen from table 2.1, the kicking out force (RF1) increases as the catenary's height decreases. As the height of the catenary decreases the shape becomes shallower and the direction of N'(φ) tends closer to the horizontal, which increases the horizontal thrusts. Therefore, the shallower shapes require a ring beam with a greater amount of reinforcing to resist the kicking out forces at the dome base.

The Best Shapes

From the results, it can be seen that the higher the catenary the smaller the kicking out forces, moments and tensile stresses in the structure. This poses a problem as a reasonable height of structure should be chosen for constructability reasons. This is why a maximum value of Y/L = 0.4 is chosen for Type C domes.

From the previous analysis, the following optimum Y/L ratios are suggested:

Structure Type (A) – Y/L > 0.5

Structure Type (C) – Y/L < 0.4

2.6.2 Sections through the Hemisphere

The equation for a circle can be used to define the shape of a hemisphere. Once the shape is defined, sections can be taken through hemispheres with different radii. The equation for a circle is:

$$x^2 + y^2 = r^2 \quad (2.21)$$

where, r is the radius of the circle and x and y are the Cartesian coordinates.

The width of the shape was set at 6.4m (21 ft). Five different shaped hemispheres were investigated: r = 3.2m (10.5 ft), r = 3.5m (11.5 ft), r = 4m (13.1 ft), r = 4.5m (14.8 ft) & r = 5m (16.4ft).

Maximum & Minimum Forces & Moments

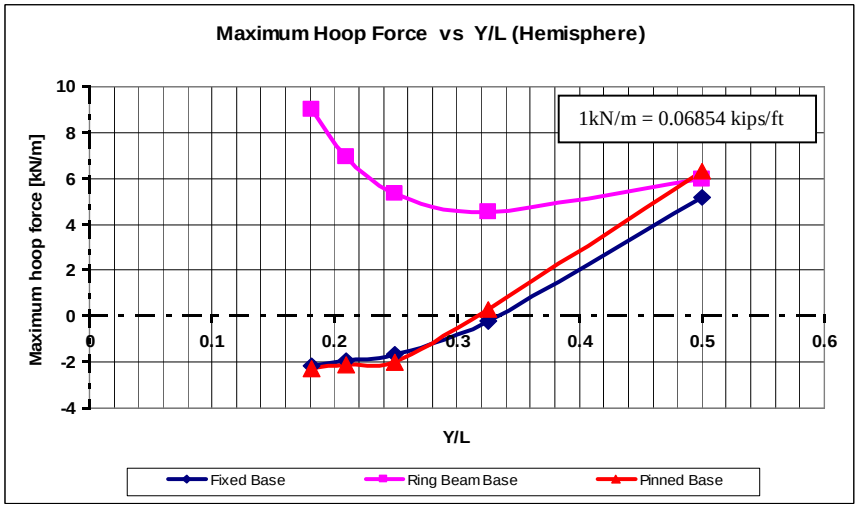

Figure 2.19 – Graph of Maximum Hoop Force vs. Y/L – Hemisphere

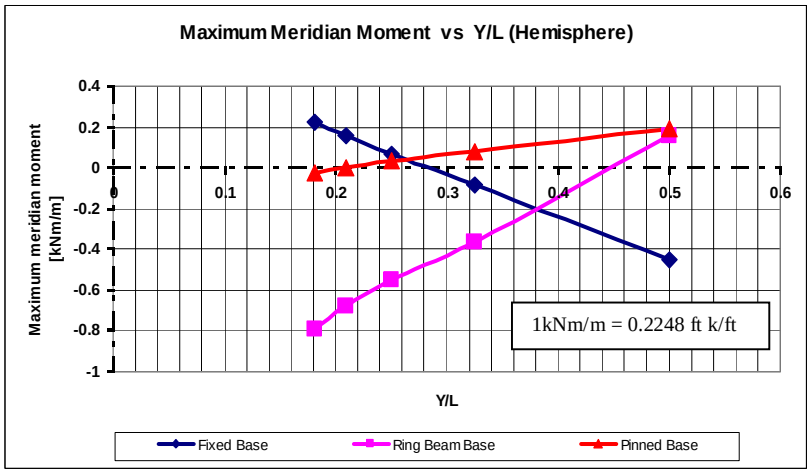

Figure 2.20 – Graph of Maximum Meridian Moments vs. Y/L – Hemisphere

For pinned and fixed base analyses the results show that an optimum range exists where the maximum hoop forces and meridian moments are minimal. This range can be seen to be between Y/L = 0.24 and 0.32. The inclusion of a ring beam increases both the hoop forces and meridian moments. When a full hemisphere is placed on a ring beam, the hemisphere behaves as if it is pinned at its base (this is in accordance with classical dome/ring theory).

The Tension Region

The tensile stresses in the best sectioned shape (Y/L = 0.32) are shown below.

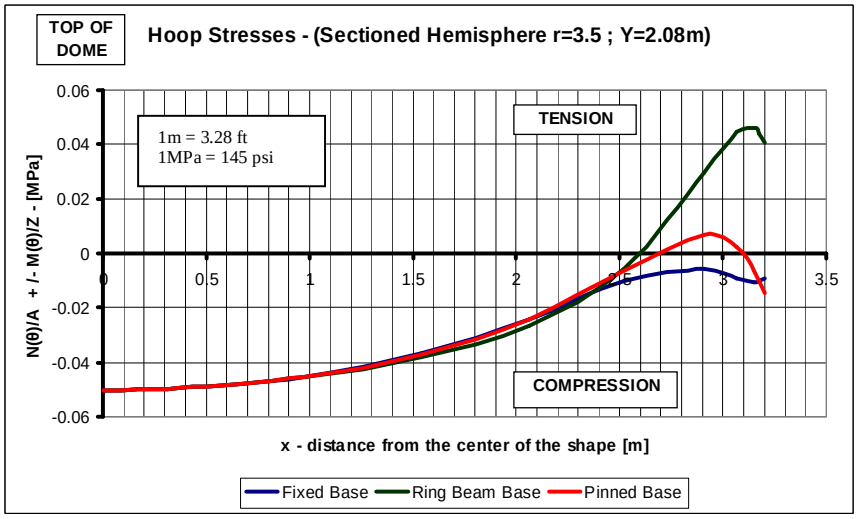

Figure 2.21 – Graph of Hoop Stresses – Sectioned Hemisphere r = 3.5

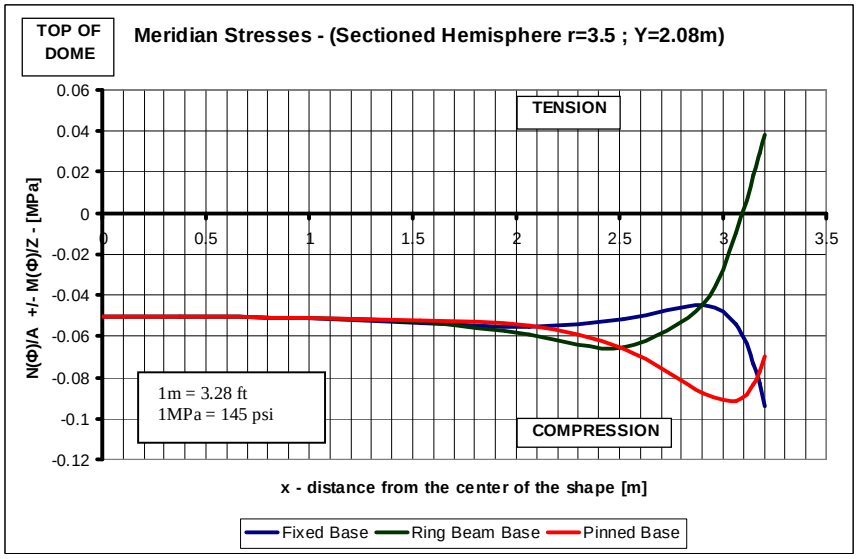

Figure 2.22 – Graph of Meridian Stresses – Sectioned Hemisphere r = 3.5

The hemispherical shape can be sectioned in such a way as to minimize the tension that exists in the structure. The above shape has a Y/L ratio of 0.32 which is in the range mentioned in the previous section. With a fixed base there is no hoop tension in the structure. When the base is pinned there is a small amount of tension in the hoop direction. When a ring beam is placed at the base, tension occurs in the lower part of the structure.

Kicking Out Forces

r Value	RF1 (kN/m)	RF2 (kN/m)	N'(Φ) (kN/m)
	Horizontal Reaction	Vertical Reaction	
3.2	2.11 (0.14 kip/ft)	12.86 (0.88 kip/ft)	12.86 (0.88 kip/ft)
3.5	4.58 (0.31 kip/ft)	8.89 (0.61 kip/ft)	9.73 (0.67 kip/ft)
4	6.06 (0.42 kip/ft)	8.00 (0.55 kip/ft)	10.00 (0.69 kip/ft)
4.5	7.34 (0.50 kip/ft)	7.73 (0.53 kip/ft)	10.85 (0.74 kip/ft)
5	8.68 (0.59 kip/ft)	7.63 (0.52 kip/ft)	11.91 (0.82 kip/ft)

Table 2.2– Fixed Base Reaction Forces – Sectioned Hemisphere
Refer to Figure 2.12 for the definition of the above variables.

Table 2.2 shows that the flatter the dome the greater the kicking out forces (RF1). This is because the component of the meridian membrane force in the

horizontal direction increases as the shape becomes shallower. The RF1 value for the full hemisphere is equal to the shear force at the base. This shows that even if the dome meets the wall vertically, there will always be a small amount of kicking out at the intersection of the wall and the dome. A ring beam may not be needed in the case of a full hemisphere as the wall will most probably be able to withstand the small outward shear force. This can be seen in section 2.7 for structure type (B).

The Best Shapes

The sectioned hemisphere has an optimum range where the membrane forces, moments and shears in the shape are at their least. However, this range yields shallow shapes (in this project as L = 6.4 m (21 ft)) that can only be used if a cylinder wall is placed below the dome. Therefore, a full hemisphere is recommended from ground level from a useable space point of view.

Structure Type (A) – Y/L = 0.5 (Hemisphere)
Structure Type (C) – 0.24< Y/L < 0.32

2.6.3 Sections through the Parabola

Six different parabolas were investigated. The variable that was changed in order to obtain the different shapes was the height of the parabola y.
The equation of the parabola is:

$$x^2 = 4Ay \qquad (2.22)$$

Where x and y are the Cartesian coordinates of the parabola.

The six parabolas investigated were limited to a base width of 6.4m and their heights were y = 1.2 (3.94 ft), y = 1.6m (5.25 ft), y = 2m (6.56 ft), y =3.2m (10.50 ft), y = 6m (19.68 ft) and y =8m (26.24 ft).

Maximum & Minimum Forces & Moments

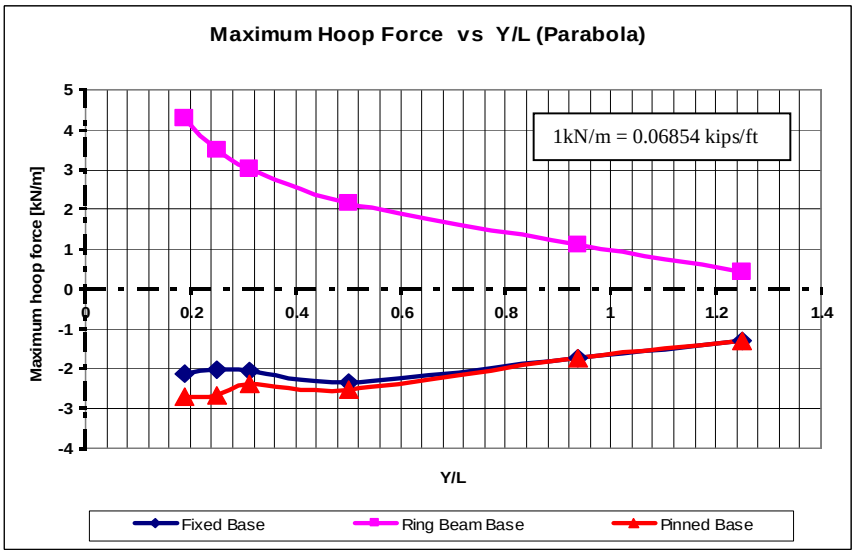

Figure 2.23 – Graph of Maximum Hoop Force vs. Y/L – Parabola

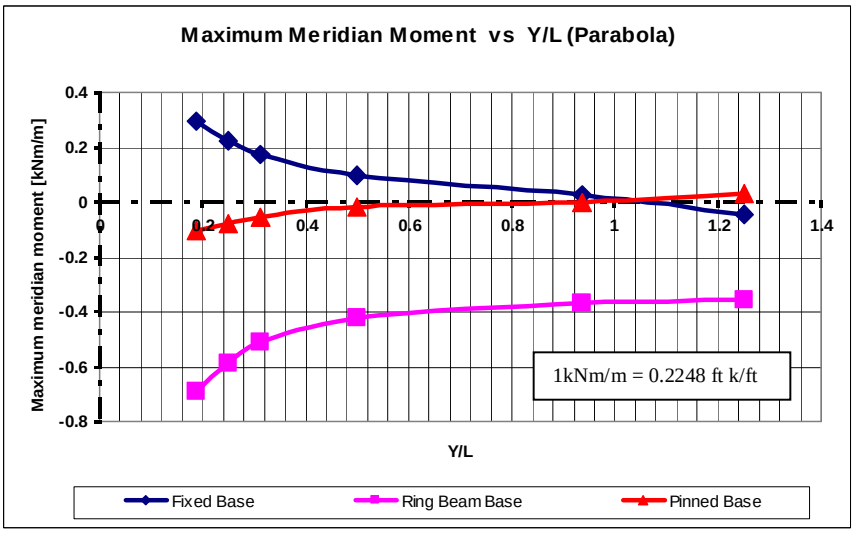

Figure 2.24 – Graph of Maximum Meridian Moment vs. Y/L – Parabola

The parabola shape makes a very efficient shell structure. The hoop forces when a pinned or fixed base is used are always compressive. The inclusion of a ring beam increases the hoop forces and meridian moments as in the previous shapes. An efficient range where hoop forces and meridian moments are at a minimum exists where $0.8 < Y/L < 1.2$. This range corresponds to a height of

between 5 (16.4 ft) and 8 meters (26.2 ft). It is interesting to note that the Musgum tribe of Central Africa built parabolic mud huts (figure 1.4) within the same height range.

The Tension Region

The tensile stresses in the best parabolic shape (Y/L = 1.2) are presented below.

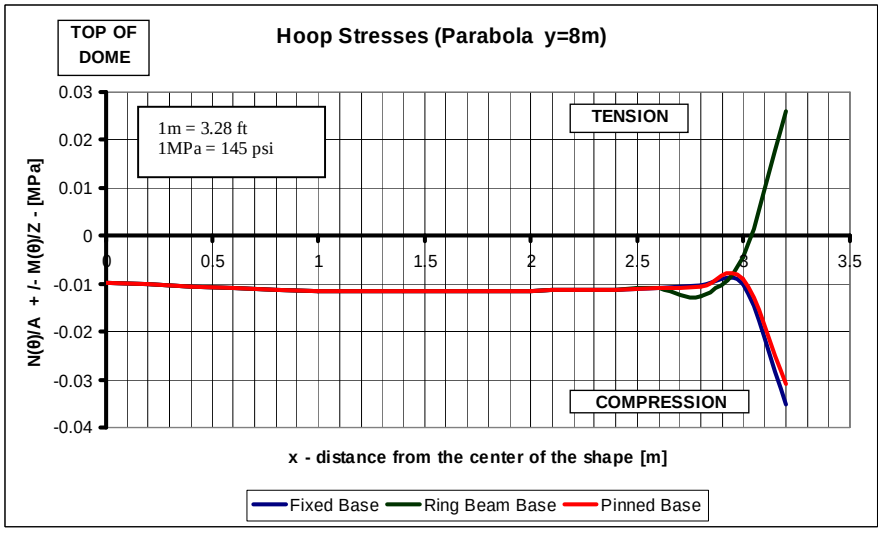

Figure 2.25 – Graph of Hoop Stresses – Parabola (y = 8m; 26.2 ft)

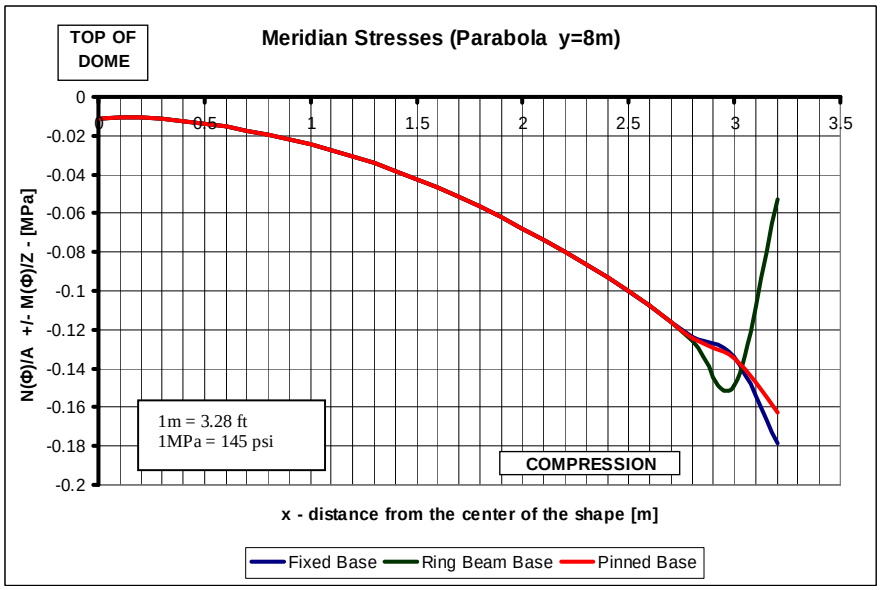

Figure 2.26 – Graph of Meridian Stresses – Parabola (y = 8m; 26.2 ft)

Once again, it can be seen that the inclusion of a ring beam produces a small degree of tension in the hoop direction of the structure. Otherwise, the entire structure is in compression. This was beneficial to the Musgums as their building material was compacted mud, which has almost no tensile strength.

Kicking Out Forces

y Value	RF1 (kN/m)	RF2 (kN/m)
	Horizontal Reaction	Vertical Reaction
1.2	8.04 (0.55 kip/ft)	7.26 (0.50 kip/ft)
1.6	6.73 (0.46 kip/ft)	7.83 (0.54 kip/ft))
2	6.00 (0.41 kip/ft)	8.51 (0.58 kip/ft)
3.2	5.10 (0.35 kip/ft)	10.90 (0.75 kip/ft)
6	4.81 (0.33 kip/ft))	17.50 (1.20 kip/ft)
8	4.90 (0.34 kip/ft)	22.54 (1.54 kip/ft)

Table 2.3 – Parabola – Fixed Base Reaction Forces
Refer to Figure 2.12 for the definition of the above variables.

The values of the kicking out forces for parabolas are very similar to the values presented for the catenary shape. This is expected, as the two shapes are very similar.

The Best Shapes

An optimum range for parabolic shaped shell structures is $0.8 < Y/L < 1.2$. This range produces very high structures which would only be viable if built from ground level (structure type A). For structure type C, the parabola is not recommended.

2.6.4 The Ellipse

The advantage of an elliptical shape is that the roof will meet the wall vertically, and therefore the meridian membrane force is transmitted vertically into the wall. The only contribution to the kicking out force will be the shear in the section and a ring beam may not be required for structure types (A) and (B). However, an elliptical roof is very flat at the top and causes difficulties in the construction of this shape. Three different ellipses were investigated. The variable that was changed in order to obtain the different shapes was the height of the ellipse, B.

The equation of the ellipse is:

$$(\frac{x^2}{H^2}) + (\frac{y^2}{B^2}) = 1 \quad (2.23)$$

Where x and y are the Cartesian coordinates of the ellipse. B is the height along the minor axis and H the height along the major axis.

The four ellipses investigated were limited to a base width of 6.4m (21 ft) and their heights were B = 1.6m (5.25 ft), B = 1.8m (5.90 ft), B =2m (6.56 ft) and B=3.2m (10.50 ft) (hemisphere).

Maximum & Minimum Forces & Moments

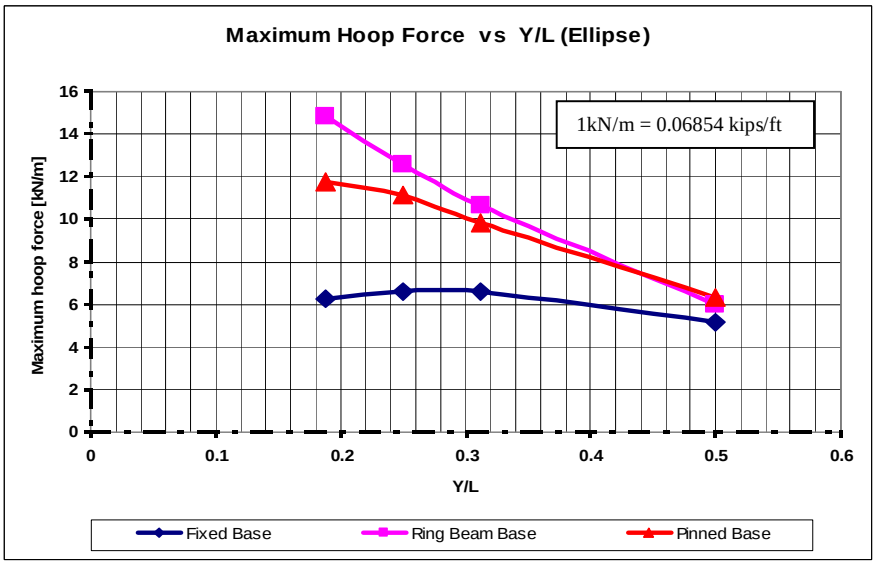

Figure 2.27 – Graph of Maximum Hoop Force vs. Y/L – Ellipse

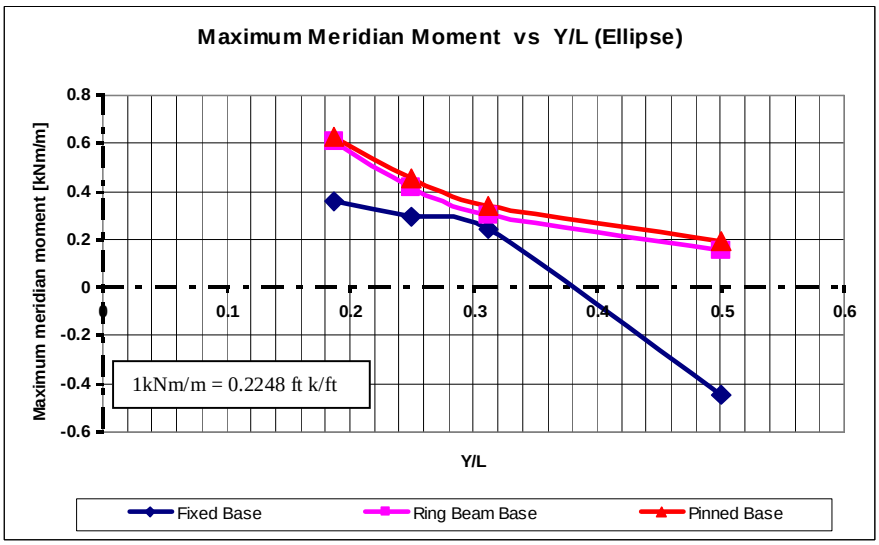

Figure 2.28 – Maximum Meridian Moment vs. Y/L – Ellipse

Figure 2.27 and figure 2.28 show that as the height of the ellipse increases the forces and moments in the ellipse decrease. The B = 3.2m (10.5 ft) ellipse (hemisphere) is the best alternative for this criterion. A considerable amount of hoop tension exists at the base of an ellipse. This is undesirable for shell structures.

Tension Region (Stresses)

The tensile stresses in the best elliptical shape (Y/L = 0.5) are presented below.

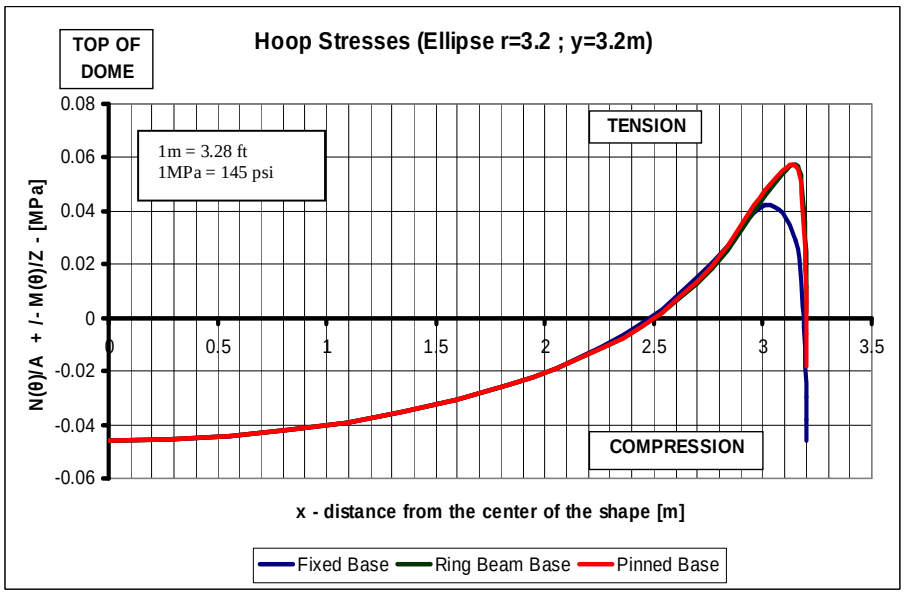

Figure 2.29 – Graph of Hoop Stresses – Ellipse (B = 3.2m; Y = 3.2m)

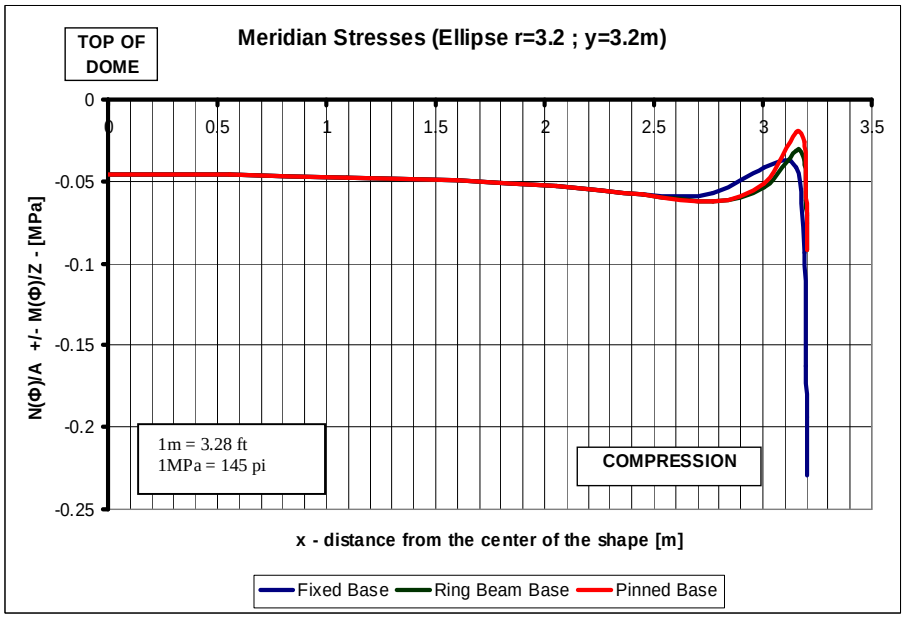

Figure 2.30 – Graph of Meridian Stresses – Ellipse (B = 3.2m; Y = 3.2m)

Kicking Out Forces

y Value	RF1 (kN/m)	RF2 (kN/m)
	Horizontal Reaction	Vertical Reaction
1.2	6.28 (0.43 kip/ft)	8.01 (0.55 kip/ft)
1.6	4.37 (0.30 kip/ft)	8.86 (0.61 kip/ft)
2	3.32 (0.23 kip/ft)	9.78 (0.67 kip/ft)
3.2	2.11 (0.14 kip/ft))	12.86 (0.88 kip/ft)

Table 2.4– Fixed Base Reaction Forces – Ellipse
Refer to Figure 2.12 for the definition of the above variables.

The kicking out force for the ellipse structure is the same magnitude as the shear force at the base of the ellipse. The above results show that as the ellipse approaches the shape of the hemisphere the kicking out force reduces.

The Best Shapes

The ellipse is a very inefficient shape and it is not recommended. The most efficient ellipse is the hemisphere, which is a suitable structure for structure type A.

2.7 Shape Analysis Results (Structure Type B)

The shapes investigated in this section were placed on top of a 1m high cylindrical wall in order to improve useable space within the structure. No ring beam was included in this analysis as the wall was assumed to resist the lateral thrust of the dome. The overall height of the structure was limited to approximately four meters and the diameter to 6.4m (21 ft). The hoop force and meridian moment diagrams are presented on the next page.

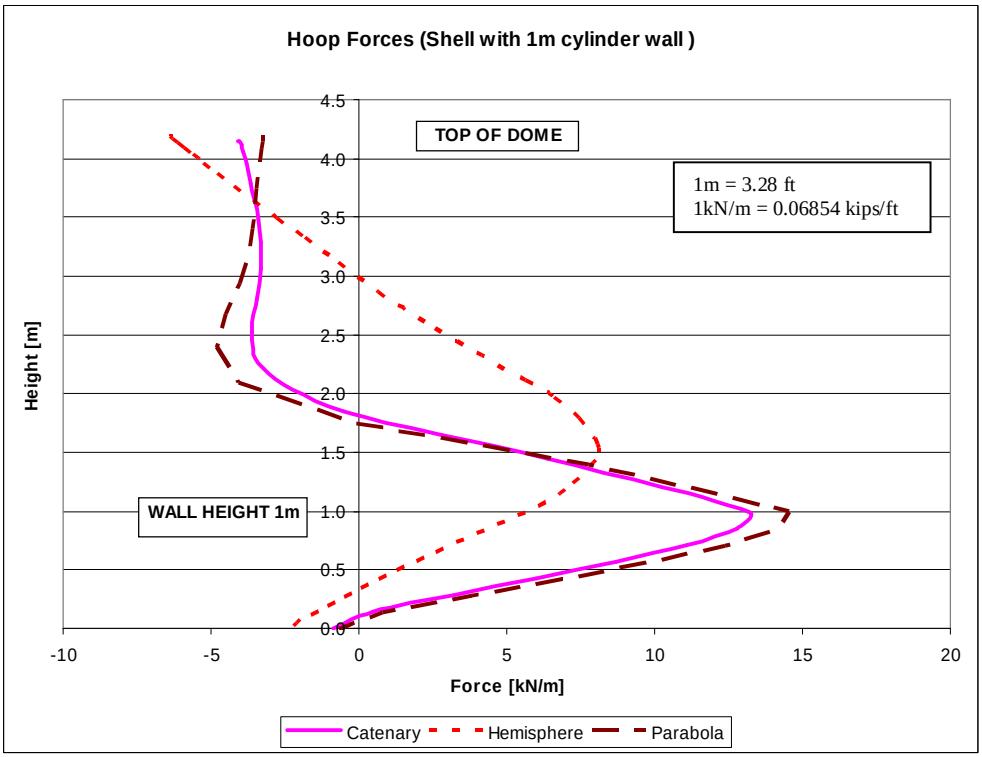

Figure 2.31 – Graph of N(θ) – Shells with 1m Cylinder Walls – Structure Type B

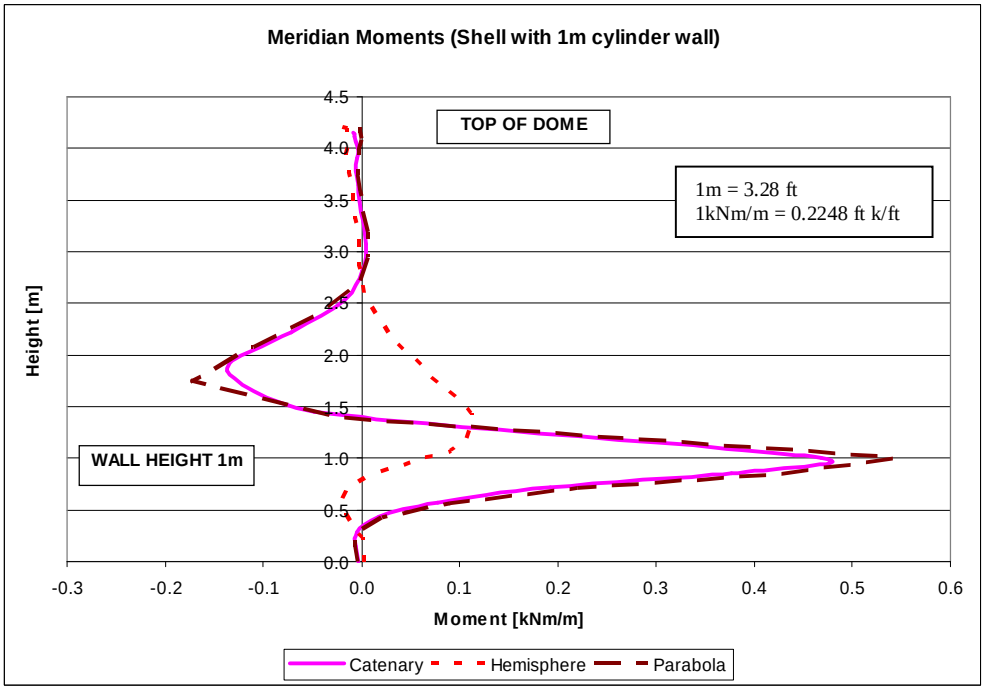

Figure 2.32 – Graph of M(φ) – Shells with 1m Cylinder Walls – Structure Type B

From figure 2.31 and 2.32 it can be seen that the hemisphere placed on top of a cylinder wall is the best option for structure type B. The kicking out force is the least for the hemisphere option and it has the most useable space within the structure. It can be concluded that the best shape that can be placed on a cylinder wall is one that meets the wall vertically (or near vertically). This is because there is no component of the meridian membrane force in the horizontal direction at the dome/cylinder wall interface, which would kick out the cylinder wall causing tension in the structure. This is the same argument as that presented in section 2.6.2 (Kicking out Forces). However, a shear force and a moment still exist at this interface and this produces some outward movement of the wall. Therefore the moments and hoop forces obtained from this analysis are greater than the results obtained in an analysis of a hemisphere pinned at its base. The problems with this type of structure are:

- The hoop forces and meridian moments are much larger than a shell from ground level.
- The maximum forces and moments occur in regions where door and window openings will be placed in the structure. These openings will increase the stresses in the structure further.

2.8 Summary of the Results

2.8.1 Tabulated Summary

This section summarizes the results of the best performing structures. It also compares the useable space within the selected optimum structures. The parameters used in measuring the useable space within the structure are shown in figure 2.33, overleaf.

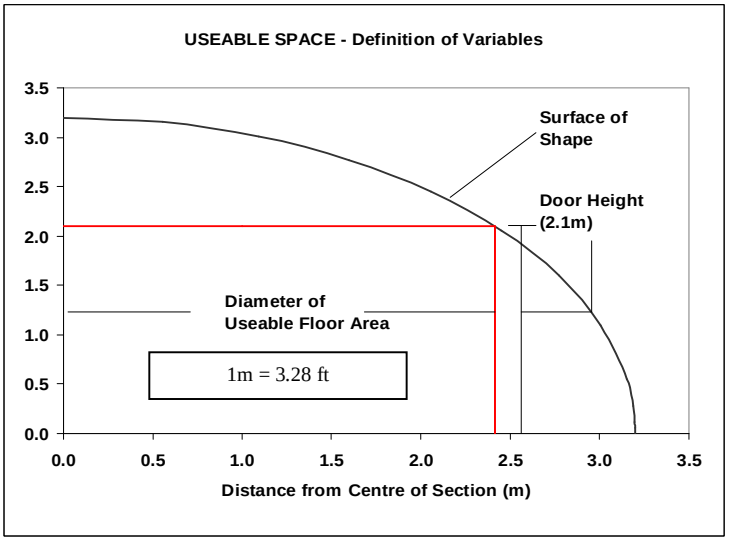

Figure 2.33 – Useable Space Parameters

Shape Evaluation Criteria	Units	Structure {A}			Structure {B}	Structure {C}
		(i) Dome from ground level (pinned base)			(ii) Hemisphere on 1m wall (pinned base)	(iii) Sectioned Hemisphere (r = 3.5) on a ring beam
		Catenary	Hemisphere	Parabola		
		a = 1.5	r = 3.2	y = 8		
Y/L						
.1. Optimum Y/L Range	-	> 0.5	0.5	0.8<Y/L<1.2	-	0.24<Y/L<0.32
.2. Actual Y/L Value	-	0.77	0.5	1.2	-	0.32
Useable Space						
.3. Floor Area	m^2	32.2 (347 ft^2)	32.2 (347 ft^2)	32.2 (347 ft^2)	32.2 (347 ft^2)	32.2 (347 ft^2)
.4. Useable Floor Area	m^2	16.4 (177 ft^2)	18.3 (197 ft^2)	20.5 (221 ft^2)	28.4 (306 ft^2)	32.2 (347 ft^2)
.5. Waste (3-4)	m^2	15.8 (170 ft^2)	14.9 (160 ft^2)	11.7 (126 ft^2)	3.8 (41 ft^2)	0
Maximum Tensile Stresses						
.6. Hoop Stresses	MPa	N/A	0.1 (0.015 ksi)	N/A	0.122 (17.7 psi)	0.046 (6.7 psi)
.7. Meridian Stresses	MPa	N/A	N/A	N/A	0.064 (9.3 psi)	0.038 (5.5 psi)
.8. Tension Region Size	-	None	Medium	None	Large	Small
Constructability						
.9. Overall Height	m	4.92 (16.1 ft)	3.2 (10.5 ft)	8 (26.2 ft)	4.2 (13.8 ft)	4.5 (14.8 ft)

Table 2.5 – Summary of the Best Shapes

2.8.2 Summary Discussion

In table 2.5 the best shapes for the given size of structure are summarized. General values for optimum Y/L ratios for the various shapes are also given. These Y/L ratios may yield the most efficient shapes structurally, but issues such as constructability and cost dictated the final shape of the structure to a greater degree. The catenary was shown to be the best structure for structure type A, the hemisphere for structure type B and the dome (sectioned hemisphere) for structure type C.

Structure (A) (catenary) was the best shape structurally. It was completely in compression when loaded. The problem with this shape is the amount of useable space within it. The curved walls from ground level limit the useable floor space within the structure. This structure had the most wasted space.

Structure (B) (hemisphere on 1m wall) had the largest tension region in the hoop direction of all the shapes. This was the structure that was chosen for construction as it provided a fair amount of useable space and its construction proved to be simpler and more cost efficient than the other options (see chapter 6). However, it is important to note that this structure was the worst with regard to structural performance (tension in the shell).

Structure (C) provided the most useable space of all the structures. It had a small tension region at its base which could easily be reinforced with bars tied into the ring beam. This structure was designed alongside structure B but proved to be more expensive to construct.

3. Materials Investigation

This section provided the necessary material properties for the design of the low-cost dome home. There are many materials that contribute to the construction of any structure and it is important that we understand their engineering properties fully. The materials investigated for the low-cost dome home included HydraForm cement stabilized earth blocks, fibre reinforced structural plaster, wire mesh reinforcement, Brickforce and Damp Proof Course (DPC). Two methods of investigation were adopted in this section. The first was a literature survey which provided the material properties of the HydraForm blocks. The second method of investigation was laboratory testing of the materials, which provided information on the tension resistance of the fibre plaster, the yield strength of the wire reinforcing (Brickforce, hard drawn wire and chicken wire mesh) and the frictional properties of the DPC's (important for stability and base fixity).

3.1 Literature Investigation

3.1.1 Cement Stabilized Earth Blocks (CEB's)

A 7MPa (1 015 psi) HydraForm Splitter Block was specified to be used in the walls and dome roof of the structure. The dimensions of these blocks were 75mm (2.95 in.) high by 110mm (4.33 in.) thick by 220mm (8.66 in.) long.

Manufacturing Process

The HydraForm Training Manual (2004) explains the procedures used to create compressed earth blocks (CEB). CEB's are made by mixing soil and cement in predetermined ratios. This mix is placed into a press and a brick is extruded vertically under a distributed pressure of 10 MPa (1 450 psi) using a diesel driven, hydraulic block making machine. The blocks are then cured for approximately 72 hours (Agremènt, 1996). According to Uzoegbo (2003) the

blocks achieve about 80% of their 28 day compressive strength in this time. Table 3.1 shows the basic soil requirements for the CEB's production.

NOMINAL COMPRESSIVE STRENGTH (MPA)	% BY MASS PASSING THE 0.075MM SIEVE		PLASTICITY INDEX (MAXIMUM)	CEMENT CONTENT (%) (CEM II/A-M 42.5)
	Min	Max		
4 (580 psi)	10	35	15	4-7
7 (1 015 psi)	10	25	10	7-10
20 (2 900 psi)	10	25	10	15-20

Table 3.1 – Basic Soil Requirements for CEB Production (Uzoegbo, 2003)

Properties

Many tests have been done at The University of the Witwatersrand on the HydraForm blocks to determine their material properties. Table 3.2 shows the results of the tests done by Magaia (2003) and R. Fernandez (2003). The final column of table 3.2 shows the recommended design values of CEB's from Houben and Guillaud (1994).

PROPERTY	S.J. MAGAIA	R. FERNANDEZ	HYDRAFORM PUBLICATIONS	HOUBEN & GUILLAUD
Density (kg/m^3)	1 900 (119 lb/ft^3)	1 950 (122 lb/ft^3)		1 700-2200 (106-137lb/ft^3)
Poisson's ratio	0.2			0.15 - 0.35
Young's Modulus (MPa)	3 500 (508 ksi)	12 400(dynamic) (1798 ksi)		700 - 7 000 (102-1015ksi)
Dry Compressive Strength (MPa)	5.4 (783 psi)	5 (730 psi)	4—7 (580-1 015 psi)	5—12 (730-1 740psi)
28 Day Tensile Strength (MPa)	1.4 (200 psi)	1.18 (170 psi)		1—2 (150-290 psi)
28 Day Bending Test (MPa)		1.02 (150 psi)		1—2 (150-290 psi)
28 Day Shear Test (MPa)				1—2 (150-290 psi)
Coefficient of thermal expansion (mm/m°C)				0.010 - 0.015

Table 3.2 – Properties of Cement Stabilized Earth Blocks

The 28 day tensile strength values in table 3.2 indicate that the blocks have a very small tensile strength. The compressive strength of the blocks is comparable to the strength of normal masonry units (e.g. stock bricks). These properties suite dome construction as the stresses within the structure are very small, and are generally compressive.

3.2 Laboratory Testing

3.2.1 Fibre Reinforced Plaster Tests

Fibre plaster was used as a structural element on the dome built by Magaia (2003). It was used to resist the tension stresses induced in the dome, and it was placed on the inside and outside surfaces of the dome. The fibres used in Magaia's plaster were sisal fibres, which over time may deteriorate due to moisture ingress and may loose their strength. The test work done in this section was aimed at determining the compressive and tensile resistances of the fibre plaster using galvanized steel fibres, in order to assess whether the plaster would be an effective structural element for the dome.

A Brief Overview of Fibre Reinforced Concrete Theory (Addis, 2001)
Fibre reinforced concrete (FRC) is defined as a composite material made with hydraulic cement, aggregates of various sizes and discrete discontinuous fibres. There are two types of fibres that can be used in FRC. The first types of fibre are low-modulus, high-elongation fibres. These include nylon and polyethylene. These fibres are capable of absorbing large amounts of energy and are used to control cracking in plastic concrete. They do not improve the strength of the concrete. The second types of fibre are high-strength, high-modulus fibres. These include steel, glass and asbestos. These fibres add strength and stiffness to the concrete.

In order to improve the strength of the concrete (plaster in this case) there are a few rules that need to be followed with regard to the choice of fibre. These are (Addis, 2001):

- Fibres should be stiffer than the matrix
- Fibre content by volume must be adequate
- There must be a good fibre-matrix bond
- Fibre length must be sufficient for anchorage
- Fibres must have a high aspect ratio (i.e. long and thin)

It is important to note that in order to achieve composite properties the volume concentration of fibres needs to be quite high. The typical recommendation for steel fibres is that the volume concentration should be more than 1%. The law of mixtures (as stated in equation 3.1) shows that as the volume concentration becomes less than this value the fibres will have no significant effect on strength or the elastic modulus of the FRC. The equation for the law of mixtures is (Addis, 2001):

$$\sigma_c = (E_f V_f + E_m V_m)\varepsilon_c \qquad (3.1)$$

Where:

E_f, E_m = Young's modulus of fibre and matrix

V_f, V_m = Volume fraction of fibre and matrix

ε_c = Strain in composite

σ_c = Stress in composite

Figure 3.1, overleaf, shows the importance of the fibre volume with regard to tensile strength gain.

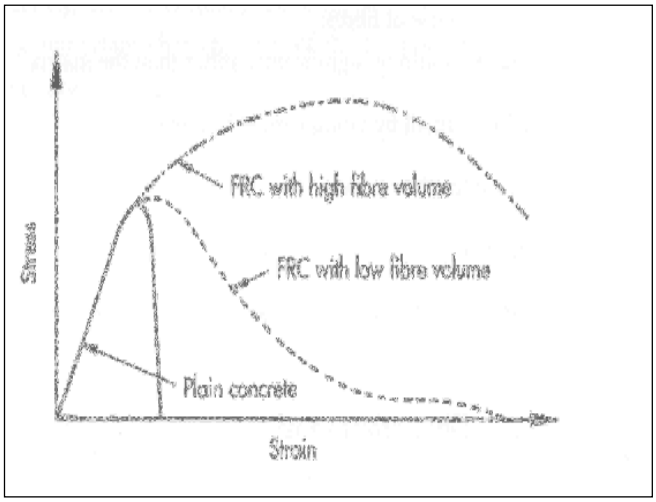

Figure 3.1 – Stress-strain behavior of FRC (Fulton 2001:253)

Materials Tested

For this investigation crimped steel fibres 0.6mm (0.024 in.) in diameter and 25mm (1 in.) long were used. These fibres were set into a mortar of designation (ii), according to SABS 0164 Part 1(1980) and BS 5628 Part 2 (2000). As discussed in the introductory chapters, it is important to avoid strong cement plasters. These are very brittle in comparison to the wall or dome and can crack allowing moisture ingress. The choice of a mortar of designation (ii) was based on the mean 28 day compressive test results presented in SABS 0164 Part1- Table1 (1980) and BS 5628 Part2 – Table1 (2000). Table 3.3 presents these results:

Mortar class	Compressive strength at 28d, MPa, min	
	Laboratory tests	Site tests
(i)	14.5 (2 103 psi)	10 (1 450 psi)
(ii)	7 (1 015 psi)	5 (725 psi)
(iii)	2 (290 psi)	1.5 (218 psi)

Table 3.3 – Mortar Compressive Strengths (SABS 0164: Part 1 Table 1)

Generally a plaster mix with a greater amount of sand, and a lesser strength would be used as the external render layer (Kohler, 1982). However, too weak

a plaster must be avoided if it is to be used as a structural unit. The table above shows that a class (ii) mortar is a similar strength to the 7MPa (1 015 psi) HydraForm building blocks.

Tension and compression tests were performed on structural plaster samples containing 20kg/m^3 (1.25 lb/ ft^3) and 40kg/m^3 (2.50 lb/ft^3) of steel fibres.

Compression Test

The aim of the compression test was to determine the effect of the fibres on the compressive strength of the plaster. The compression tests were done using a Tinnius-Ohlsen press. The specimens tested were 100mm (3.94 in.) cubes. According to Addis (2001), three cubes for each sample taken need to be tested and the results of each test should be within 15% of the average result. In order to obtain a valid compressive strength six cubes were tested at 28 days to obtain the 28 day compressive strength. The results are presented in table 3.4.

Amount of fibre	Days	Stress
		(MPa)
20kg/m^3 (1.18% by volume) (1.25 lb/ ft^3)	28.00	10.24 (1 480 psi)
	28.00	9.87 (1 430 psi)
	28.00	10.24 (1 480 psi)
Average	28.00	**10.12 (1 460 psi)**
40kg/m^3 (2.35% by volume) (2.50 lb/ft^3)	28.00	9.30 (1 350 psi)
	28.00	9.53 (1 380 psi)
	28.00	9.45 (1 370 psi)
Average	28.00	**9.43 (1 370 psi)**

Table 3.4 – Compressive Strength Tests Results

If we compare these results to the compressive strength of class (ii) mortar in SABS 0164 (1980) (7MPa (1 015 psi) in laboratory testing), we can see that there is an improvement in strength when using fibres in the plaster mix. This result, as well as the fact that by introducing too many fibres the mix may decrease in compressive strength, was observed in the test work done by Magaia (2003). It was also observed that the compressed cubes did not fail in

the usual hourglass shape. This suggests that the tensile stresses induced in the cube at ninety degrees to the compressive force (Poisson's effect) are resisted to some extent by the fibres.

Tension Test

The main reason for using a structural plaster is to resist tension stresses in the structure. The tensile strength of concrete is not normally tested by placing specimens in direct tension. Instead, specimens are tested in flexure (bending) or by splitting (Addis, 1998). However, the tests performed on the fibre plaster were axial tension tests. I- shaped specimens were used for the testing. The specimens consisted of prismatic elements 300mm (11.8 in.) long, with cross sections of 100 X 130mm (3.94 X 5.11 in.) at both ends, and a reduced section of 60 X 100mm (2.36 X 3.94 in.) in the centre portion to ensure failure in this region. The specimens were placed into special clamps and an axial load was applied until failure. Using this type of axial test to determine the tensile resistance of the fibre plaster may not be the most ideal method. The test may under predict the tensile strength of the specimen due to a small amount of eccentricity of the loading, as well as badly distributed or clumped fibres. Every effort was made to ensure a concentric loading and a good distribution of fibres. The results of the tension tests are shown in table 3.5, overleaf.

Amount of fibre	Days	Loaded Mass (kg)	Force (kN)	Stress (MPa)
20kg/m^3 (1.18% by volume) (1.25 lb/ ft^3)	28.00	270.00	2.65	0.44 (64 psi)
	Specimen cracked before testing			
	Specimen cracked before testing			
Average	28.00	270.00	2.65	**0.44 (64 psi)**
40kg/m^3 (2.35% by volume) (1.50 lb/ft^3)	28.00	625.00	6.13	1.02 (148 psi)
	28.00	629.00	6.17	1.03 (149 psi)
	Specimen cracked before testing			
Average	28.00	627.00	6.15	**1.03 (149 psi)**

Table 3.5 – Tension Test Results – Fibre Plaster

The tensile strengths shown in table 3.3 are extremely small. In order to determine whether these results are reasonable, we would need to compare them to the tensile strength of an un-reinforced specimen. Unfortunately, these tests were not performed and so the un-reinforced tensile strength was approximated using empirical formulas (Addis, 1998). These formulas (equations 3.2 & 3.3) apply to concrete, and they relate tensile strength to compressive strength. It is important to note that there is no general relationship between compressive and tensile strength in concrete (Addis, 2001).

Flexural strength = 0.11 x compressive strength (3.2)

Splitting tensile strength = 0.07 x compressive strength (3.3)

Using an un-reinforced compressive strength of 7MPa (1 015 psi), equation 3.2 is equal to 0.77MPa (112 psi) and equation 3.3 is equal to 0.49MPa (71 psi). From these results we can see that the 20 kg/m^3 (1.25 lb/ ft^3) (fibre plaster mix showed no significant increase in tensile strength when compared to the un-reinforced splitting test empirical formula. Whereas the 40 kg/m^3 (1.50 lb/ft^3) mix showed an improvement over the splitting test empirical result by a factor of 2.1.

Possible Problems with Fibre Plaster

According to Professor Arnold Wilson of Brigham Young University, Utah (2005): 'In areas of calculated tension, rebar or wire mesh is much preferred over fibre reinforcement. Fibre reinforcement can experience a zipper effect. Once a crack is started it will continue to grow and develop because fibres offer only small resistance. When solid reinforcement (bar or mesh) is met by the crack it will usually stop'. For this reason the use of wire mesh was employed on the dome surface instead of fibre plaster.

3.2.2 Brickforce, Wire Wrapping & Wire Mesh Tests

Chicken wire mesh was used on the outside and inside of the dome to help resist temperature stresses (see chapter 4) and to aid in minimizing cracking of the plaster. Shrinkage of the cement plaster causes a build up of stresses in the material. These stresses cause the plaster to pull away from the wall. In the case of soft brickwork the shrinking plaster can sometimes damage the wall. Moisture movement in the wall worsens the effects of this type of cracking (Williams-Ellis, 1947). Therefore, it is important to use a low strength (low shrinkage) plaster and to reinforce the brickwork to prevent cracking.

Hard drawn wire was also used in the form of Brickforce[4] and wire wrapping (stitching) around the openings of the final structure (see chapter 6). This reinforcing was used to resist the high stresses around the window and door openings.

Uniaxial Tension Tests

Uniaxial tension tests were performed on the different wire elements in the structure in order to determine their yield strength. Figure 3.2 shows the parameters used to describe a typical stress-strain curve of a material.

[4] A wire ladder placed in the mortar between brick courses.

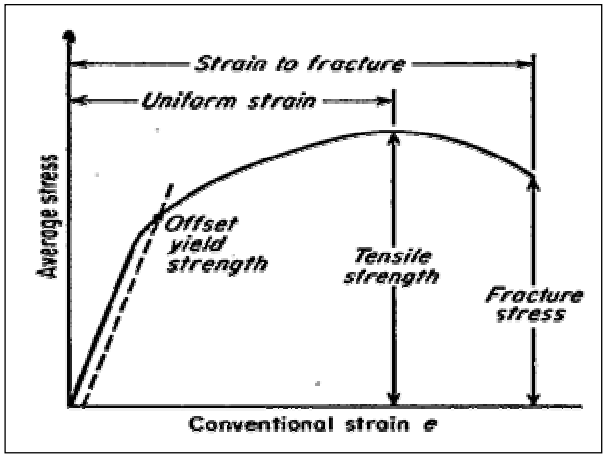

Figure 3.2 – Stress-Strain Curve Parameters

Certain materials do not show a specific yield point when uniaxial tension tests are performed on them. For this reason, a proof (or offset) stress is defined. This stress is determined by using a strain (e) of between 0.1 - 0.5%, as seen in figure 3.2. In these tests a strain of 0.1% was used in order to find the minimum yield strength of the material.

Brickforce & Hard Drawn Wire Wrapping Results

Brickforce consist of 2 hard drawn 2mm (0.08 in.) or 2.8mm (0.11 in.) diameter wires connected together at intervals by transverse welded wires the length of one or two brick courses. One of these wires (2.8mm (0.11 in.), actually 2.66mm (0.10 in.)) was tested using the uniaxial tension test. Three tests were performed and the graph of the minimum yield stress is presented below. The minimum 0.1% proof stress was found to be 500MPa (72.5 ksi).

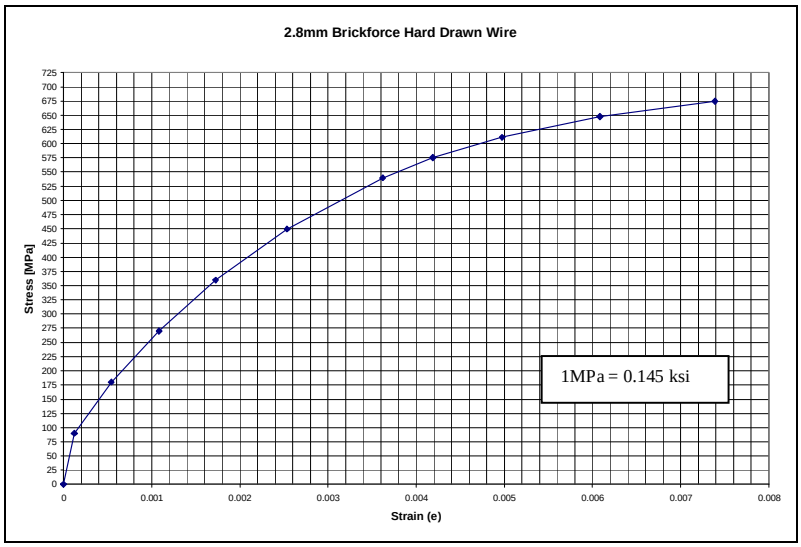

Figure 3.3 – Graph of Brickforce Yield Stress

The wire wrapping (brickwork stitching) was specified as 2mm (0.10 in.) hard drawn steel wire. The wire diameter was measured as 1.98mm (0.10 in.) and the minimum yield stress from three tests was found to be 490 MPa (71.1 ksi) (see graph 3.2). According to Allens-Meshco (steel wire manufacturers) the minimum yield strength for hard drawn wire can be taken as 485 MPa (70.3 ksi). This value is similar to the values obtained from the tests.

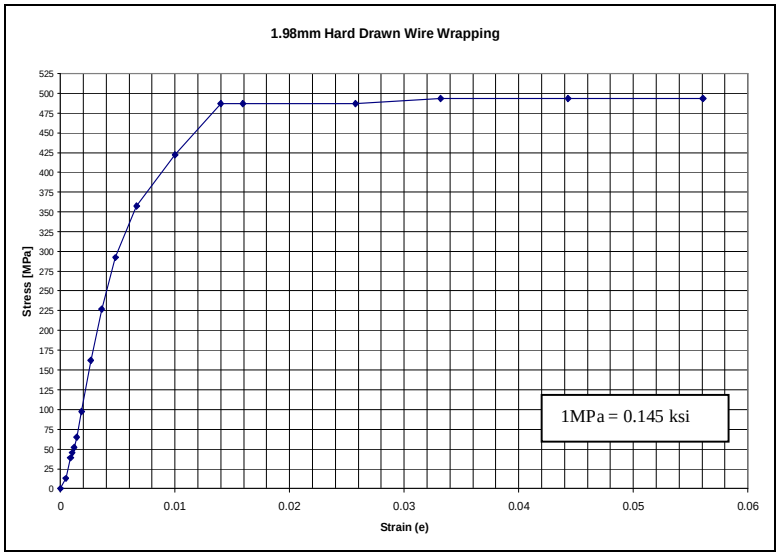

Figure 3.4 – Graph of Wire Wrapping Yield Stress

Chicken Mesh Results

The chicken wire mesh specified consisted of 0.71mm (0.03 in.) diameter galvanized wire with 13mm (0.51 in.) apertures. According to CWI-Wire (wire mesh manufacturers) the yield strength is usually around 320 MPa (46.4 ksi). The minimum yield strength found in these tests using the proof stress method (e = 0.001) was 300MPa (43.5 ksi).

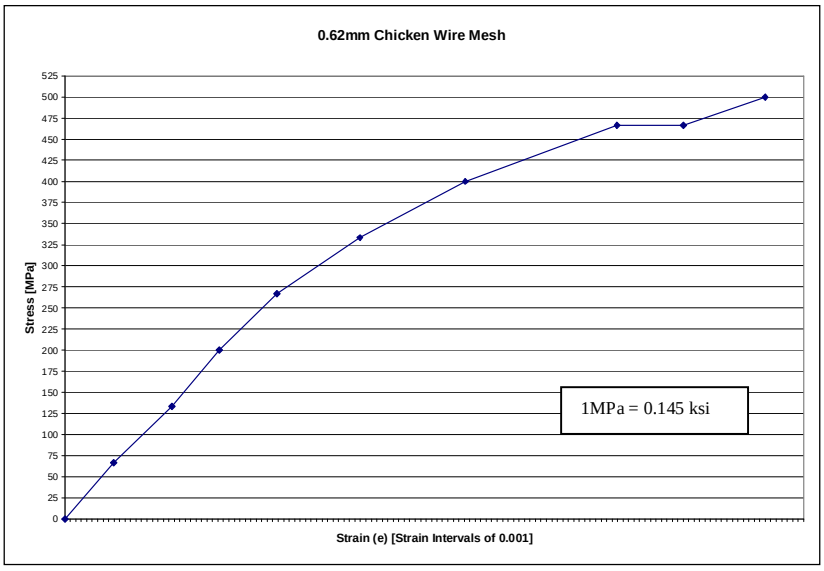

Figure 3.5 – Graph of Chicken Mesh Yield Stress

3.2.3 Plastic Damp Proof Course (DPC) Friction Tests

DPC's are used for the prevention of moisture movement in walls. Sometimes they are placed in critical areas where there are large compressive and bending forces. It is very important that these materials be chosen carefully to ensure that they can transfer these forces. Two common examples of DPC's are (Curtin, 1982):

- Horizontal DPC's which prevent vertical moisture movement and are generally located in areas of high compression and bending

- Vertical DPC's which prevent horizontal movement of moisture between different leaves of the wall. These are placed in areas of high shear.

For this investigation, standard horizontal plastic DPC's were used. These are flexible and are useful in areas where movement is expected.

Location of the DPC's in the Dome Home

In the final structure (structure type (B) in the shape investigation – dome on 1m cylinder wall) a DPC layer was placed at the base of the cylinder wall between the wall and the ring foundation. This DPC serves the purpose of preventing moisture ingress into the structure, as well as providing a plane along which movement can take place. This possible plane of movement is important as thermal stresses on the structure can be quite large and would cause the walls to crack if the structure did not have a movement joint.

Stability Concerns

The use of the DPC's at ground level is a concern with regards to stability. Horizontal loading such as wind loading can cause the walls to slip if the coefficient of friction between the DPC and the underlying material (e.g. foundation) is too small. A rough test method was adopted to approximate the coefficient of friction at the DPC interfaces.

Test Method and Apparatus

The basic requirements for measuring the coefficient of friction, μ, are:

1. A means of applying a normal force, N,
2. A means of measuring the tangential force, F, ($\mu = F/N$)

The second requirement can be measured using the geometry of the system if the inclined plane method (BS-4618, 1975) of investigation is used. This test is

done by increasing the inclination of a plane surface with a test specimen placed on top of it, until the specimen slides. The coefficient of friction can then be determined using the equation:

$$\mu = \frac{F}{N} = \frac{W \sin\theta}{W \cos\theta} = \tan\theta \qquad (3.4)$$

Figure 3.6 defines the variables in the above equation.

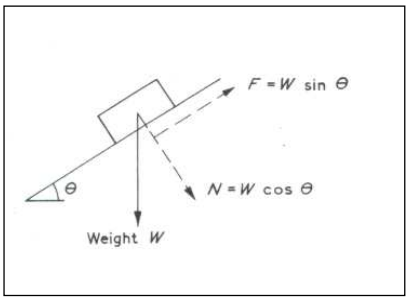

Figure 3.6 – Line Diagram of the Inclined Plane Method

The apparatus for this experiment included a plane of mortar built into a stiff wooden frame (mortar mix (ii) SABS 0164-Part1), a concrete block (or mortar block), the plastic DPC material, a jack and measuring equipment. The apparatus can be seen in figure 3.7.



Figure 3.7 – Inclined Plane Friction Test Apparatus

The plane of mortar represents the interface between the wall and the DPC, and the concrete block represents the interface between the foundation, and the DPC. In practice, the DPC would be placed in a mortar layer. These tests approximate the behavior of this layer in its cracked state. The DPC material was tightly wrapped around the concrete block and stapled on the non-contact surface to ensure that the DPC did not slip. The mortar was set into a stiff wooden frame in order to avoid warping of the mortar plane. The frame incorporated a circular bearing, which can be seen at the base of the frame shown in figure 3.7. This bearing ensured a smooth change in the inclination of the mortar plane. A jack was placed underneath the testing rig and was jacked up very slowly, in order to avoid vibration, until the specimen slipped. Once slip occurred, the angle of slip (θ) was measured using a protractor. This value was very rough, and therefore another method was used to improve the accuracy of this measurement. A string was hung from the centerline of the plane and tensioned by tying a bolt to it. This created a triangle whose height and base length were measured in order to determine the tangent of θ.

Three sets of tests were done. The first set excluded the DPC material. The second set of tests was done using one layer of DPC material wrapped around the concrete block. The third set of tests was done using a DPC wrapped around the mortar plane and the concrete block.

Test Results

The results of the concrete block (mortar block) sliding down the mortar plane were:

Test Description & Specimen	A [cm]	B [cm]	θ [°]	Protractor Reading	$\mu_{Average}$
Test 1	33.3	22	33.5	35	0.68
Test 2	34.3	19.8	30.0	30	0.58
Test 3	34	20.3	30.8	31	0.60
Test 4	32.5	22.5	34.7	35	0.70
Test 5	33.4	21.5	32.8	33	0.65
Test 6	33.2	21.5	32.9	33	0.65
Test 7	33	21.1	32.6	35	0.67
Test 8	32.9	21.3	32.9	33	0.65
Test 9	31.5	22.5	35.5	36	0.72
Final Average					**0.65**

Table 3.6 - Concrete Block Sliding Down Mortar Surface

The final coefficient of friction, μ=0.65, is similar to the coefficient of friction between brick and concrete (μ=0.6). A difference in these results was expected as the roughnesses of the elements are slightly different in each case. This test proved that the test method could yield reasonable approximations of the coefficient of friction.

In structure B, a single DPC layer was used at ground level and sliding was a concern at this interface. The results for one layer of DPC wrapped around the concrete block can be seen on the next page.

Test Description & Specimen	A [cm]	B [cm]	θ [°]	Protractor Reading	$\mu_{Average}$
Test 1	31.5	23.5	36.7	37	0.75
Test 2	31.6	23.3	36.4	35	0.72
Test 3	31.5	23.4	36.6	36	0.73
Change DPC					
Test 4	32.7	21.8	33.7	33	0.66
Test 5	32.1	22.2	34.7	34	0.68
Test 6	32.9	21.3	32.9	35	0.67
Change DPC					
Test 7	32.9	21.3	32.9	33	0.65
Test 8	33.4	20.5	31.5	32	0.62
Test 9	31.9	22.3	35.0	34	0.69
Final Average					0.69

Table 3.7 - One Layer of DPC Wrapped around Concrete Block

The results from table 3.7 show that there was a slight increase in the coefficient of friction when the DPC material was introduced. This increase could be due to a sticking action between the plastic and mortar surfaces. However, the results show that a single layer of DPC has very little effect on the coefficient of friction. This result is beneficial with regard to stability.

Due to the circular shape of the structure placing of the DPC at wall level is difficult and therefore a large amount of lapping of the DPC must be done. This was a concern with regard to stability, and therefore tests were done with 2 layers of DPC. The results are presented on the next page.

Test Description & Specimen	A [cm]	B [cm]	θ [°]	Protractor Reading	$\mu_{Average}$
Test 1	35.2	17.5	26.4	24	0.47
Test 2	35.5	16.5	24.9	25	0.47
Test 3	35	17.4	26.4	25	0.48
Change DPC					
Test 4	34.4	18.2	27.9	27	0.52
Test 5	33.5	20.4	31.3	31.3	0.61
Test 6	35.6	16.5	24.9	25	0.46
Change DPC					
Test 7	35.2	16.7	25.4	25	0.47
Test 8	33.6	19.3	29.9	30	0.58
Test 9	33.4	19.9	30.8	30	0.59
Final Average					0.52

Table 3.8 - Two Layers of DPC Wrapped around Concrete Block and Mortar Surface

These results show a slight reduction in the coefficient of friction. However, in practice the vertical force from the wall will compress the DPC's together and the two layers may stick, behaving as a single layer of DPC. Damage to the DPC's with time will also affect the coefficient of friction. The roughness of the mortar and the foundation will also vary on site. These factors highlight the difficulties and possible errors that can be made when investigating the coefficient of friction of surfaces which include plastics. Therefore, during the design stage it is important to adopt safety factors which reflect this uncertainty.

Stability calculations were performed. The coefficients of friction presented in this section were used and large safety factors were adopted due to the rough nature of the results presented above. However, these calculations proved that the coefficient of friction between the wall and the foundation was not critical under normal loading conditions.

4. Structural Analysis

The analysis presented in this section is based on a 28m^2 (301 ft^2) dome that was constructed as a prototype. This structure corresponds to structure type (B) from the shape investigation and can be seen in figure 4.1 below. An alternative structure was designed but proved to be too expensive. This structure can be seen in Appendix B.



Figure 4.1 – Prototype 28m^2 (301 ft^2) (Structure type (B))

The structural analysis of the dome home was done using a limit states approach. The load combinations according to SABS 0160 – 1989 were calculated and then inputted into the final analysis model on Abaqus™. A three dimensional analysis was performed on the structure. This type of analysis was necessary because of the effects of unsymmetrical loading, such as wind loading, and openings in the final structure for doors and windows. The load combination that produced the greatest forces and moments in the structure was used in the final design of the structural elements.

4.1 The Model

4.1.1 The Dimensions of the Structure

The dimensions of the final structure are shown in figure 4.2.

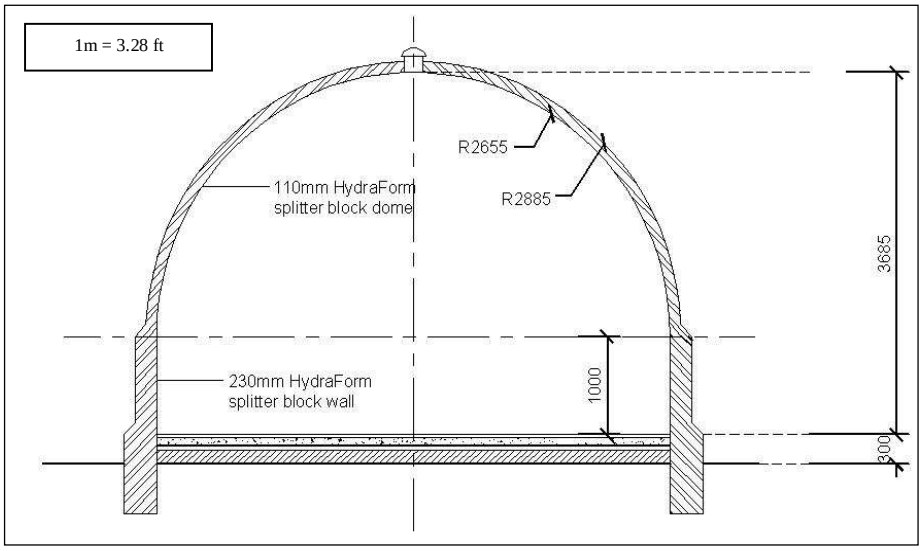

Figure 4.2 – Dimensions of the Final Structure (Prototype 28m^2 (301 ft^2) Dome)

4.1.2 The Finite Element Analysis (FEA) Model

The model was created in Abaqus^{TM} in a 3-D environment. The dome and cylinder wall were modeled using quadratic shell elements (quadratic deformation function) with mid side nodes. These functions yield a more accurate solution than linear deformation functions. The arches around the windows and door were modeled using solid elements (hexahedron brick elements) and shell to solid coupling was used to link the arches and the shell structure. The inclusion of the arches in the model is important as they stiffen the structure. Figure 4.3, overleaf, shows the FEA model of the structure.

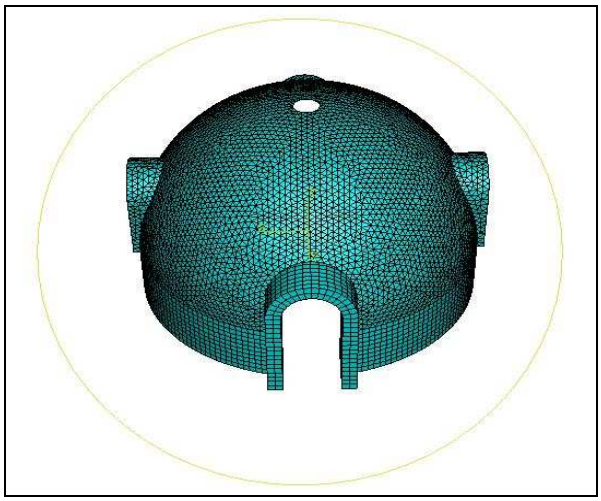

Figure 4.3 – 3D FEA Model (Final Structure)

4.2 Loading Calculations

The loads presented in this section exclude ultimate and serviceability limit state load factors. In the finite element analysis of the structure the load factors presented in section 4.3 were used.

4.2.1 Dead Load (Self Weight)

The dead load is the overall self weight of the structure including finishes. The dome homes self weight can be broken up into the contributions of the three major structural elements; namely, the dome, the cylinder wall and the foundation. The self weight was calculated by finding the downward pressure on the structural elements and dividing that pressure by the thickness of the structural unit resisting the load (in order to obtain the body force [kN/m^3] that could be inputted into Abaqus^{TM}).

The values of the dead loads are:

Dome: (brick self weight + plaster self weight) / (thickness of the wall)

= [(1950 x 9.81 x 0.11) + (2300 x 0.03 x 9.81)] / [1000 x 0.11]

= 25.3 kN/m^3 (0.093 lbf/in^3)

Wall : (brick self weight + plaster self weight) / (thickness of the wall)

= [(1950 x 9.81 x 0.23) + (2300 x 0.03 x 9.81)] / [1000 x 0.23]

= 22.1 kN/m^3 (0.081 lbf/in^3)

4.2.2 Live Load

The live load was obtained from Clause 5.4.3.3 of SABS 0160 (1989). The code suggests that the live load that produces the most severe effect on the structure be used. A choice of a concentrated load of 0.9kN (0.20 kips) applied over an area of 0.1m^2 (1.08 ft^2), or a uniformly distributed load (UDL) of 0.5kN/m^2 (0.073 psi) is presented. 0.5kN/m^2 is the maximum UDL suggested for an inaccessible roof.

4.2.3 Wind Load

One of the major benefits of dome structures is their favorable resistance to wind loads. The dome structure is aerodynamic and the pressures that arise on the surface are very small. Figure 4.4 (Billington, 1982) shows the equations used to determine the wind pressure on a dome, as well as the wind pressure on a cylinder wall.

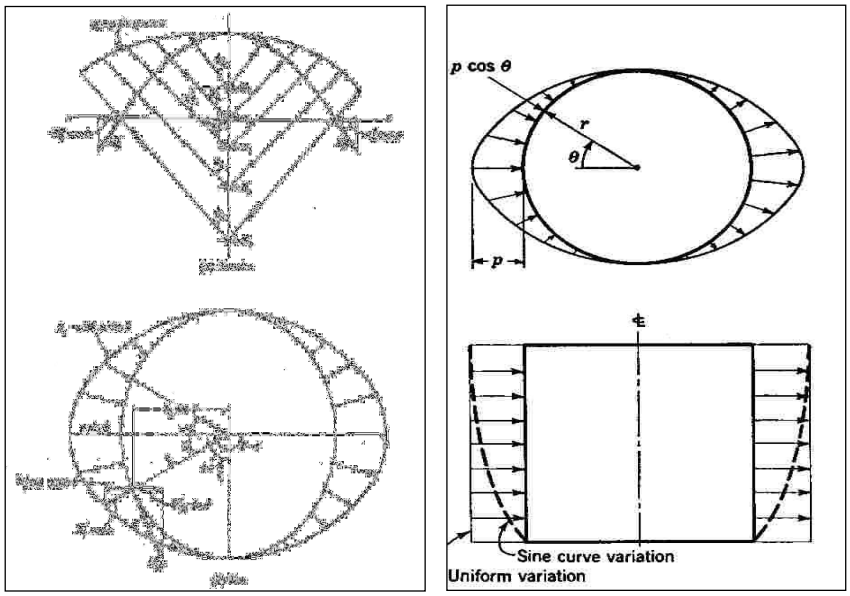

Figure 4.4 – Wind Pressure on a Dome and a Cylinder (Billington, 1982:74)

From figure 4.4**:** p_z = pressure on the surface of the structure

p = free stream velocity pressure

The wind loading was calculated using the following equations, taken from SABS 0160 (1989) assuming Johannesburg, South Africa conditions:

$$q_z = p = k_p v_z^2 = 0.88 \text{ [kN/m}^2\text{]} \qquad (4.1)$$

$$0.128 \text{ [psi]}$$

where: $k_p = 0.53$ (constant depending on site altitude)

$v_z = (v \times k_z)$ = characteristic wind speed at height, z.

$k_z = 1.02$ = wind speed multiplier, depending on height of the structure and the

nature of the surrounding terrain

v = 40 m/s = regional basic wind speed

$$p_z = C_p q_z = 0.88\, C_p \text{ [kN/m}^2\text{]} \qquad (4.2)$$

$$0.128 C_p \text{ [psi]}$$

where: C_p = pressure coefficient depending on the surface of the structural unit

Therefore from Billingtons' formulae:

C_p for a dome = $\sin\phi \cos\theta$

C_p for a cylinder = $\cos\theta$

The wind load was applied in patches to the finite element model, by breaking it up into sections. This is done by partitioning the dome and cylinder surfaces and applying the applicable pressure to that section of the model. The smaller the partitions the more accurate is the loading. Figure 4.5 illustrate how the dome and cylinder surfaces were partitioned in order to model wind loading, using patch loading.

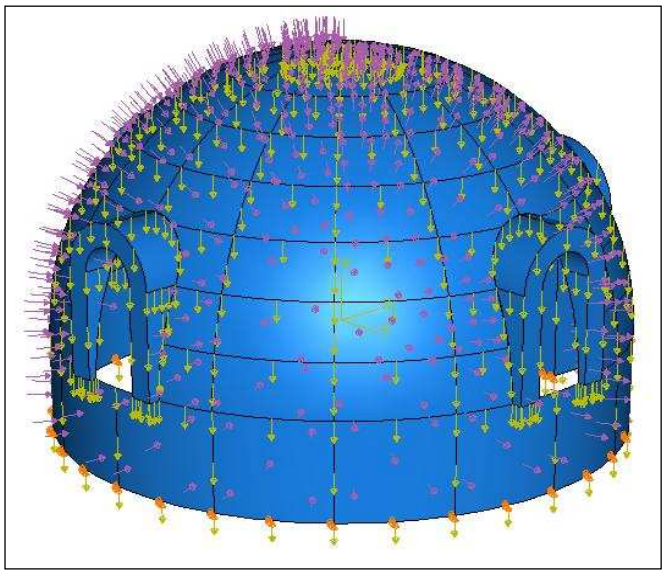

Figure 4.5 – Partitioned Model (Wind Load- Patch load)

4.2.4 Temperature Load

According to Billington (1982), "even a 10ºF temperature drop will produce large hoop tension and a moment more than the gravity-load moment. Actual temperature drops can often be as high as 70ºF, so that the tensions and moments due to temperature could control the design". This statement was made for a fixed base dome example.

Temperature Effects on General Structures

In our everyday encounters with buildings, temperature and shrinkage effects can be seen. Temperature load can be equated to a volume increase/decrease of the structure (as can shrinkage).Two typical examples of the effect of this type of loading are show below.



Figure 4.6 – Two Examples of Cracking Induced by Volume Changes

The first picture, in figure 4.6**,** shows cracking of a brick infill panel wall. The concrete column has contracted causing large stresses in the wall and finally resulting in cracking. The second picture shows a brick wall resting on a concrete foundation. Shrinkage may be one of the reasons why the wall has cracked (horizontal crack). However, temperature variations between the foundation and the wall will cause differential movement of the two elements, which will create high stresses and cracking at the wall/foundation interface.

The masonry design approach to this type of problem is not to increase the strength of the structural units, but to include expansion joints in areas of differential movement (or volume change). The inclusion of a DPC material acts like an expansion joint. It creates a slip plane along which movement due to shrinkage and temperature variations can be accommodated without creating large stresses.

Temperature Effects on Dome Structures

Figure 4.12 shows a dome in the Sparrow Aids Village (Johannesburg, South Africa). The cracking observed in this structure is postulated to be attributed to thermal stresses. It is important to note that failures of domes have been directly attributed to large and rapid temperature changes [Gred, Paul (1986), "Students Narrowly Escape Dome Collapse", Engineers Australia, August 22,

1986], and therefore this type of loading should be considered during the structural analysis of a dome.

Two types of loading must be considered when analyzing the temperature effects on a dome structure. These are:

- Global temperature changes over the entire structure.
- Local temperature changes (part of the structure experiences temperature changes).

When analyzing for temperature loads (or shrinkage) using classical thin shell theory, a uniform volume change is assumed to occur throughout the structure and the slope of the dome is assumed to remain constant. This assumption is not physically correct as during the day one side of the structure will have more sunlight than another side (causing differential temperature in the structure). When using Billingtons' (1982) analysis method, a global temperature change is assumed. No forces result from the membrane condition, and the errors are calculated using the following equations:

D_{10} = (Radius) x (Temperature Change) x (Coefficient of Expansion) (4.3)

$D_{20} = 0$ (4.4)

The analysis is completed in the same manner as the dead load analysis after this step (i.e. Corrections etc.).

For localized temperature changes, an FEA is required. Monolithic Dome™ of Texas avoids the effects of temperature load by applying a layer of insulation to their domes. This is an effective, yet costly, method of resisting temperature changes and was therefore not considered for the low-cost dome constructed.

4.3 Load Combinations

The load combinations for the ultimate and serviceability limit states of this structure, as determined from SABS 0160 (1989), were:

ULTIMATE LIMIT STATE	SERVICEABILITY LIMIT STATE
1.5 (Dead load)	1.1 (Dead load) + 1.0 (Live load)
1.2 (Dead load) + 1.6 (Live load)	
0.9 (Dead load) + 1.3 (Wind load)	
1.2 (Temperature load) + 0.9 (Dead load)	

Table 4.1 – Load Combinations According to SABS 0160 (1989)

4.4 Finite Element Analysis Results

The analysis results are presented graphically. The exact values of forces and moments for some of the load combinations can be seen in Appendix A. The arches in the openings, the skylight and window and door openings all have a significant effect on the structural analysis results. The effects of these openings on the structure are discussed before the results of the ultimate limit state (ULS) and serviceability limit state (SLS) load combinations are presented. The results that follow are presented along sections through the structure. Three critical sections were taken and they are shown in figure 4.7.

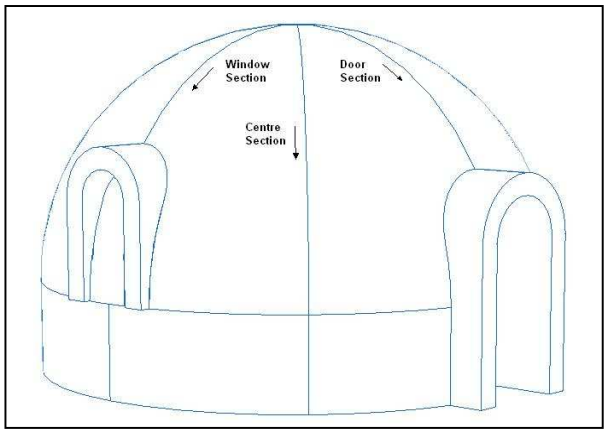

Figure 4.7 – Sections along Which Results are Presented

4.4.1 The Effects of the Skylight Openings and Point Loading

The Skylight Opening

Billington (1982) presents the membrane equations for the thin shell analysis of a 'Concentrated Load around a Skylight Opening'. These equations are useful as they highlight the fact that a ring compression is induced at the top of the dome and that bending occurs in the region of the skylight. Figure 4.8 shows a point load acting on the free upper edge of the dome

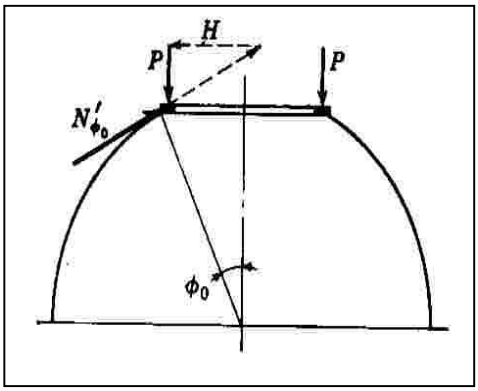

Figure 4.8 – Concentrated Load around a Skylight Opening (Billington, 1982:45)

The load P acts vertically and cannot be resisted by the meridian thrust alone (Billington, 1982). Therefore, a horizontal thrust must occur. This thrust is determined by equation 4.5:

$$H_{\phi 0} = \frac{P}{\tan \phi_0} \qquad (4.5)$$

This horizontal thrust induces a ring compression into the edge of the shell, which can be very large and a stiffening edge ring may be required. The magnitude of the ring compression is:

$$C_{\phi 0} = aP \cos \phi_0 \qquad (4.6)$$

Point Loading (Live Loading)

The effect of a point load in the region of the skylight was investigated in the live load analysis of the structure. A point load of 0.9kN (0.20 kips) was placed at the apex of the dome (on the edge of the skylight opening) and a third of the way up the dome surface. This load may represent a person standing on the

dome. The results are presented in figures 4.9 and 4.10. The graphs also show the forces and moments in the structure without a skylight.

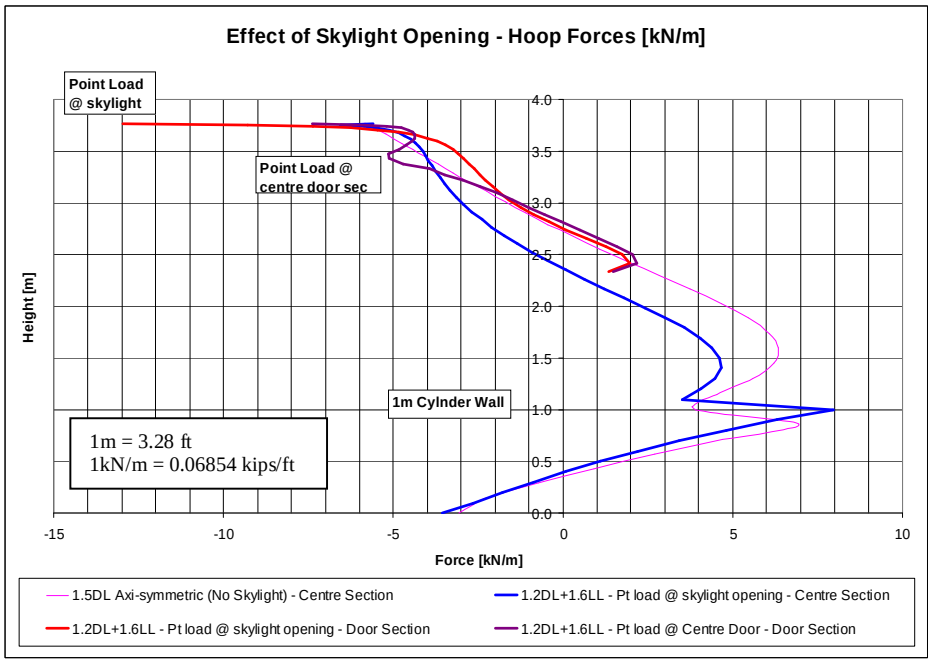

Figure 4.9 – Graph of the Effect of Skylight Opening on Hoop Force

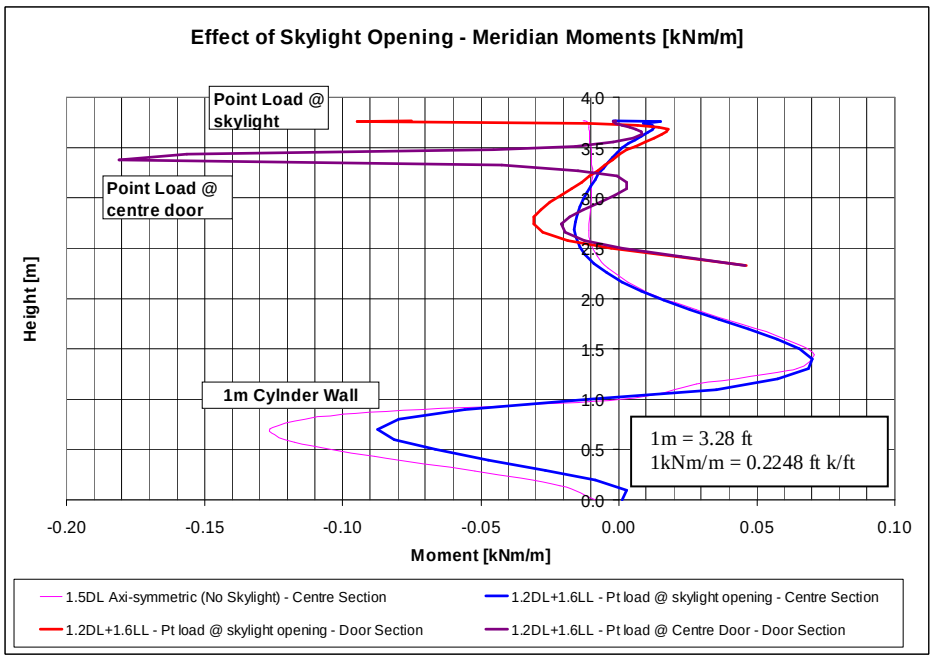

Figure 4.10 – Graph of the Effect of Skylight Opening on Meridian Moments

Figure 4.9 shows the hoop compression that occurs in the top of the dome when a skylight is included, as well as localized compression in the regions where point loads occur. Figure 4.10 shows that the skylight has no appreciable effect on the moments in the dome, but when a point load is applied to the dome (over an area of $0.1m^2$ ($1.08\ ft^2$) moment is induced in the region of the load.

4.4.2 The Effects of Window and Door Openings

Openings in shell structures cause high stress concentrations which need to be accurately quantified. Classical shell theory cannot accurately calculate the forces and moments around openings in shell structures due to the complex nature of the shell theory equations. Therefore FEA was used to find the effects of the window and door openings in the dome. Figure 4.11 shows the difference in the pattern of stress concentration around unsupported and supported (arches) openings in the dome. Note that this figure exaggerates the deflected shape of the dome.

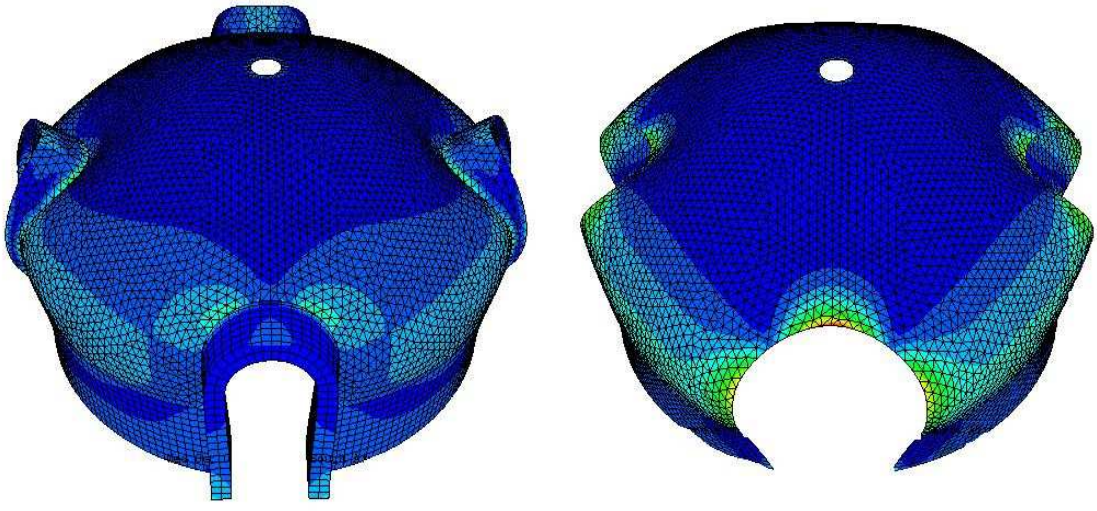

Figure 4.11 – Stress (Von Mises) around Supported and Unsupported Dome Openings

The red, green and light blue regions in figure 4.11 are regions of high stress concentration. The inclusion of arches in the openings reduces these stresses and changes their pattern of distribution. Three regions of high stress can be identified from figure 4.11.

These are:

- At approximately 45 degrees to the top of the door and window openings.
- Directly above the window openings.
- Around the bottom third of the dome structure.

It is interesting to note that these regions coincide with crack patterns observed around the openings in existing structures. Cracking in other regions was also observed. This type of cracking was more random and is thought to be caused by thermal and shrinkage stresses in the structure. Figure 4.12 shows the crack patterns observed on the Sparrow Aids Village Domes (un-reinforced domes, i.e. no chicken mesh or wire wrapping).

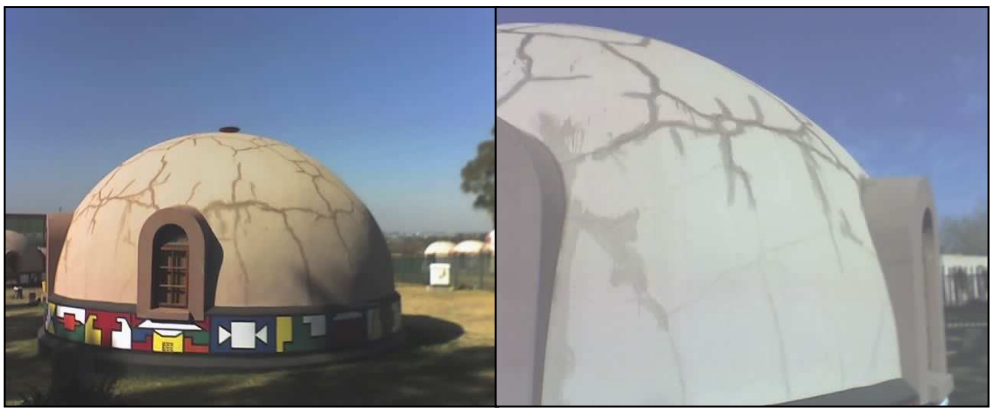

Figure 4.12 – Cracks Patterns around Openings at the Sparrow Aids Village

The cracks, shown in figure 4.12, cause waterproofing problems. A special waterproofing paint was applied to these structures in order to counteract this unsightly problem. An alternative solution to this is to insulate the outside of the structure. However, this is an expensive procedure and tensile stresses around openings are not resisted by using this approach. Another approach is

to try and prevent cracking by reinforcing the dome. This was the approach adopted in this investigation. The causes of cracking are discussed further in section 4.4.4 (b) - Window and Door Sections.

The influence of the arches in reducing the hoop forces and moments in the structure are shown in figures 4.13 and 4.14.

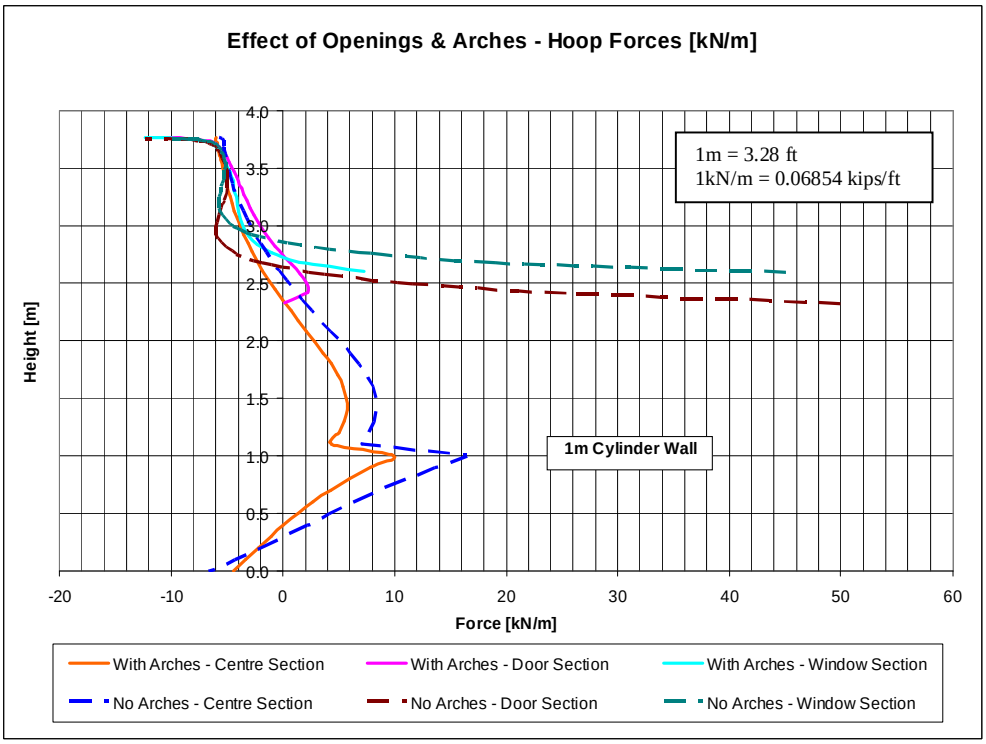

Figure 4.13 – Graph of Hoop Forces around Window Openings

From figure 4.13, we can see that the arches are beneficial as they stiffen the structure and reduce the tensile hoop forces that occur in the regions of window and door openings.

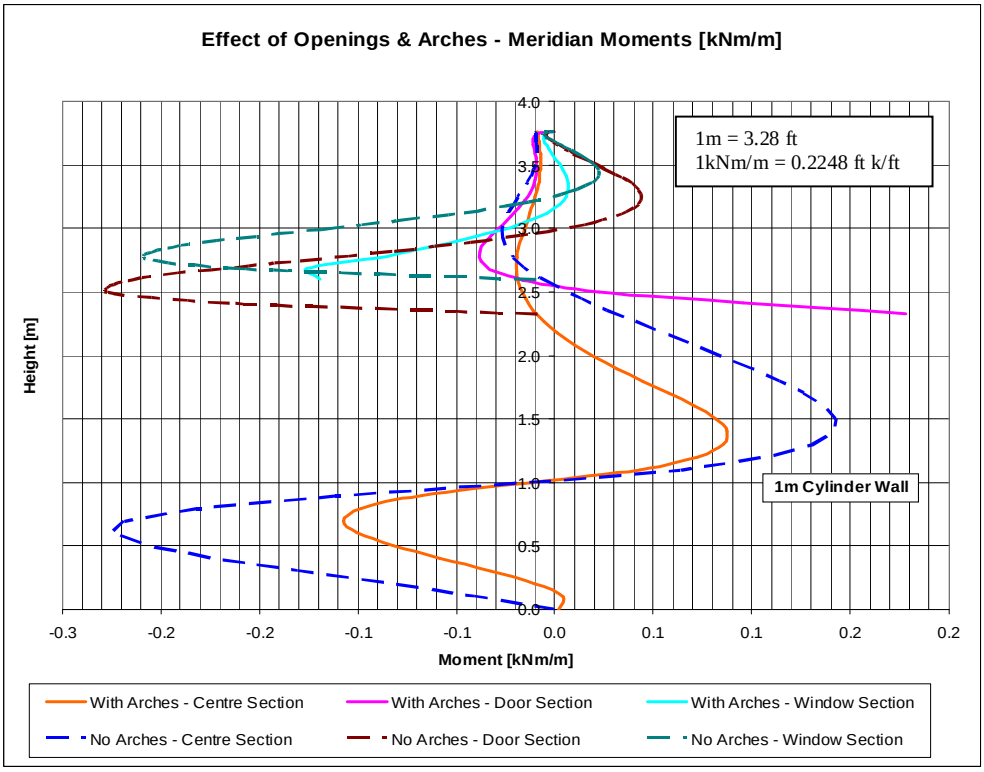

Graph 4.14 – Graph of Meridian Moments around Window Openings

From figure 4.14 we can see that the arches reduce the tension region on the inside face of the structure above the door and window openings (see figure 4.11). In these regions, cracking is observed in existing dome structures, as seen in figure 4.15.

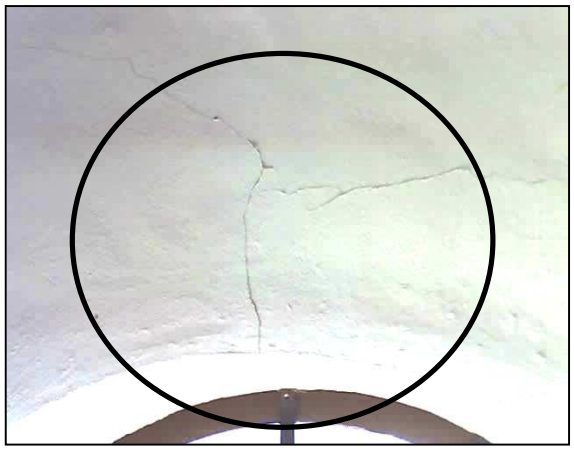

Figure 4.15 – Cracking on the inside face of a Window

4.4.3 The Effects of Temperature Loading

The temperature loading was broken up into a global temperature increase of the whole structure and a local temperature increase on half the structure. The local temperature increase was an attempt to model the heating of one side of the structure by the sun. A temperature increase of 20 degrees Celsius was used. The results were dependant on the fixity of the cylinder wall to the foundation (i.e. fixed base, pinned base or sliding base). As discussed earlier in this chapter slip joints, in the form of DPC's, can be included in the structure to reduce the effects of temperature loading. The following graphs show the results of temperature loading on the dome and cylinder wall for different fixities. Note the marked improvement when a sliding joint is used (i.e. movement of the structural element is not restricted).

Temperature Increase over the Whole Dome

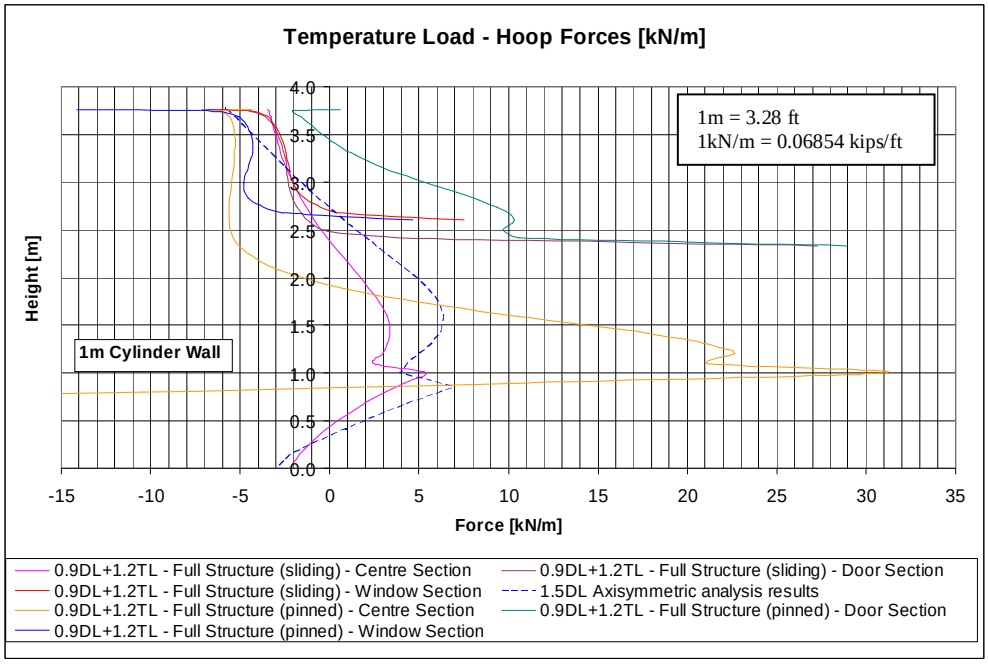

Figure 4.16 – Graph of Hoop Force (1.2TL+0.9DL)

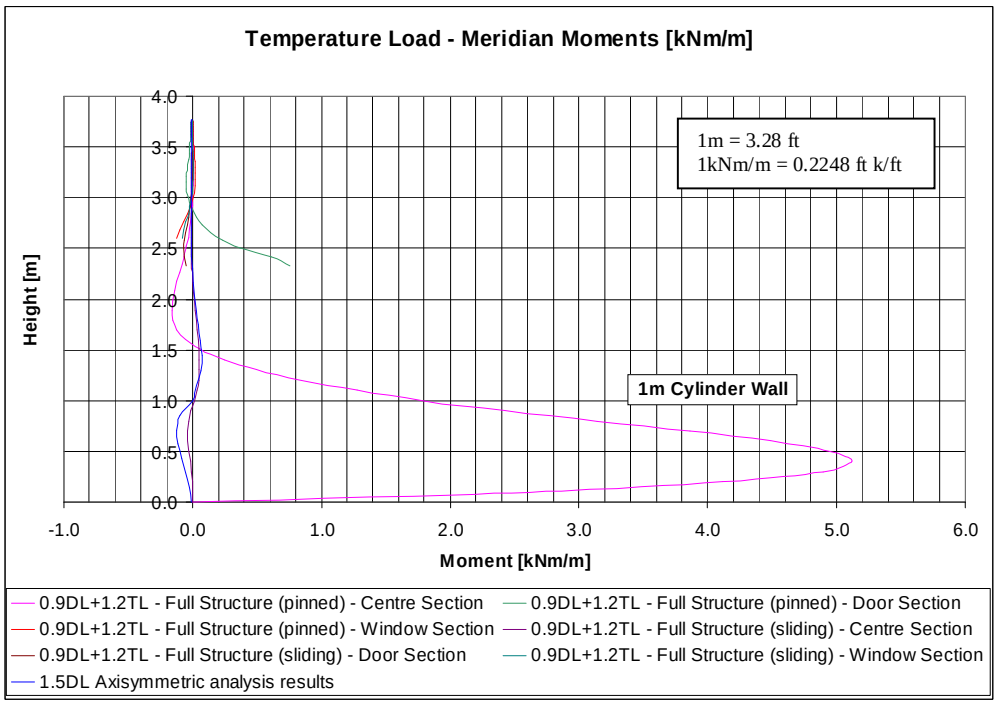

Figure 4.17 – Graph of Meridian Moment (1.2TL+0.9DL)

From figures 4.16 and 4.17, we can see that a slip joint at the base of the structure substantially reduces the hoop forces and meridian moments in the structure. The load combination of 1.5DL produces greater hoop forces and meridian moments along the centre section than the temperature load case with a sliding (slip joint) base. In the regions of openings, the hoop forces are greater than the 1.5DL load combination due to the stiffening effect of the arches (restraining movement). Therefore, it is important to provide reinforcing in these regions to resist these forces.

Temperature Increase over Half the Dome

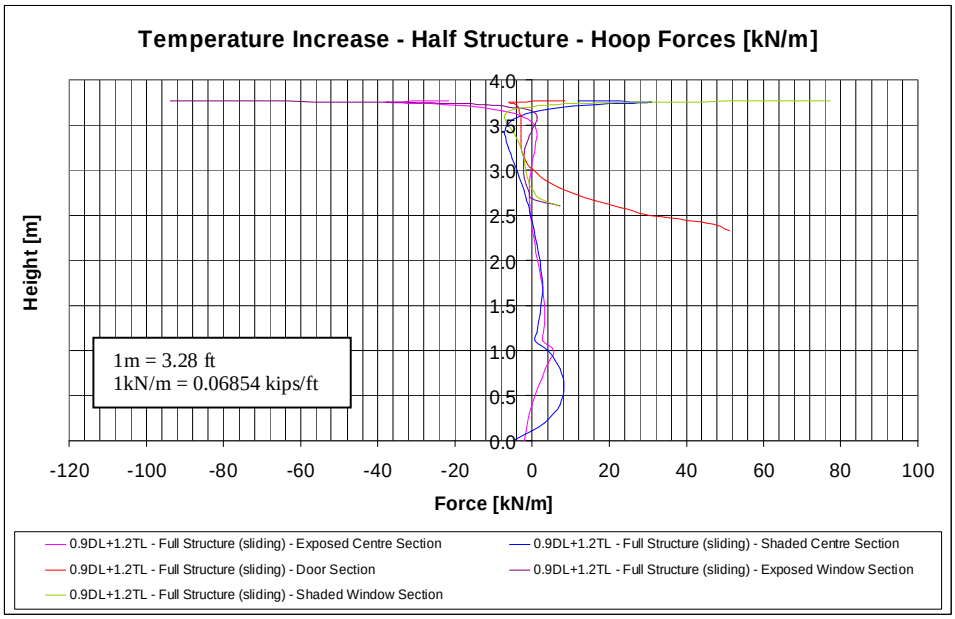

Figure 4.18 – Graph of Hoop Force (1.2TL+0.9DL - Half Structure)

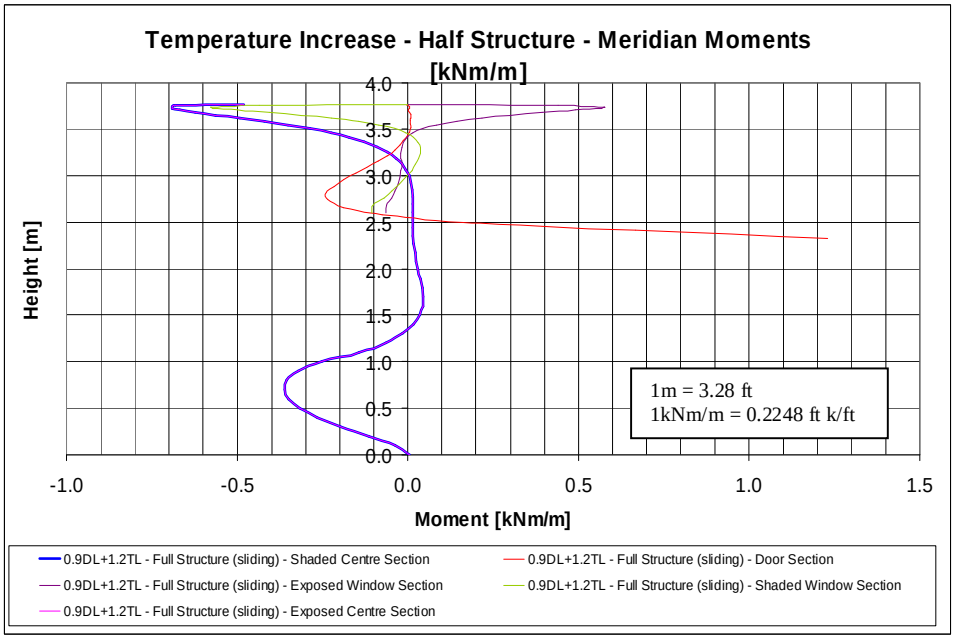

Figure 4.19 – Graph of Meridian Moment (1.2TL+0.9DL - Half Structure)

The results presented in figures 4.18 and 4.19 are for a temperature increase of 20 degrees Celsius of on half of the structure. The results show a significant

increase in the hoop forces and meridian moments in the top of the structure between the regions of temperature increase and no temperature increase. This loading case was not considered in the design of the structure as this pattern of temperature increase is a simplification of the actual situation. However, figures 4.18 and 4.19 are useful in showing us that the forces and moments induced due to differential heating of different regions of the structure can be quite large.

The inclusion of a DPC at ground level ensures a slip joint at the base of the structure which allows movement of the structure and reduces the effects of temperature loading. However, the temperature load case is still critical to the ultimate limit state analysis of the structure in the regions of openings and was considered when designing the structural elements. In concrete structures where the bases are fixed, or built into a ring beam, reinforcing will need to be provided in order to resist temperature loading. Large forces build up due to the fact that the foundation is cooler than the structure, causing a differential temperature distribution.

4.4.4 Final Design Results

The results presented in this section were used in the material design of the dome and cylinder wall. The material design is presented in the next chapter. The exact values of the forces and moments can be seen in Appendix A. Figures 4.20 to 4.25 show the ultimate limit state results for the dome. The forces and moments were taken from critical vertical sections through the structure as shown in figure 4.7.

The Ultimate Limit State

(a) Centre Sections

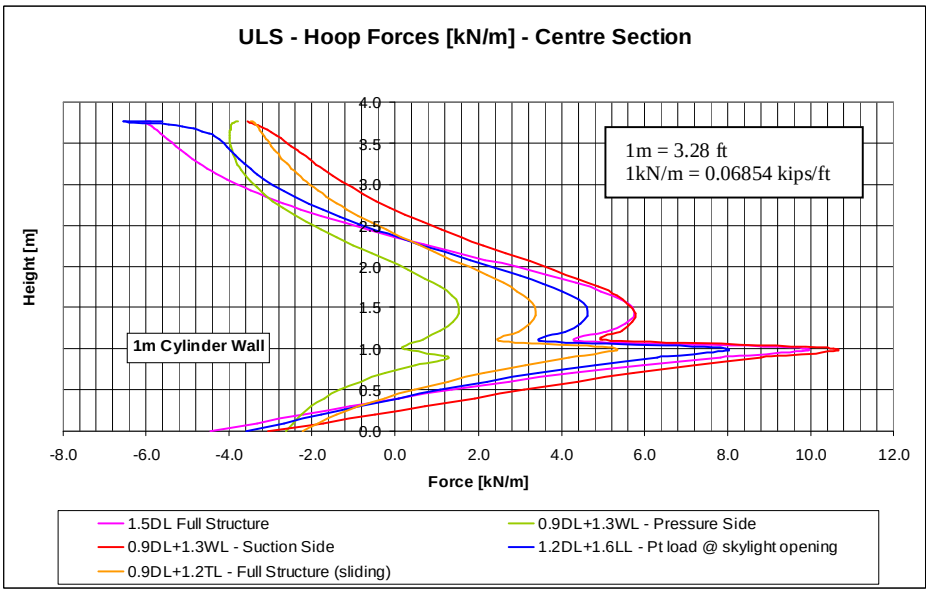

Figure 4.20 – Graph of Hoop Forces (ULS) – Centre Section

From the above graph we can see that the suction side of the structure under wind loading and the load combination 1.5DL produce the greatest tensile hoop forces.

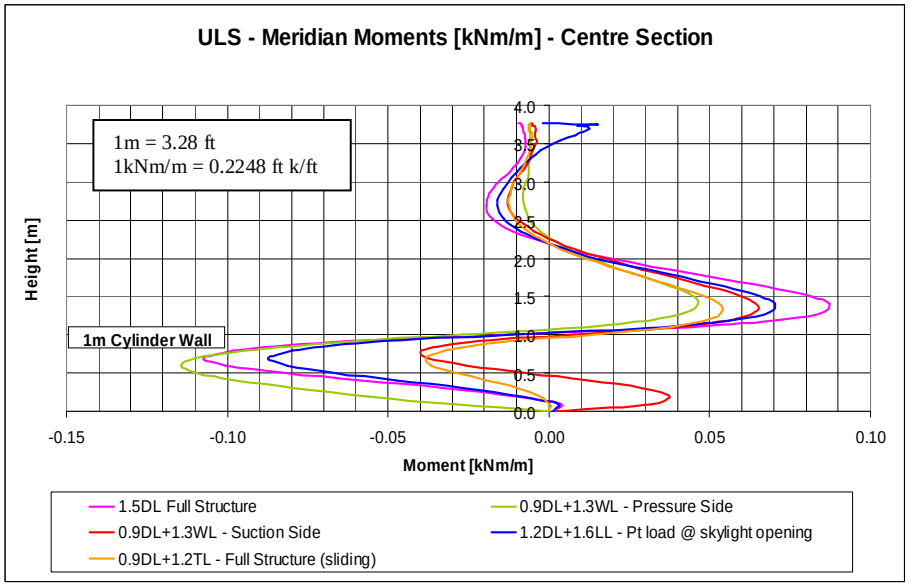

Figure 4.21 – Graph of Meridian Moments (ULS) – Centre Section

(b) Door Sections

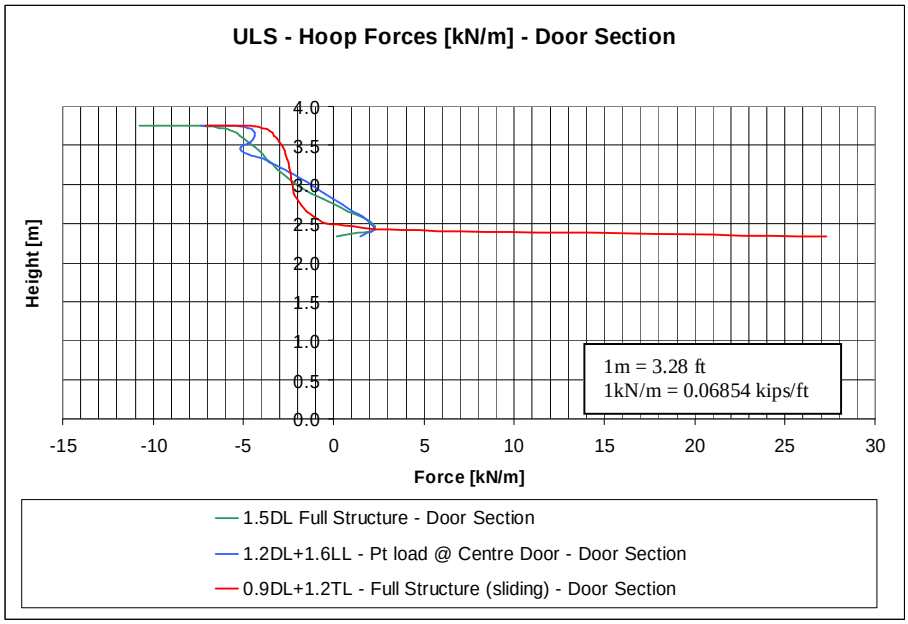

Figure 4.22 – Graph of Hoop Forces (ULS) – Door Section

Figure 4.22 shows the critical load combination with regard to tensile hoop forces is the 0.9DL+ 1.2TL load case. This load case also produces moments at the dome arch interface (figure 4.23).

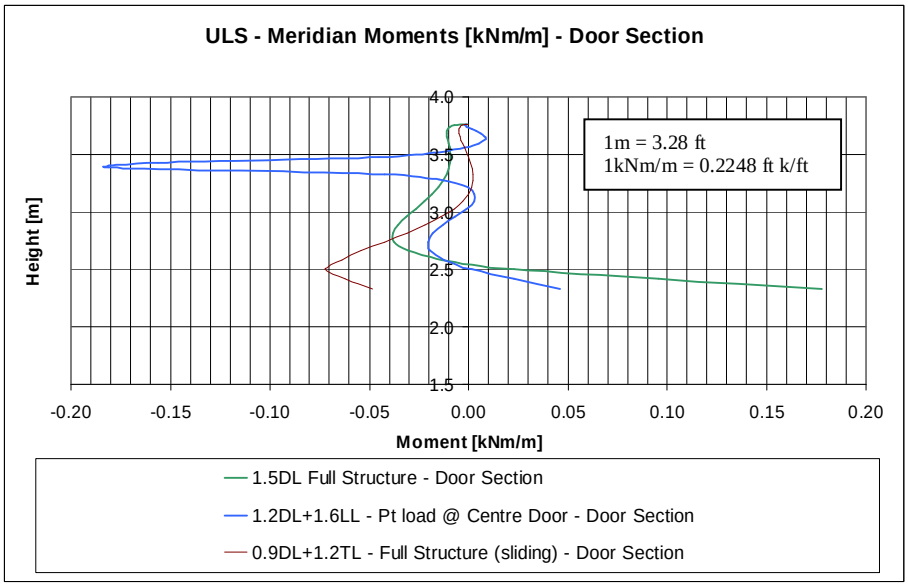

Figure 4.23 – Graph of Meridian Moments (ULS) – Door Section

(c) Window Sections

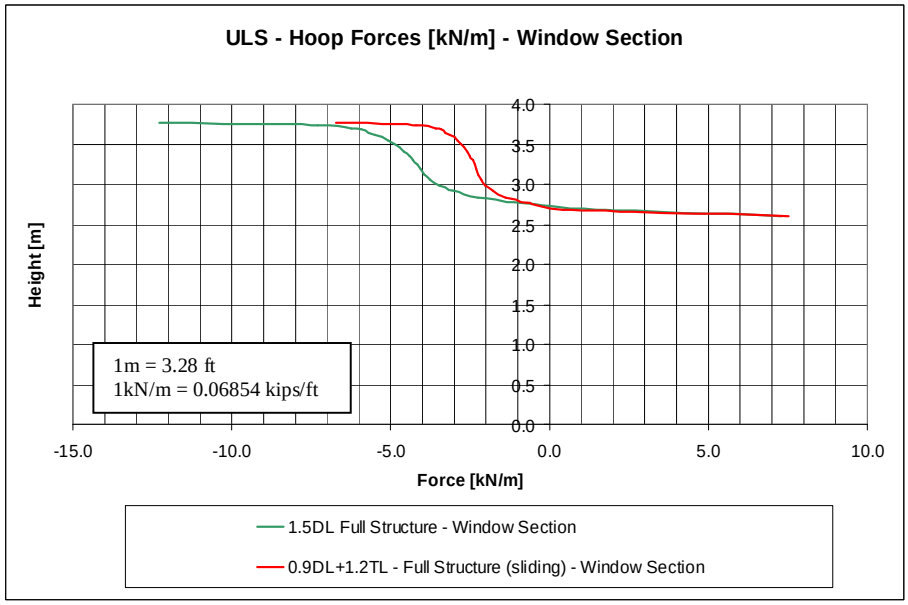

Figure 4.24 – Graph of Hoop Forces (ULS) – Window Section

As in the previous section, the temperature loading load case is critical. The arches provide resistance to the volume increase of the structure and tension results in the regions around the arches.

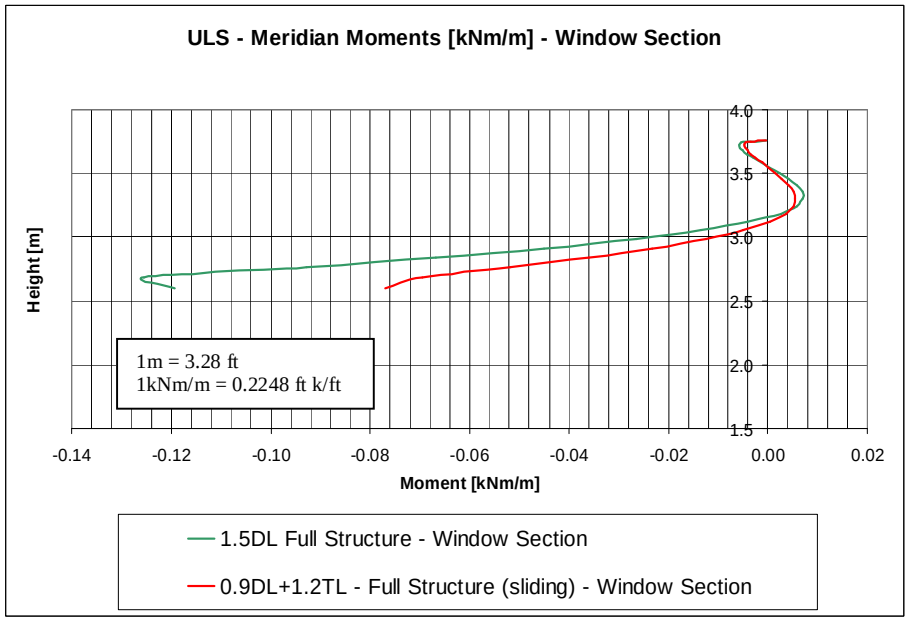

Figure 4.25 – Graph of Meridian Moments (ULS) – Window Section

Stresses in the Dome

In order to decide which of the load combinations produces the greatest amount of tension in the dome, and hence the worst loading case, the elastic stress formula can be applied in the hoop and meridian directions. This stress formula can be used if the section is uncracked according to masonry design procedures (Curtin, 1982). Formulae for cracked section analyses are presented in the next chapter.

$$\sigma = \frac{N}{A} \pm \frac{M}{Z} \qquad (2.19)$$

The variables in this formula are defined in section 2.5.3. The graphs below show the stresses in the meridian and hoop directions on the inner and outer surfaces of the dome, due to different loadings. Results are presented for the centre section and the window and door sections. In the meridian direction, the dome is in compression only. Positive values denote tension, negative values denote compression.

(a) Centre Sections

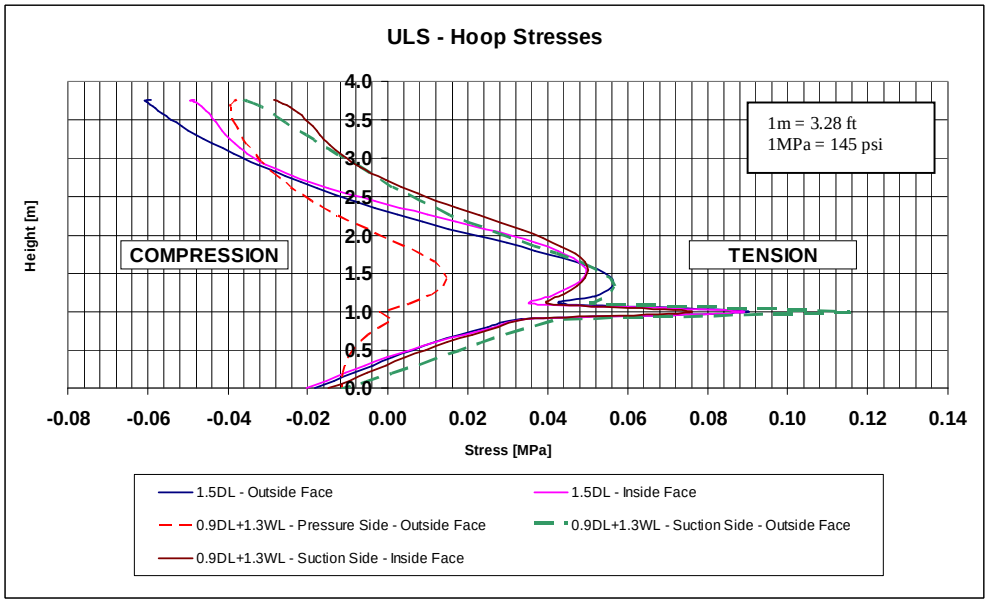

Figure 4.26 – Graph of Hoop Stresses – Centre Section

Figure 4.26 shows that the load case producing the maximum tensile stress in the hoop direction was the 0.9DL+1.3WL (suction side) load case.

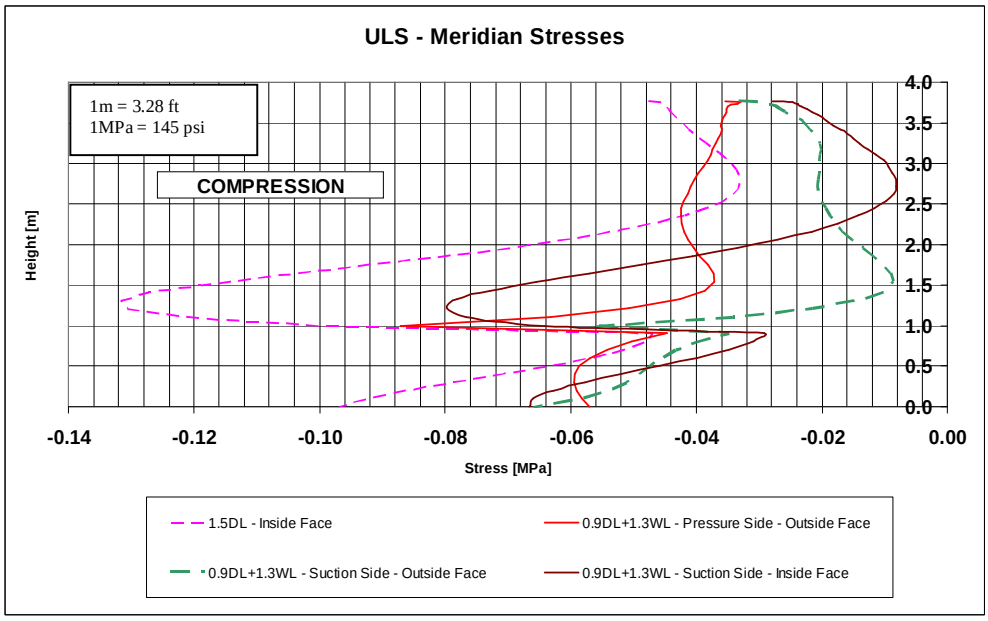

Figure 4.27 – Graph of Meridian Stresses – Centre Section

The largest compressive stress in the dome was created by the 1.5DL load combination, and the compressive resistance of the dome was based on this maximum value. From the above graphs we can deduce that the most critical load cases along the centre section are the 1.5DL (compression) and 0.9DL+1.3WL (suction side) load cases.

(b) Window and Door Sections

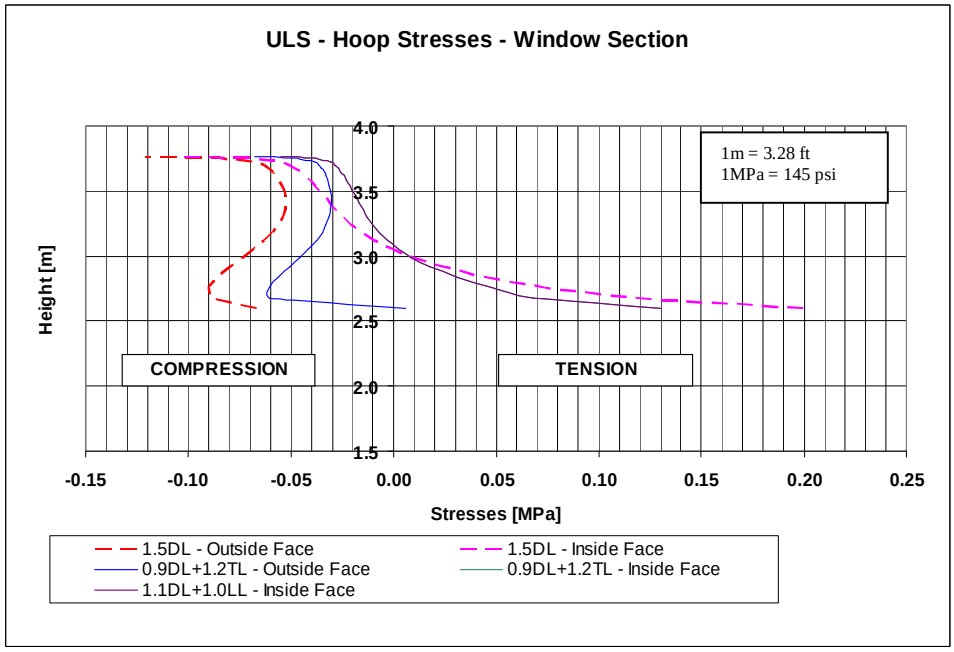

Figure 4.28 – Graph of Hoop Stresses – Window Section

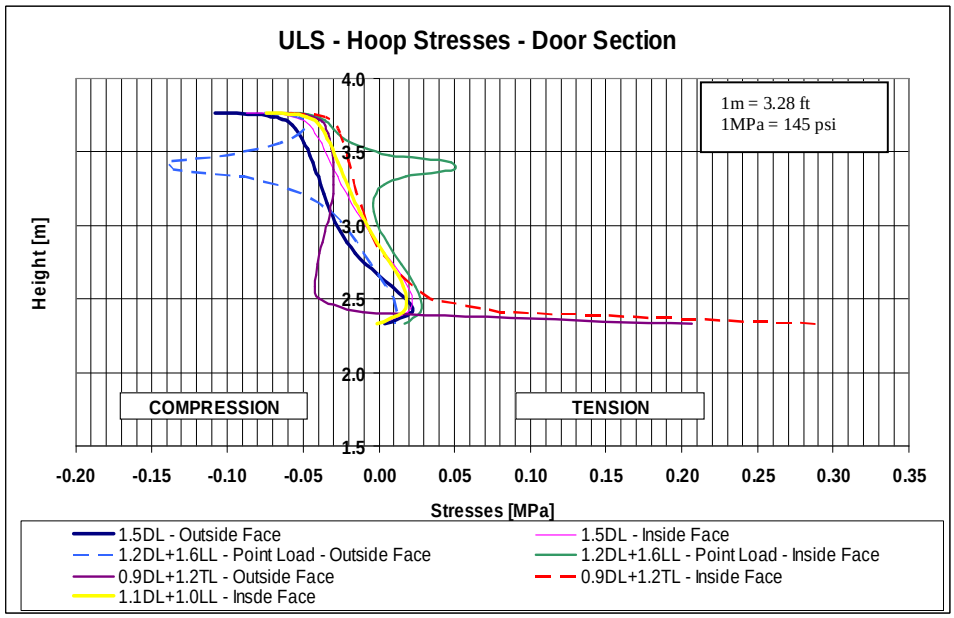

Figure 4.29 – Graph of Hoop Stresses – Door Section

The above results show that tension occurs at the intersection between the dome and arch at the window opening. The hoop tension acts laterally and

produces a crack similar to the one shown in figure 4.15. In section 5.2.1, it will be shown that a conservative estimate can be made about the tensile strength of the dome in the hoop direction (according to BS 5628-1:1992). The value of this direct tensile strength was found to be 0.097 MPa. This shows that under certain loading conditions, especially temperature loading, cracks will begin around the windows and doors of an un-reinforced dome and propagate from these points (as seen in figure 4.12). In the meridian direction, tension is also observed in these critical areas (figures 4.30 and 4.31). BS 5628-1:1992 does not allow a direct tensile strength to be along a mortar joint. Therefore, we can assume that these meridian tensile forces will cause the structure to crack in a horizontal ring pattern beginning at tops of the windows and doors. This horizontal ring can be seen in figure 4.12.

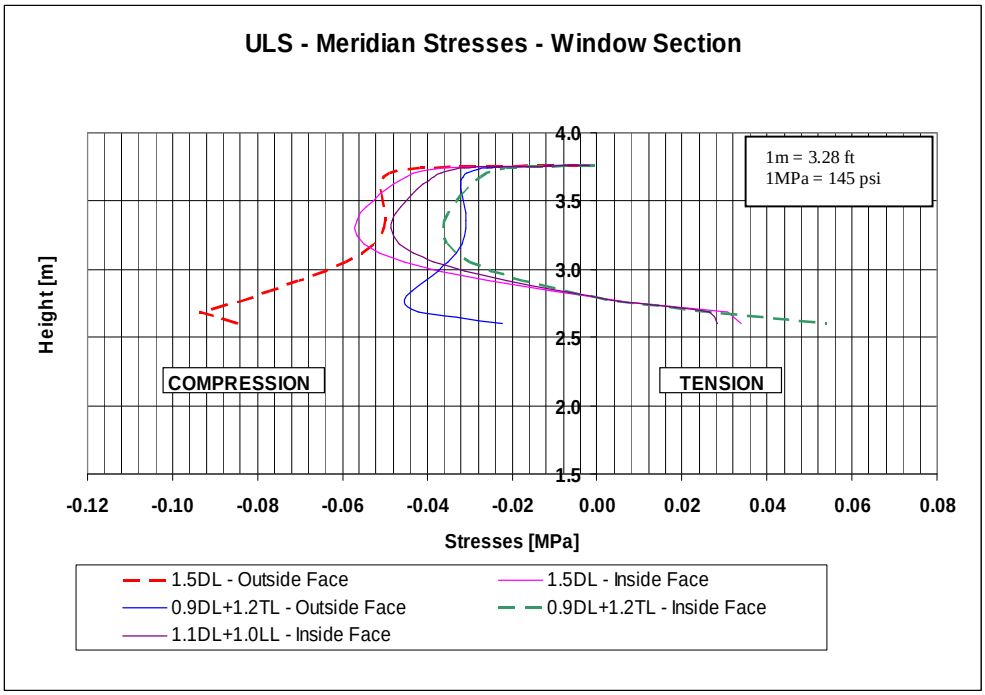

Figure 4.30 – Graph of Meridian Stresses – Window Section

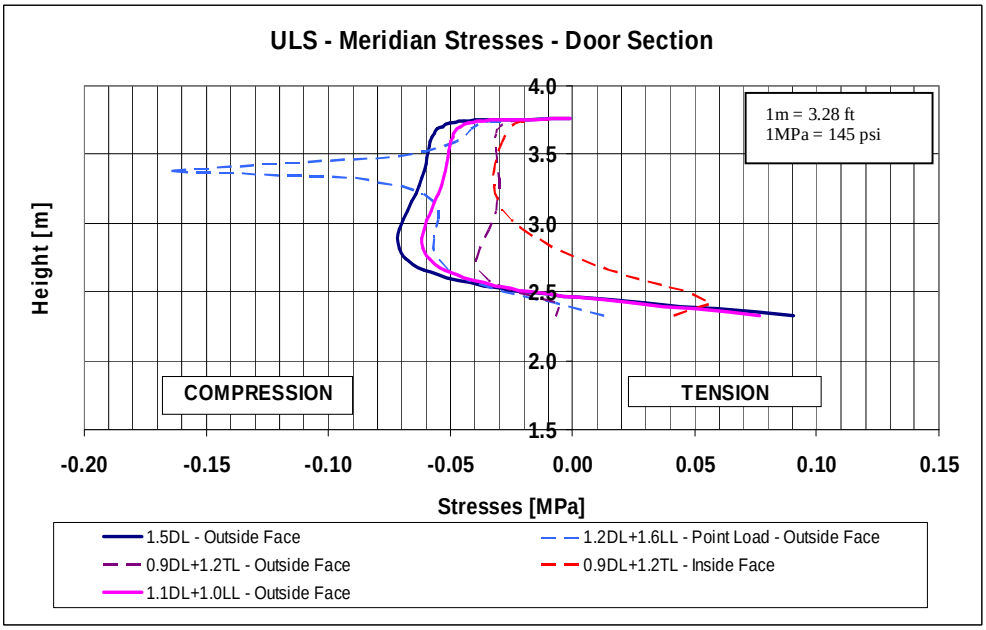

Figure 4.31 – Graph of Meridian Stresses – Door Section

Along the sections taken above the door and window openings the 1.5DL and 0.9DL+1.2TL load cases were critical. It was found that some form of reinforcing was required in these areas.

The Serviceability Limit State (SLS) Results

The serviceability limit state is important as it is used to check that the deformations of the structure are within allowable tolerances. The figures below are screen captures of the deflections obtained for the 1.0DL + 1.1LL load combination. The maximum deflection is shown in the top left of the figure. U2 is the vertical deflection of the structure and U1 the horizontal deflection.

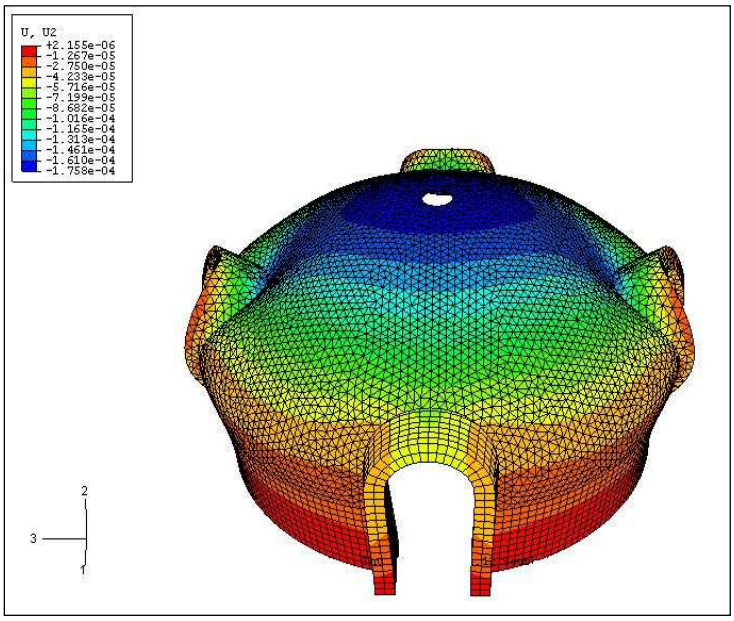

Figure 4.32 – Serviceability Deflections – U2

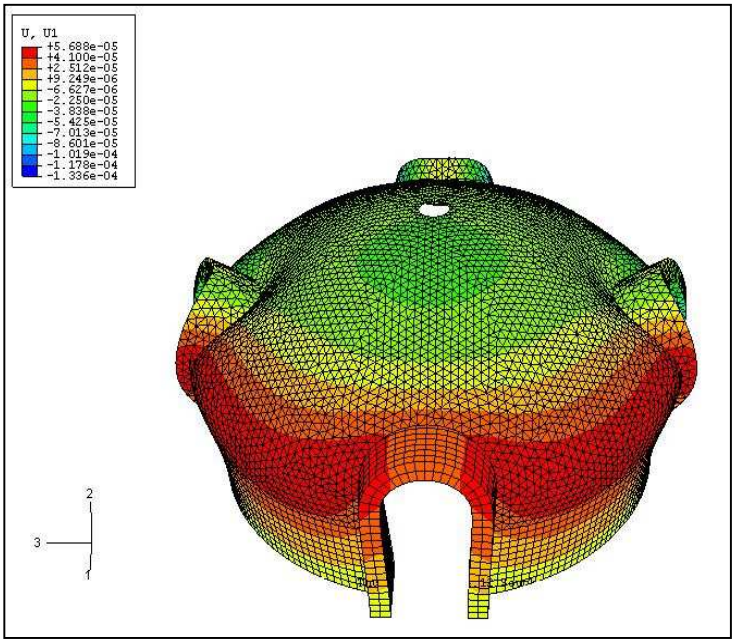

Figure 4.33 – Serviceability Deflections – U1

The maximum downward deflection is 0.28mm and the maximum outward deflection 0.13mm. These deflections are extremely small and do not pose a problem for any internal finishes.

.5. Design of Structural Elements

The two main structural materials in the dome structure were masonry and concrete. The walls were built using HydraForm 7MPa (1 015 psi) soil cement blocks and the foundation was built out of reinforced concrete. The design of these elements was done in accordance with SABS 0164-1 (1980), BS 5628-1 (1992) (masonry) and SABS 0100-1 (2000) (reinforced concrete). The 'Check List for Structural Design' published by the Joint Structural Division of the SAICE and IStructE was used as a guide for the masonry and concrete design sequence.

5.1 Design Theory

5.1.1 Masonry Design

Masonry design can be approached in two ways. The first method is a rational design where the loads on the structure and the material resistances are calculated and compared. The second method is an empirical method in which standard details and standard construction procedures are adopted (SABS 0400). For the purposes of this design a rational approach was used. This approach includes the calculation of the compressive, flexural, tensile and shear strength of the dome and cylinder wall. These strengths were compared to the stresses caused by axial forces and bending moments in the hoop and meridian directions (as seen in the Structural Analysis section of this report).

Compressive Strength

In the design of walls, loaded with an axial compressive force, the stress throughout the wall is an equal compressive stress and the following formula can be used to calculate the walls resistance to the compressive load.

$$Design\ Strength = \frac{\beta f_k}{\gamma_m} \qquad (5.1)$$

where: f_k = characteristic compressive strength

β = capacity reduction factor

γ_m = Material safety factor = 3.5

The characteristic compressive strength, mentioned above, depends on the class of mortar used (class II in this case), the strength of the masonry units used and the size of the units. The size of the unit is brought into the equation by defining a shape factor.

$$Shape\ Factor = \frac{height\ of\ block}{least\ horizontal\ dimension} \qquad (5.2)$$

The shape factor, mortar class and the compressive strength of the masonry unit are used to determine the characteristic compressive strength by interpolating f_k values between Table 2(b) and Table 2(d) in BS 5628-1 (1992).

The capacity reduction factor (β) depends on the slenderness of the wall. This factor is used to reduce the calculated resistance of slender walls which have a propensity to buckle. Table 7 of BS 5628-1(1992) lists appropriate β values to be used for a specific slenderness of wall. This value can be assumed equal to 1 in cases where buckling is not an issue and the ultimate design compressive stress can be calculated.

Finally, the material safety factor can be determined depending on the construction and manufacturing quality of the blocks. A safety factor of 3.5 was used. This value is based on normal manufacturing and construction quality (BS 5628-1 Table 4(a) (1992)).

Equation 5.1 is used to determine the resistance of a masonry unit to a compressive stress. However, we can see from the results of the analysis that the dome and wall experience tensile and compressive forces as well as bending moments.

Combined Moment and Axial Force

The dome and cylinder wall have moments and axial forces acting on them in two directions; namely, the meridian and hoop directions. These forces create tensile and compressive stresses in the wall. There are two approaches to designing a wall of this type. The first assumes an uncracked wall section in which the wall can resist a small amount of tension. The second assumes a cracked section in which the tensile strength of the wall is exceeded and the wall cracks. Figure 5.1 shows three different cases of stress within a wall section and the appropriate design approach for each case.

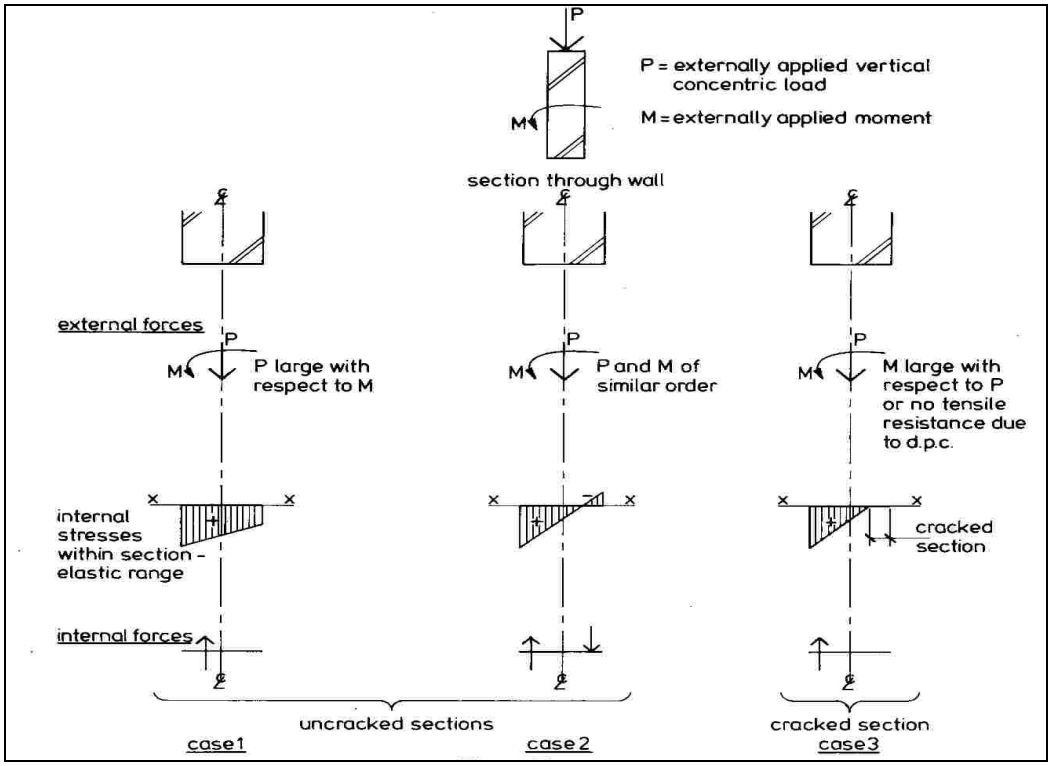

Figure 5.1 – Stresses in a Masonry Wall (Curtin, 1985:60)

(a) Uncracked Section Design Approach

The moment resistance of an uncracked section can be determined using the following formulae:

$$M_R = \frac{f_{kperp}}{\gamma_m} \times Z \quad ; \quad M_R = (\frac{f_{kpar}}{\gamma_m} + g_d) \times Z \qquad (5.3 \ \& \ 5.4)$$

where: f_{kperp} = characteristic flexural strength perpendicular to bed joints

f_{kpar} = characteristic flexural strength parallel to bed joints

γ_m = material safety factor = 3 (BS 5628-1 Table 4(b) (1992))

g_d = design vertical stress (axial stress)

Z = elastic section modulus

It is important to note that axial stresses can increase as well as decrease the moment of resistance of the section depending on whether they are compressive or tensile. The characteristic flexural strength is a measure of the tensile resistance of the section under bending. It depends on the mortar class, the type of masonry unit and the bond between the two. BS 5628-1 (1992) clause 24.1 allows half the value of the characteristic flexural strength to be used as resistance to direct tensile stresses. However, it is important to note that direct tension parallel to the bed joints (meridian direction) should not occur (Curtin, 1985). Since masonry is not an isotropic material, the flexural tensile strengths in the vertical and horizontal planes differ (hence f_{kperp} and f_{kpar}). Figure 5.2 shows the two possible failure planes in a masonry wall due to flexure.

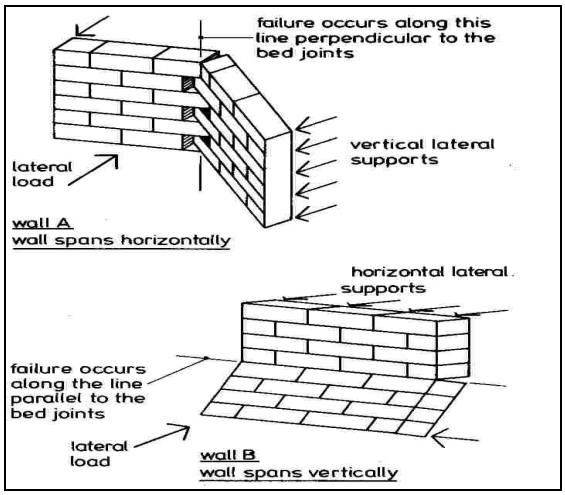

Figure 5.2 – Masonry Flexural Failure Planes (Curtin, 1985:61)

(a) Cracked Section Design Approach

This approach is best described in the Structural Masonry Designers Handbook (Curtin, 1985). It states, "the design moment of resistance to lateral loading is provided solely by the gravitational stability moment produced by the self weight of the member and any net dead load about the appropriate lever arm." Figure 5.3 shows the stress block assumed for the cracked masonry wall design.

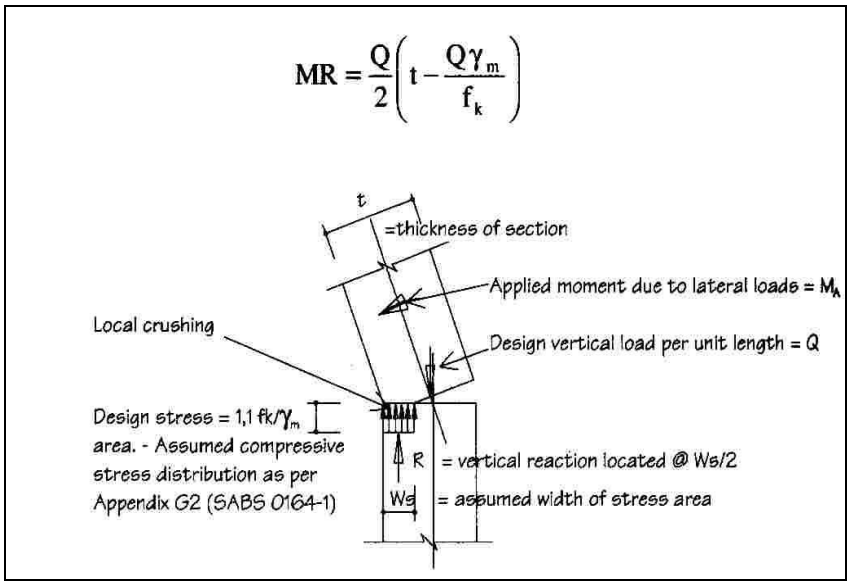

Figure 5.3 – Cracked Section Stress Block (Crofts & Lane, 2000:154)

Both cracked and uncracked methods of design are applicable to the ultimate limit state, and both methods were used to check the resistance of the dome and cylinder walls. The stress blocks were modified in order to accommodate tension in the sections. Two materials were investigated in order to resist this tension. The first was a fibre plaster and the second was a steel mesh. It was found that three states of stress could exist in a section of a masonry wall. These were:

- compressive stress only
- compressive and tensile stress
- tensile stress only

These states of stress could exist in the hoop and meridian directions, as in both directions moments and axial forces act. The derivations of these stress blocks and their moment resistances are presented in the sections below. The results for a stress block using fibre plaster and the results for a stress block using reinforcing steel (steel mesh) are presented. The fibre plaster stress blocks are shown for interest sake, as fibre prototype structure.

Stress Blocks Using Fibre Plaster & Reinforcing Steel

(a) Compressive Stress

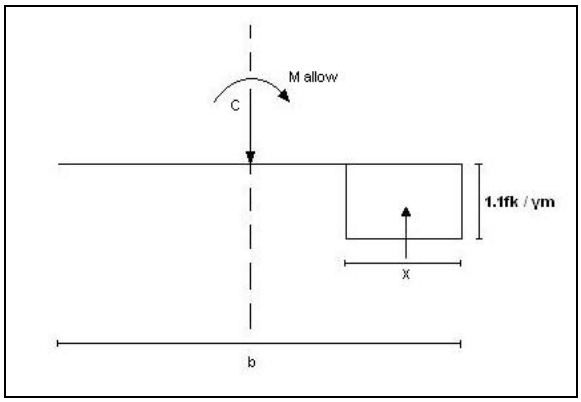

Figure 5.4 – Design Stress Block - Compressive Stress

Using static equations:

$$\sum Vertical\ Forces = 0: \qquad x = \frac{C \times \gamma_m}{1.1 f_k} \qquad (5.5)$$

$$\sum Moments = 0\ about\ the\ centroid$$

$$M_{allow} = \frac{1.1 f_k}{\gamma_m} \times x \times (\frac{b}{2} - \frac{x}{2}) \qquad (5.6)$$

where: C = compressive force, N_φ or N_θ

M = moment, M_φ or M_θ

(b) Compressive and Tensile Stress

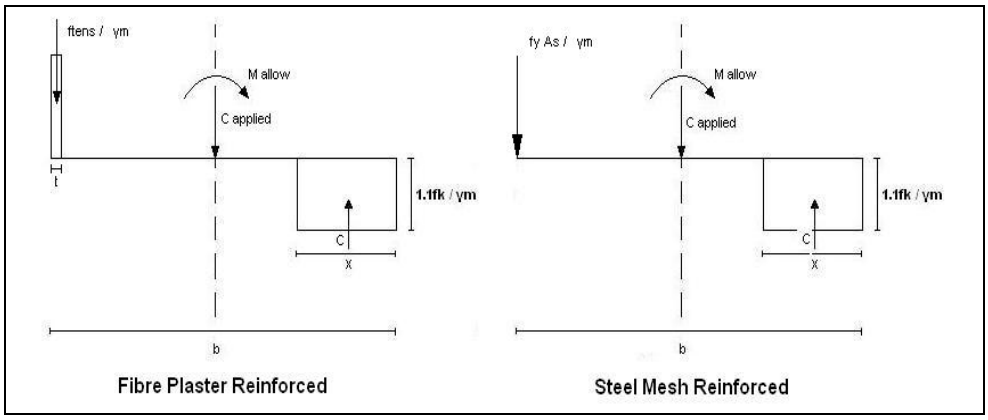

Figure 5.5 – Design Stress Blocks – Compressive and Tensile Stress

For the fibre plaster option:

$$\sum Vertical\ Forces = 0: \ C_{applied} + T - C = 0 \qquad (5.7)$$

$$x = (C_{applied} + \frac{f_{tens}}{\gamma_m} t) \times \frac{\gamma_m}{1.1 f_k} \qquad (5.8)$$

$$\sum Moments = 0\ about\ the\ centroid$$

$$M_{allow} = C(\frac{b}{2} - \frac{x}{2}) + T(\frac{b}{2} - \frac{t}{2}) \qquad (5.9)$$

where: f_{tens} = tensile strength of the fibre plaster

t = thickness of the fibre plaster

For the steel mesh option:

$$\sum Vertical\ Forces = 0 : C_{applied} + T - C = 0 \qquad (5.10)$$

$$x = (C_{applied} + \frac{f_y A_s}{\gamma_m}) \times \frac{\gamma_m}{1.1 f_k} \qquad (5.11)$$

$\sum Moments = 0$ *about the centroid*

$$M_{allow} = C(\frac{b}{2} - \frac{x}{2}) + T(\frac{b}{2}) \qquad (5.12)$$

where: f_y = yield strength of the steel

A_s = area of the steel

(c) Tensile Stress

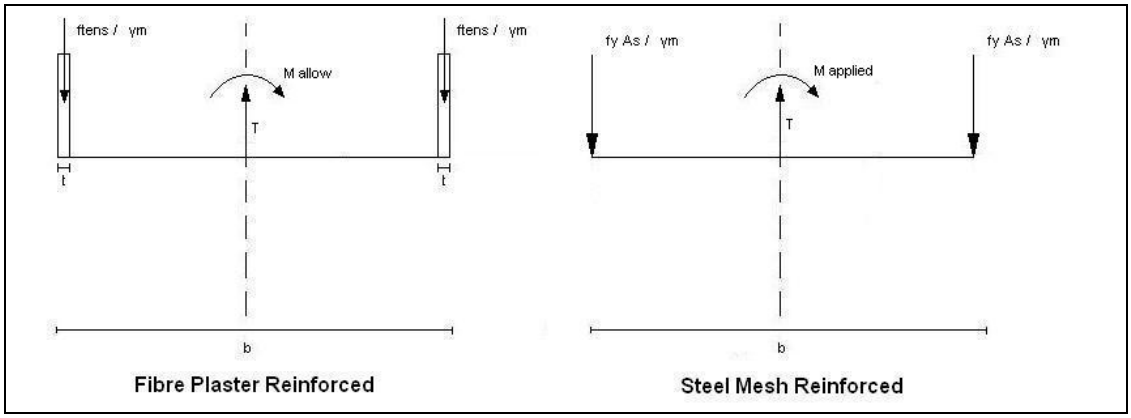

Figure 5.6 – Design Stress Blocks - Tensile Stress

For the fibre plaster option:

$\sum Moments = 0$ *about the RHS*

$$M_{allow} = \frac{f_{tens}}{\gamma_m} t(b - \frac{t}{2}) - T(\frac{b}{2} - \frac{t}{2}) \qquad (5.13)$$

For the steel mesh option:

$\sum Moments = 0$ *about the RHS*

$$A_s = \frac{(\frac{Tb}{2} + M_{applied})}{f_y b} \qquad (5.14)$$

Design Shear Strength

From the equations above, the compressive strength, moment capacity and tensile strength of dome can be determined. Another important variable in the design of masonry structures is the shear strength of the structure. When a shell or finite element analysis is performed, the membrane shear stress is calculated and this must be resisted by the masonry.

The shear strength of a masonry unit is given by the following formula:

$$v_b \leq \frac{f_v}{\gamma_{mv}} \qquad (5.15)$$

where: v_b = applied shear stress

f_v = characteristic shear strength

γ_{mv} = material safety factor = 2.5

The characteristic shear strength depends on the mortar class and the axial force in the section. The formula for the characteristic shear strength is:

$$f_v = (0.35 + 0.6 g_A)\ N/mm^2 \qquad (5.16)$$

where: g_A = design vertical load (Compressive) per unit area of the wall.

5.1.2 Foundation Design

The foundation design was done in accordance with SABS 0100-1 (2000). The formulae for the foundation design are presented in the latter sections of this chapter. It is assumed that these formulae are well known; thus, detailed explanations are not provided. The main considerations for designing the foundation were:

- the bearing pressure on the soil
- the flexural reinforcement
- the shear stress in the foundation

The bearing pressure was limited to 100 kPa (14.5 psi). This pressure allows the structure to be built almost anywhere in South Africa. The disadvantage of using this limiting value was that the foundation was restricted to a certain size, and economy of the foundation could not be improved where soil conditions are better. The serviceability criteria of overturning and sliding did not affect the foundation. These calculations have been omitted in the following sections. A detail of the foundation can be seen in figure 5.19. The foundation is relatively deep. This depth allows the foundation to act as a beam when differential ground settlements occur and prevents the structure from cracking.

5.2 Design Calculation Results

5.2.1 The Dome

Properties

The characteristic compressive strength (f_k), as discussed previously, depends on the shape of the masonry unit used. Figure 5.7 shows the HydraForm Splitter block (7 MPa; 1.02 ksi) used in the dome construction.

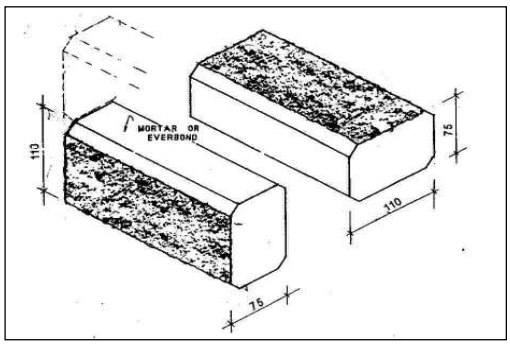

Figure 5.7 – HydraForm Splitter Block

The design properties (in accordance with SABS 0164-1 (1980), BS 5628-1 (1992)) of the masonry used for the dome construction were:

- shape factor = 0.68
- characteristic compressive strength (f_k) = 3.38 N/mm^2 (490 psi)
- material safety factor for compression (γ_m) = 3.5
- capacity reduction factor (β) = 1.0 (assuming no buckling)
- characteristic flexural strength perpendicular to bed joints (f_{kperp}) = 0.58 N/mm^2 (84 psi)
- characteristic flexural strength parallel to bed joints (f_{kpar}) = 0.24 N/mm^2 (35 psi)
- material safety factor for flexure and tension (γ_m) = 3
- elastic section modulus (Z) = 0.002 m^3 (0.071 ft^3)
- area (A) = 0.11 m^2 (1.18 ft^2)

(a) Centre Section Results (see figure 4.7)

The load case producing the greatest compression stresses in the meridian direction of the dome was the 1.5DL load case. The load case producing the largest tension stresses was the 0.9DL+1.3WL (suction side) load case in the hoop direction. The material resistances are plotted against the critical load cases below.

Hoop Direction

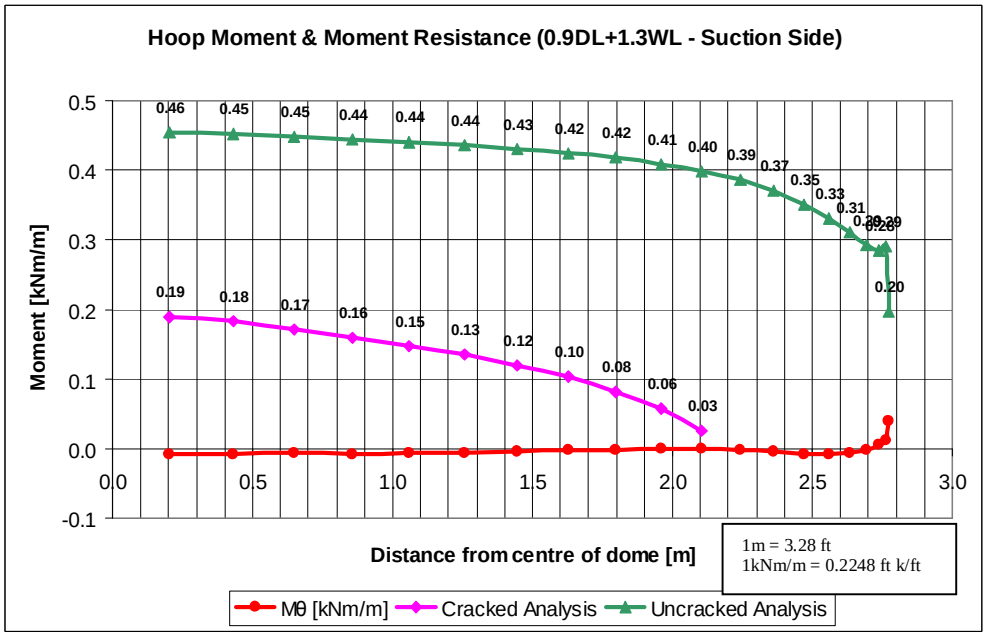

Figure 5.8 – Graph of Hoop Moment & Resistance – Centre Section (Dome)

The uncracked analysis assumes the section has a small amount of flexural tensile strength (f_{kperp}) and therefore will be able to resist tensile stress, unlike the cracked analysis which has no tensile strength and depends on the gravitational stability moment due to the axial compressive force. The cracked analysis moment of resistance line in figure 5.8 stops where the stress in the section changes to tensile stress. This analysis assumes the masonry cannot resist any tensile stress and so other materials such as wire mesh or fibre plaster need to be introduced in order to resist the tension in this region.

It is important to check that the maximum compressive and tensile resistances are not exceeded. The following graph shows the stresses and the material resistances in the section (uncracked). Positive values denote tension and negative compression.

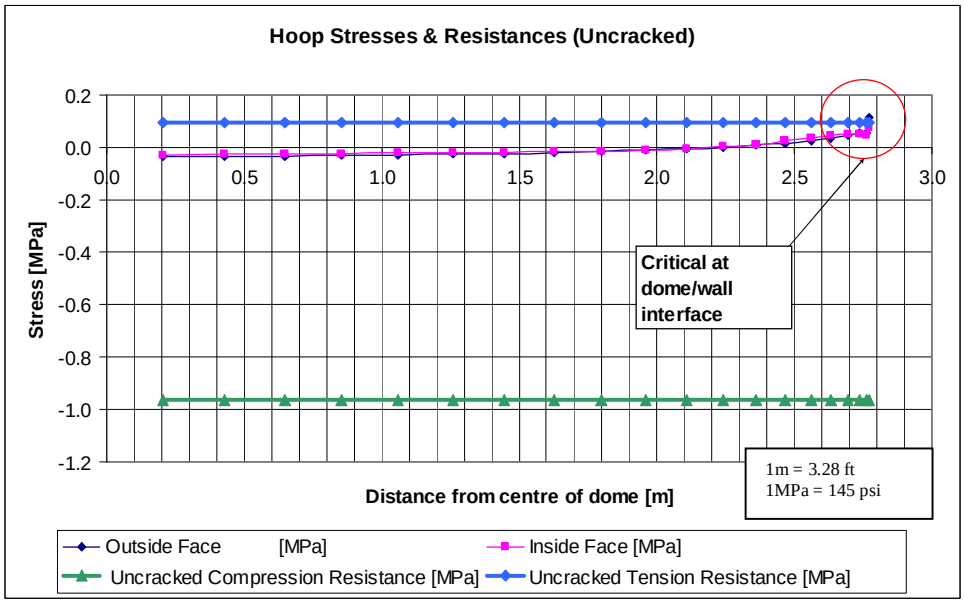

Figure 5.9 – Graph of Hoop Stresses & Resistances – Centre Section (Dome)

From graph 5.9 we can see that the stresses are within the allowable limits. The tension resistance line is based on the equation:

$$Tensile\ Resistance = \frac{f_{kperp}}{2\gamma_m} \qquad (5.17)$$

As stated earlier, BS 5628-1 (1992) clause 24.1 allows half the value of the characteristic flexural strength to be used as resistance to direct tensile stresses in the appropriate direction (hoop direction in this case). Figure 4.20 shows that the dome/cylinder wall interface is critical with regard to tension. In the final structure a concrete lintel was built around the structure at this point providing strength at this interface (see figure overleaf).



Figure 5.10 – Final Structure - Concrete Lintel

Meridian Direction

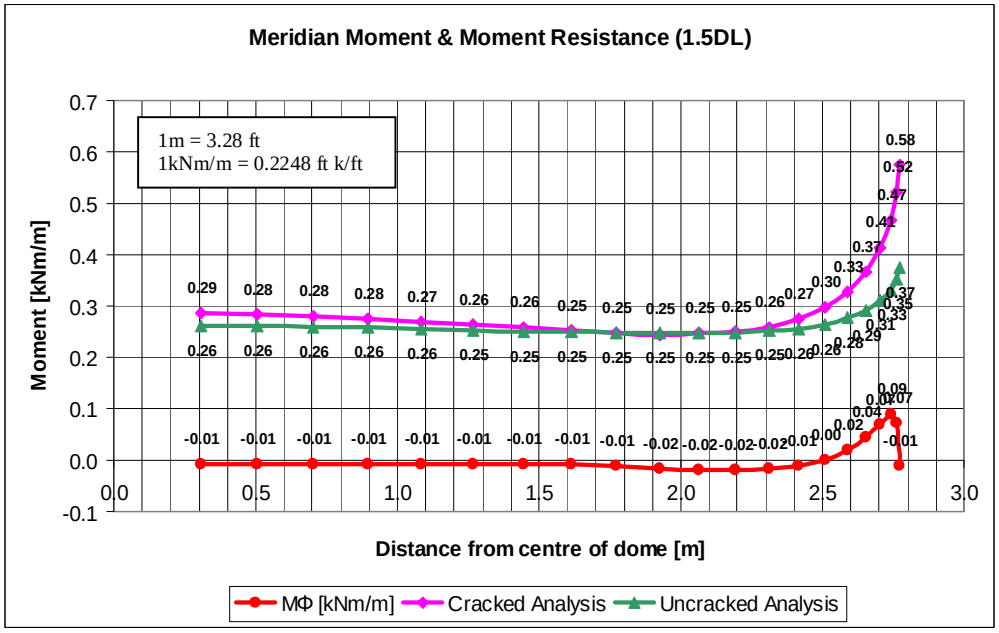

Figure 5.11 – Graph of Meridian Moment & Resistance – Centre Section (Dome)

In the meridian direction the stresses in the dome are all in compression. The above graph shows the cracked moment resistance and the uncracked moment resistance of the dome. The moment resistance increases as the compressive forces in the meridian direction increase. These forces add to the gravitational stability moment (cracked analysis) and therefore increase the moment

capacity. This is also true for the uncracked analysis where the term g_d in equation 5.4 increases with increasing axial compression.

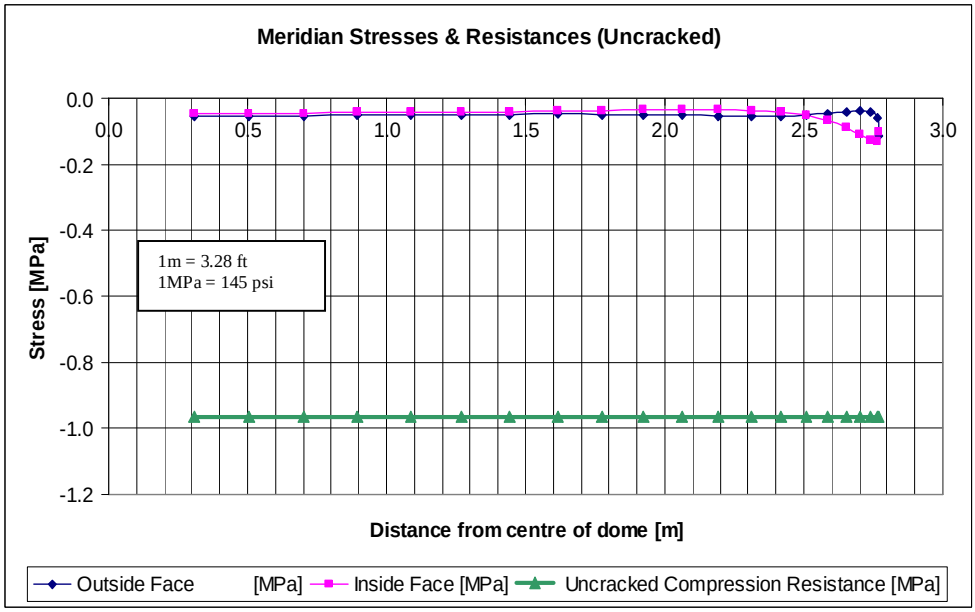

Figure 5.12 – Graph of Meridian Stresses & Resistances – Centre Section (Dome)

In the meridian direction the stresses are all in compression. From graph 5.4 we can see the compressive strength is more than adequate to resist these stresses. Figures 5.9 and 5.12 illustrate the domes large reserve of compressive strength.

(b) Door and Window Opening Section Results

Wire wrapping was provided in the areas of high stress around the window and door openings. This detail can be compared to the stress distribution shown in figure 4.11 and the cracking discussed in section 4.4.4. Figure 5.13, overleaf, shows a detail of the wire wrapping around the door.

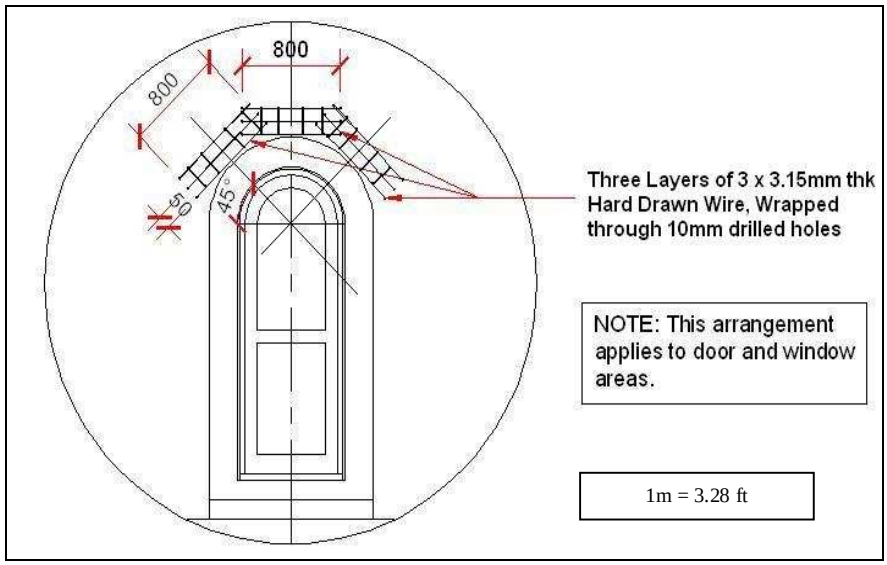

Figure 5.13 – Wire Wrapping Detail

An alternative solution to this problem is to provide BrickForce^{TM} (wire reinforcing) between the different courses of bricks in the dome. The problems with this solution are that stress concentrations cannot adequately be targeted as the spacing of the wire is determined by the brick course height and no steel is provided in the meridian direction. Wire wrapping can be concentrated in areas of high stress and adequate areas of steel can be provided in these regions. This solution requires less material and cost savings can be made. Tables 5.1 and 5.2 show the results of the wire wrapping calculations. It was assumed that in the areas of high stress (tension) the masonry had cracked and therefore it made no contribution to tensile strength.

	FORCE (F) [KN/M]	**MOMENT (M) [KNM/M]**	**RESULTANT TENSILE FORCE (F +/- M/B) [KN/M]**	**AREA OF STEEL REQUIRED [MM^2/M]**
Hoop Direction 1.5DL (ULS)	2.23 (0.15 kips/ft)	0.003	2.26 (0.16 kips/ft)	5.35
0.9DL + 1.2TL	**41.24 (2.83 kips/ft)**	**-0.083 (-0.02 ft k/ft)**	**42.0 (2.88 kips/ft)**	**107 (0.051 in^2/ft)**
1.1DL +1.0LL (SLS)	1.99 (0.14 kips/ft)	0.005	2.04 (0.14 kips/ft)	4.83
Meridian Direction 1.5DL (ULS)	0.28 (0.02 kips/ft)	0.178 (0.04 ft k/ft)	1.90 (0.13 kips/ft)	4.50
0.9DL + 1.2TL	**2.82 (0.19 kips/ft)**	**-0.062 (-0.01 ft k/ft)**	**3.38 (0.23 kips/ft)**	**8.02 (0.004 in^2/ft)**
1.1DL +1.0LL (SLS)	0.04	0.154 (0.04 ft k/ft)	1.44 (0.10 kips/ft)	3.41

Table 5.1 – Wire Wrapping Calculation – Door Section

	FORCE (F) [KN/M]	**MOMENT (M) [KNM/M]**	**RESULTANT TENSILE FORCE (F +/- M/B) [KN/M]**	**AREA OF STEEL REQUIRED [MM^2/M]**
Hoop Direction 1.5DL (ULS)	7.32 (0.50 kips/ft)	-0.268 (-0.06 ft k/ft)	9.76 (0.67 kips/ft)	23.1
0.9DL + 1.2TL	**7.51 (0.52 kips/ft)**	**-0.125 (-0.028 ft k/ft)**	**8.65 (0.59 kips/ft)**	**20.5 (0.027 in^2/ft)**
1.1DL +1.0LL (SLS)	6.29 (0.43 kips/ft)	-0.225 (-0.05 ft k/ft)	8.32 (0.57 kips/ft)	19.8
Meridian Direction 1.5DL (ULS)	-2.77 (-0.19 kips/ft)	-0.119 (-0.03 ft k/ft)	-	Not Necessary
0.9DL + 1.2TL	**1.73 (0.12 kips/ft)**	**-0.080 (-0.02 ft k/ft)**	**5.83 (0.40 kips/ft)**	**5.83 (0.007 in^2/ft)**
1.1DL +1.0LL (SLS)	-2.41 (-0.17 kips/ft)	-0.101 (-0.02 ft k/ft)	-	Not Necessary

Table 5.2 – Wire Wrapping Calculation – Window Section

Under normal loading conditions the area of steel provided by the Brickforce would be sufficient. However, from these results we can see that temperature load has a significant effect on the structure and is probably the largest contributor to cracking of masonry dome structures.

5.2.2 The Cylinder Wall

Properties

The cylinder wall was a double brick, splitter block (figure 5.7) wall. The design properties of the masonry used for the cylinder wall construction were:

- shape factor = 0.68
- characteristic compressive strength (f_k) = 3.38 N/mm^2 (490 psi)
- capacity reduction factor (β) = 0.44 (meridian direction, slenderness = 1/0.23 = 6.52; e_x = 0.3t); 1 (hoop direction)
- characteristic flexural strength perpendicular to bed joints (f_{kperp}) = 0.38 N/mm^2 (55 psi)
- characteristic flexural strength parallel to bed joints (f_{kpar}) = 0.16 N/mm^2 (23 psi)
- elastic section modulus (Z) = 0.0082 m^3 (0.29 ft^3)
- area (A) = 0.23 m^2 (2.48 ft^2)

Results

From the analysis section we can see that the 1.5DL and 0.9DL+1.3WL (suction side) load cases are the most critical for the cylinder wall. The 1.5DL is critical because it yields the greatest compressive stress in the meridian direction of the structure. The 0.9DL+1.3WL (suction side) load case yields the greatest tension region in the hoop direction of the structure.

Hoop Direction

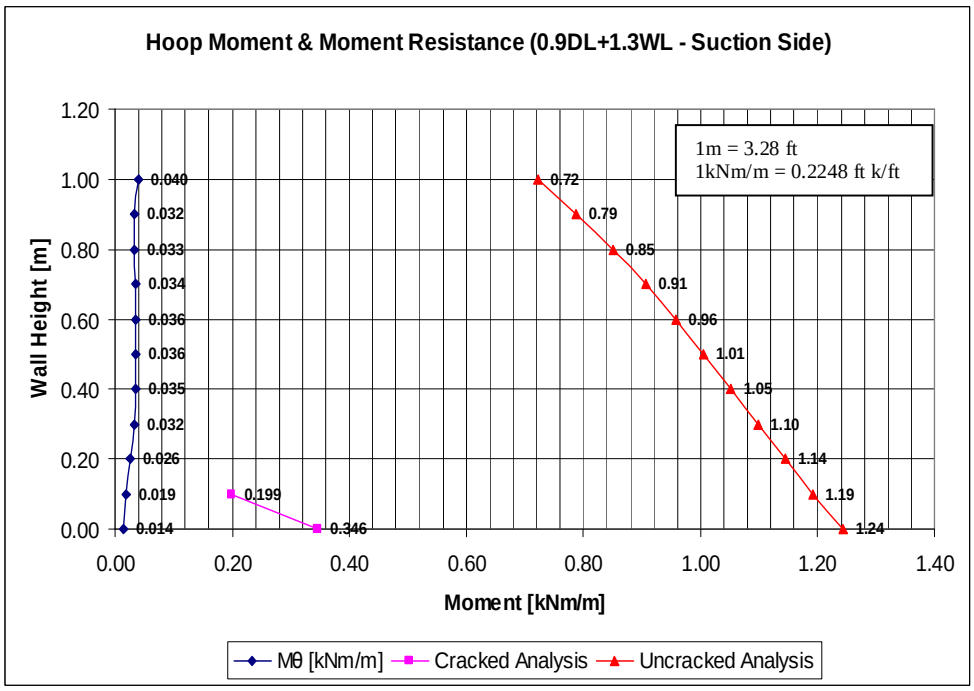

Figure 5.14 – Graph of Hoop Moments & Resistances – Centre Section (Cylinder Wall)

The uncracked moment resistance in the hoop direction is large in comparison to the applied loads. The cracked moment resistance is shown for the compression zone in the hoop direction only. This illustrates the fact that the majority of the wall is in tension. The stresses in the hoop direction do not exceed the allowable (uncracked) stress limits, figure 5.15, and therefore the wall requires no reinforcing.

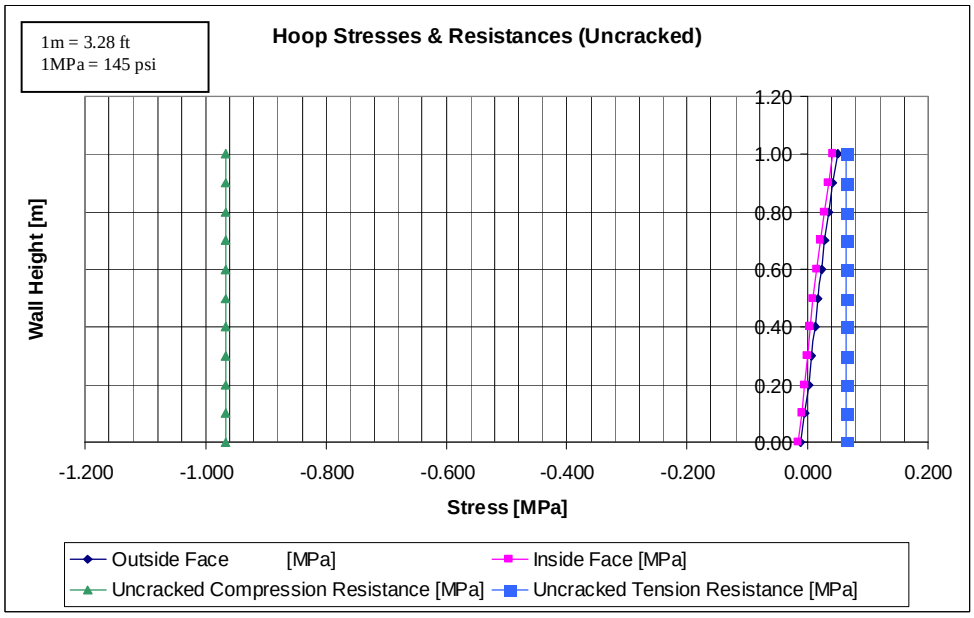

Figure 5.15 – Graph of Hoop Stresses & Resistances – Centre Section (Cylinder Wall)

Meridian Direction

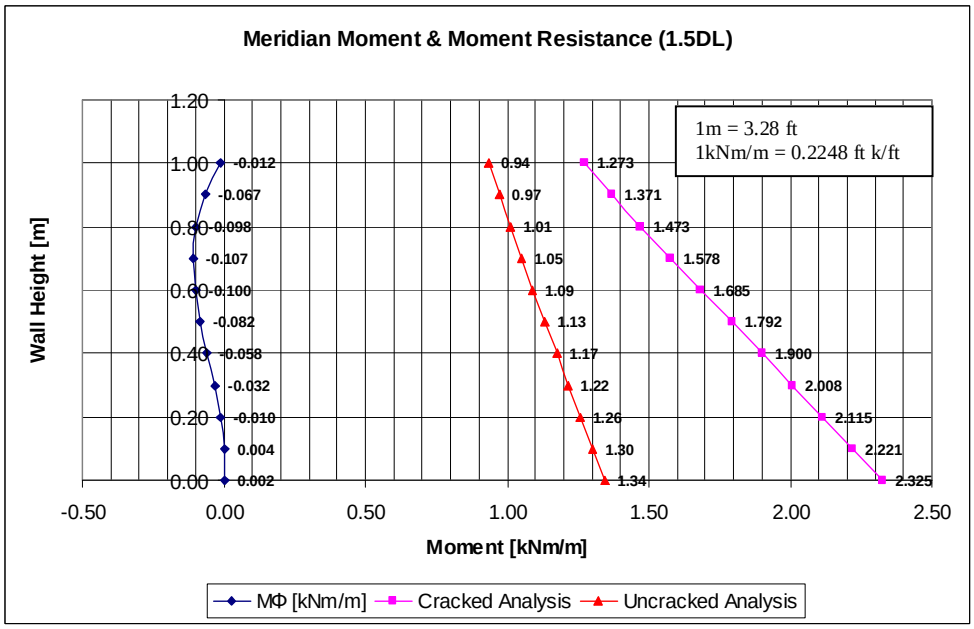

Figure 5.16 – Graph of Meridian Moment & Resistance – Centre Section (Cylinder Wall)

The stresses in the meridian direction of the cylinder wall are all compressive. The moment and compression resistances of the blocks are well within allowable limits.

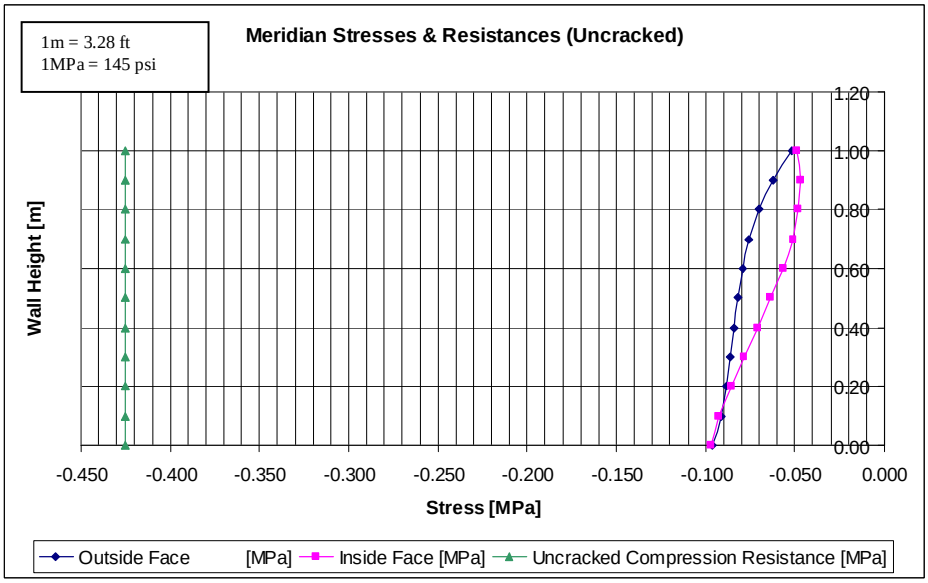

Figure 5.17 – Graph of Meridian Stresses & Resistances – Centre Section (Cylinder Wall)

Shear Strength of the Dome

Equation 5.15 shows the shear strength of a masonry unit. In this section the beneficial effect of axial stress is ignored and the characteristic shear strength for the dome and cylinder wall is assumed to be 0.35 N/mm^2 (51 psi). From the graph below, we can see that the shear strength is sufficient.

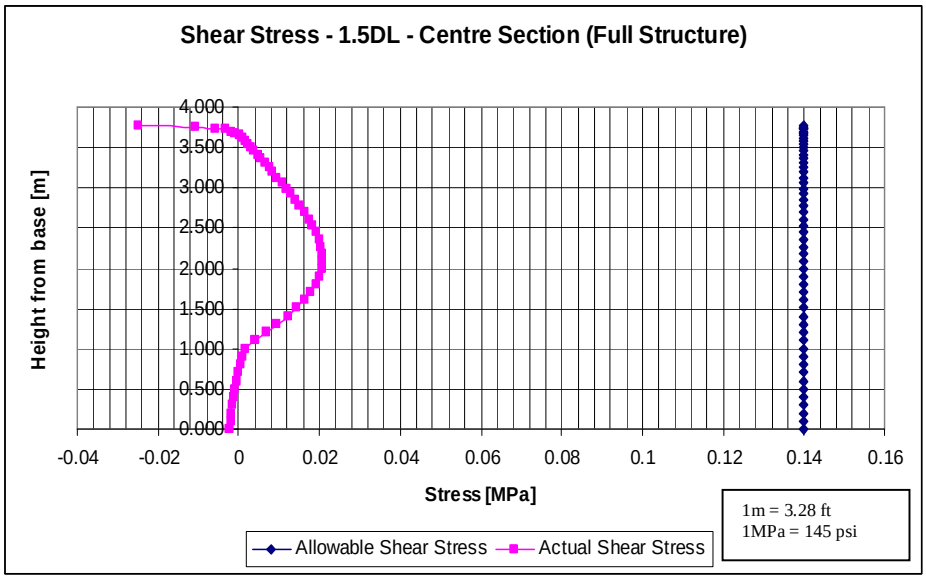

Figure 5.18 – Graph of Shear Stress in the Structure

5.2.3 The Foundation Design Results

Loading

The loading on the foundation was broken up into the serviceability and ultimate limit state loadings:

ULTIMATE LIMIT STATE (1.5DL)	SERVICEABILITY LIMIT STATE (1.0DL +1.1LL)
M_{Φ} = 0 (pinned)	M_{Φ} = 0 (pinned)
$N_{\Phi max}$ = 22.24 kN/m (1.52 kips/ft)	$N_{\Phi max}$ = 17.82 kN/m (1.22 kips/ft)
+ 5.25 kN/m (factored foundation (0.34 kips/ft) self weight)	+ 3.85 kN/m (factored foundation self (0.26 kips/ft) weight)
= 27.5 kN/m (1.88 kips/ft)	= 21.7 kN/m (1.49 kips/ft)

Table 5.3 – Foundation Loading

Bearing Pressure

The bearing pressure on the soil was calculated as:

$$\sigma = \frac{P}{ab} \qquad (5.18)$$

where: a = width of the foundation (brickwork and concrete, see figure 5.19)

b = length of the foundation

$\sigma = 56\ kPa \prec 100\ kPa$ (Allowable bearing pressure)

(8.1 psi < 14.5 psi)

Flexural Reinforcing

The design of the flexural steel was based on minimum steel considerations according to SABS 0100-1 (2000) Clause 4.11.4. Three Y12's were used, forming a beam which provides resistance to ground settlement. A detail of the foundation can be seen in figure 5.10.

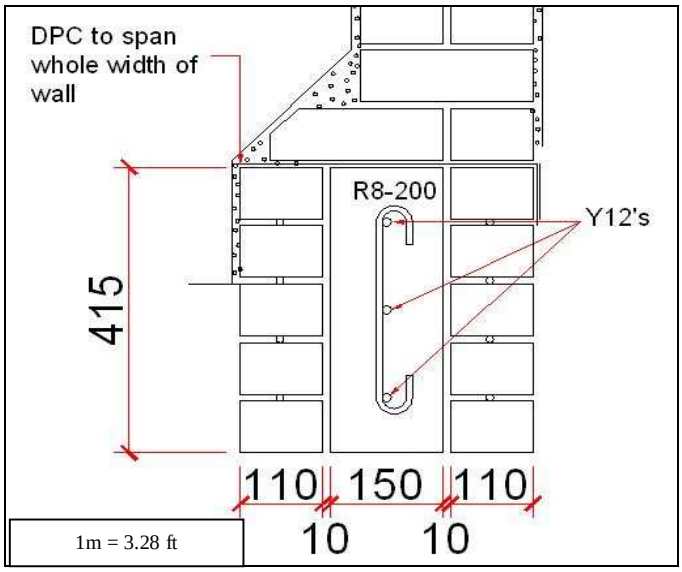

Figure 5.19 – Foundation Detail

5.2.5 Overall Stability

The stability of the dome structure (resistance to sliding on the DPC) was a concern. This was checked by calculating the friction coefficient that would allow sliding of the roof under a lateral load (wind load in this case), and comparing it to the coefficient of friction obtained from the tests in the materials investigation section of this report. It was found that the safety factor for sliding far exceeded the required safety factor of 1.5. It is important to note that no seismic or vibration analysis was done on this structure as it was designed for Johannesburg, South African conditions.

6. Construction and Cost Analysis

The construction of domes can be very complicated and therefore very costly. There are four techniques used to construct accurately shaped domes. The first technique involves complex shuttering systems using specially shaped trusses. These trusses are connected to form a doubly curved surface and covered with plywood sheeting. This option is very costly and would not be appropriate for housing. The second technique uses soil to form a temporary shutter in the shape of the dome. This technique must be used very carefully. If the soil is not compacted correctly the shape of the dome will be compromised which could lead to failure of the dome. The other two techniques are briefly discussed in the next two sections. They are building with a guiding template and using an inflatable formwork. The inflatable formwork was invented in order to construct concrete domes, but has since been used effectively in the construction of brick domes by Dome Space of South Africa.

6.1 Reinforced Concrete Dome Construction

The quickest method of constructing a reinforced concrete dome is to use an inflatable balloon formwork. The formwork is attached to a foundation ring beam and is then inflated. Two types of air forms can be used. The first type is inflated and construction workers enter the air form through an air-lock. When they are inside they spray an insulating layer, attach reinforcing to the insulation and then spray a concrete (Shotcrete) layer onto the walls of the air form to form the structure. The second type of air form is inflated and the insulation and concrete are sprayed onto the outer surface. This method of construction is less costly as it does not require an airlock, but it cannot be used on very large domes. Figure 6.1, overleaf, shows the Monolithic™ EcoShell method of construction.

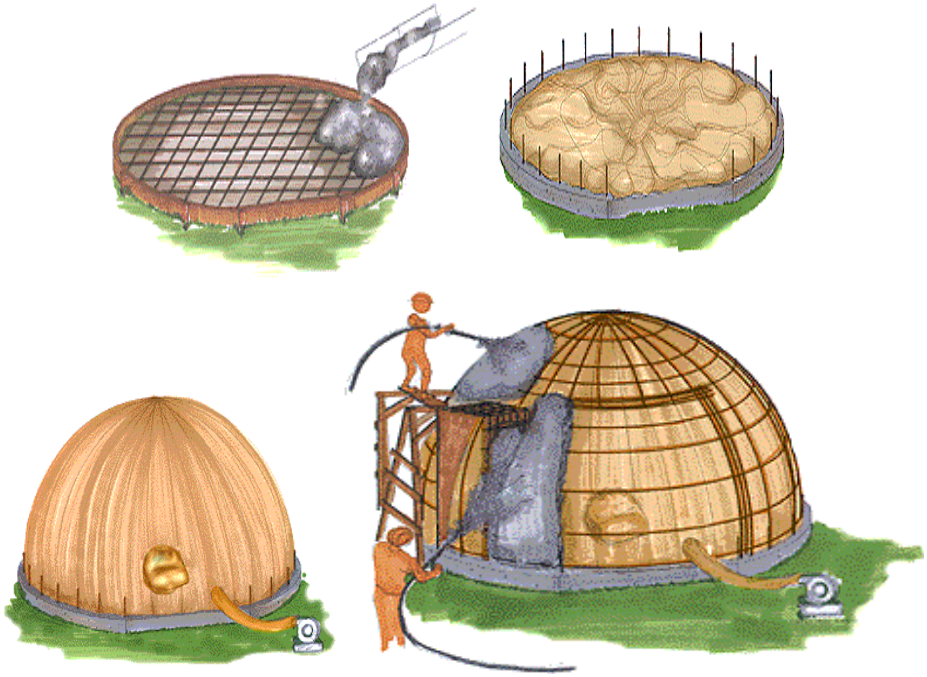

Figure 6.1 – EcoShell Dome Construction Method ()

6.2 Brick Dome and Vault Construction

Brick domes and vaults have been constructed over the ages. In the last century Hassan Fathy was the pioneer of the ancient Nubian techniques of dome and vault construction. These techniques were used in arid regions (shortage of wood for formwork) to build domes and vaults without any formwork. Today these techniques are being used in India, at the Auroville Building Centre, to construct low cost as well as aesthetically pleasing housing. The technique used to construct domes involves a tracing arm that is put in the centre of the structure and used to trace the shape of the dome. The dome is built in rings using a thin layer of earth mortar that is very sticky (high clay content) and prevents the bricks from sliding off each other**.** Figure 6.2, overleaf, shows a typical tracing arm being used to construct a dome.

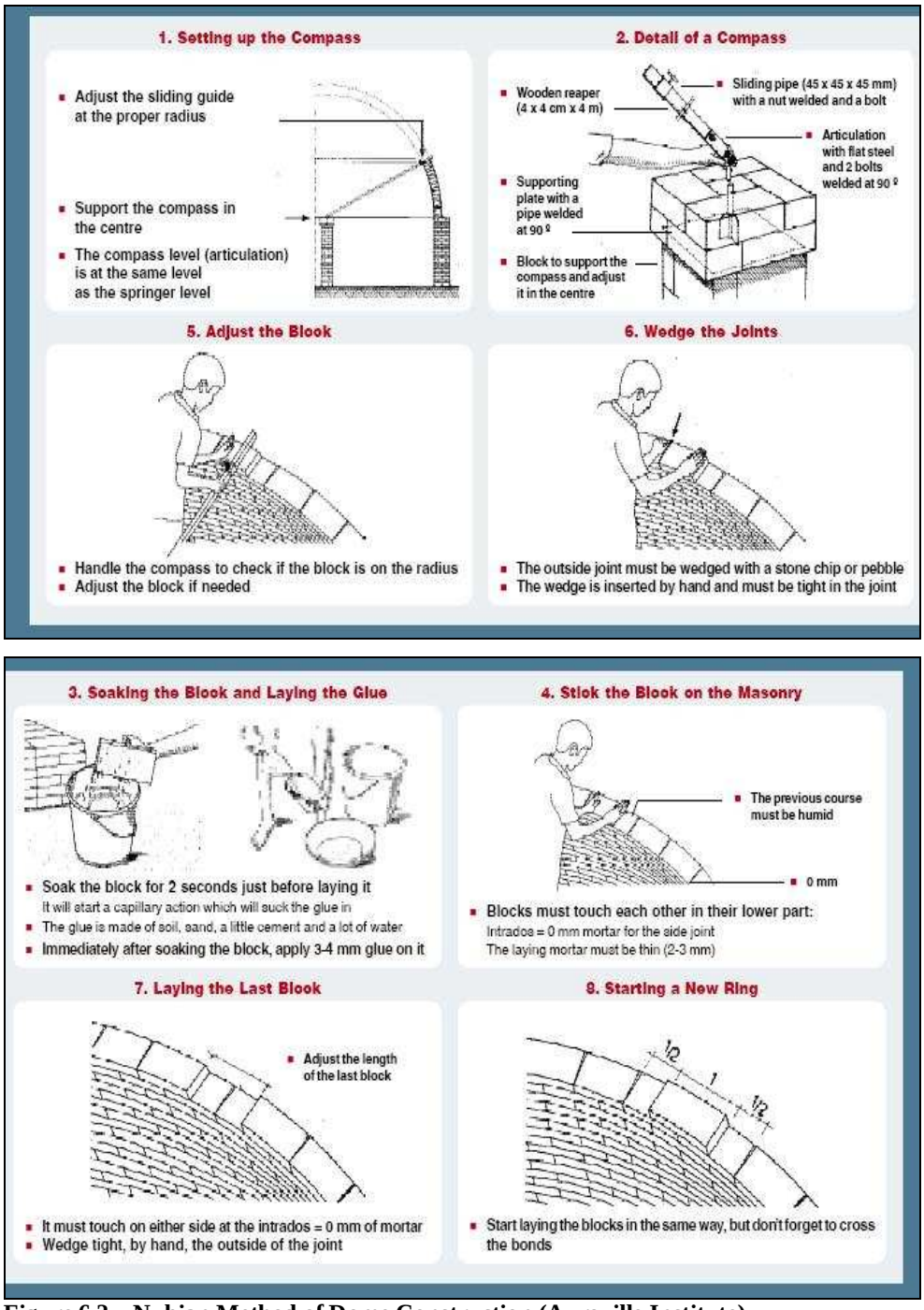

Figure 6.2 – Nubian Method of Dome Construction (Auroville Institute)

The inflatable air form technique has also been used successfully in brick dome construction. This technique was used to construct the dome home

discussed in this thesis. The benefits of this method of construction are that the air form makes sure an accurate dome surface is constructed, the construction time is reduced and the air form can be re-used many times. The disadvantages of this method are increased initial costs, for the formwork and associated equipment, and the possibility of damage to the air form. However, if the structure is used for low-cost housing the air form cost will be spread over many houses and will not be prohibitive.

6.3 Construction Procedure of the Prototype 28m^2 Dome

The Central Johannesburg College provided the site for the construction of the dome. The dome was built by Dome Space (Pty) Ltd. over a period of two weeks. Materials used in the construction of the dome were sampled and laboratory tests were performed in order to check their adequacy. The soil cement blocks used in the construction were provided by HydraForm South Africa.

6.3.1 Site Preparation & Setting Out

The site was cleared of all vegetation. A metal stake was driven into the ground at the location of the centre of the dome. A piece of wire cut to the correct radius was connected to the centre stake and to a spirit level and used to mark out the location of the ring foundation. Figures 6.3 and 6.4 show the measuring out of the foundation.



Figure 6.3 – Setting Out Equipment for the Foundation



Figure 6.4 – Setting Out of the Foundation

6.3.2 The Foundation

Figure 6.5 shows the digging of the foundation. The soil was extremely rocky and hard which provided a stable base for the structure. The soil conditions suggested that the worst case allowable bearing pressure of 100 kPa (14.5 psi) used in the design was a conservative estimate.



Figure 6.5 – Digging the Foundation

Once the foundation had been dug and the measurements had been checked, short foundation walls were built. These walls can be seen in figure 6.6. The building of these short walls replaced costly shuttering which would generally be used in the casting of the concrete in the foundation. These walls were tied into the concrete using Brickforce™.



Figure 6.6 – Short Foundation Walls

Reinforcing was provided in the concrete section in the form of three Y12 (high tensile steel bars) and R8 stirrups (mild steel stirrups) placed at 300mm centres (11.8 in.) around the ring foundation. This arrangement allowed the foundation to act like a beam and resist settlement. Figure 6.7 shows the fixing of the reinforcing steel and the placing and compacting of the concrete.



Figure 6.7 – Placing of Foundation Reinforcing & Concrete

6.3.3 The Cylinder Wall

Before the construction of the cylinder wall could begin, the HydraForm soil-cement blocks needed to be split. Once split, one block would provide three smaller blocks. The tools used to split these blocks were provided by HydraForm and can be seen in figure 6.8.



Figure 6.8 – Splitting the Splitter Blocks

The split blocks were then stacked and used for the construction of the cylinder wall and dome. The masons preferred using the blocks with straight edges (the outer pieces from figure 6.8) for the dome construction as they provided more evenly finished brick courses. Figure 6.9 shows the construction of the cylinder wall to window height.



Figure 6.9 – Construction of the Cylinder Wall

6.3.4 The Inflatable Formwork

The inflatable formwork used for the construction of the dome was developed by Dome Space (Pty) Ltd. It was put into place after the construction of the cylinder wall, as seen in figure 6.10, overleaf.



Figure 6.10 – The Inflatable Formwork

The balloon, shown in figure 6.10, is partitioned into two chambers. The first chamber is in the shape of a ring around the base of the balloon. This chamber was filled with water to stabilize the formwork and to flatten the bottom of the formwork. The yellow pipe in figure 6.10 was used to fill this chamber. The second chamber was inflated with air to form the shape of the dome. Due to the large surface area of the balloon very little pressure was required to keep it inflated. A mark was made on the balloon at door height in order to regulate the pressure in the balloon. Wooden arch moulds were placed in the door and window openings in order to provide an accurate shape for the masons to follow.

6.3.5 The Dome Construction

In figure 6.10, one of the masons is attaching a rope to the balloon formwork. This was done so that the chicken wire mesh for the inside face of the dome could be attached to the inflatable and built into the wall as the dome was constructed. Figure 6.11 shows the chicken mesh being built into the wall. The technique used to build the mesh into both faces of the dome wall was:

- The mesh was attached in layers to ropes hanging off the inflatable
- The brick courses were built in rings around the structure
- The mesh was folded over the bricks and lapped on the outside

This method of construction enabled the mesh to be provided on the inside and out side faces of the dome. The mesh provides ductility and strength to the masonry structure. It reduces the amount of plaster cracking due to shrinkage of the plaster, as well as reducing cracking in regions around the openings in the dome due to temperature loading. It is very important when constructing the dome to lay the bricks slightly away from the dome. This allows small increases in volume of the balloon without pushing the dome outward.



Figure 6.11 – Dome Construction

6.3.6 The Arches and Skylight Construction

Figure 6.12 shows the construction of the arches around the openings in the dome. The bricks were laid in such a way that the dome was supported by the arch.



Figure 6.12 – Construction of the Arches

The stiffness and shape of the formwork of the arch is important. If a flexible formwork is used then the arch may be built inaccurately. This was the case with the door arch. The formwork moved inwards causing inaccuracies in the arch (see figure 6.13).



Figure 6.13 – Door Arch

Figure 6.14 shows the dome in its un-plastered state. At the top of the structure a small masonry ring wall was constructed in order to house the skylight and passive vent system provided by SOLATUBE South Africa.



Figure 6.14 – Un-plastered Dome

6.3.7 Wire Wrapping Around the Openings

Wire wrapping was placed around the openings of the structure to resist localized stresses, as discussed in chapters 5 and 6. The holes were drilled at an upward angle of 45º (from the ground) in order to prevent water ingress into the structure. The wire was stitched through these holes (see figure 6.15).



Figure 6.15 – Wire Wrapping around Door Opening

6.3.8 Plastering, Painting & Finishing of the Dome

At the intersection between the dome and the cylinder wall a concrete lintel was placed. Figure 6.16 shows a section of the lintel.



Figure 6.16 – Concrete Lintel

Figure 6.16 also shows the wire mesh which was nailed down before plastering. The structure was left for a week un-plastered in order to allow settlement and shrinkage of the structure. Finally the structure was plastered and painted. The plaster mix used was 5: 1 sand and cement mix with 2.5kg (5.5 lb) of Coprox^{TM} (waterproofing) added to the mix. The final product can be seen in figure 6.17 below.



Figure 6.17 – The Completed 28m^2 (301 ft^2) Dome

6.4 Construction Materials Investigation

The construction materials were investigated in order to check the quality of the structure. Three sets of tests were performed. These were:

- Standard Cube Compressive Strength tests on the mortar.
- Non-destructive Strength tests on the foundation and floor slab.

The masonry units were specified as 7MPa (1 015 psi). This was checked by the manufacturers, HydraForm South Africa.

6.4.1 Mortar Strength Tests

A class II mortar, according to SABS 0164:1 (1980), was used. The required strength and mix proportions of the mortar can be seen in figures 6.18 and 6.19 respectively.

Mortar class	Compressive strength at 28d, MPa, min	
	Laboratory tests	Site tests
(i)	14.5 (2.10 ksi)	10 (1.45 ksi)
(ii)	7 (1.02 ksi)	5 (0.73 ksi)
(iii)	2 (0.29 ksi)	1.5 (0.22 ksi)

Table 6.1 – Requirements for Mortar (SABS 0164:1 Table 1)

Mortar Class	Common Cement, kg	Lime, litres	Sand (measured loose and damp), litres, max	Masonry Cement or Common Cement with mortar plasticizer, kg	Sand litres, max
I	50 (110 lb)	0 - 10	130	50 (110 lb)	100
II	50 (110 lb)	0 - 40	200	50 (110 lb)	170
III	50 (110 lb)	0 - 80	300	50 (110 lb)	200

Table 6.2 – Mix Proportions for Mortar (SABS 0249 Table 5)

Cube samples (100mm (3.94 in.) cubes) were taken during the construction of the dome. The cubes were tested at 7, 14 and 21 days in order to check the

strength of the mortar. Figure 6.18 shows the average results of the tests. It is important to note that the compressive strength of the mortar in the structure will tend to the strength of the masonry units. This is due to the triaxial effect present when a thin layer of mortar (in the bed joint) is placed under compression and the mortar units above and below it provide restraint (Crofts & Lane, 2000). However, it is still useful to use the test results below to measure the quality of the construction.

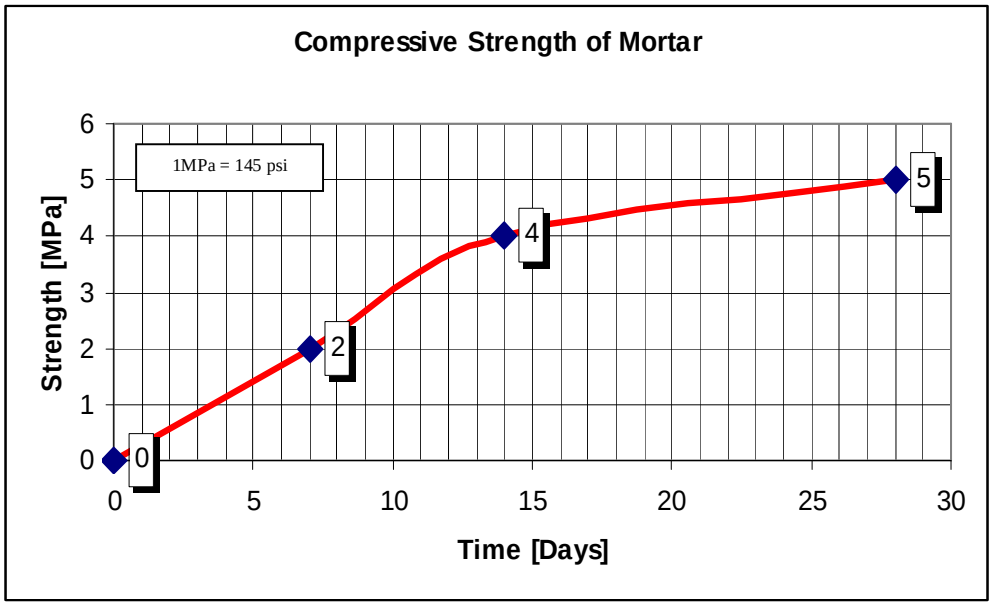

Figure 6.18 – Graph of the Strength of the Mortar

In the tests, it was observed that a small amount of organic matter (grass) was present in the mortar mix. This should be prevented as it has a negative impact on the strength of the mortar. The tests showed that the mortar was adequate with regard to compressive strength considerations for class II mortar. A possible improvement to the mortar mix would be the inclusion of hydrated lime. Lime helps retain moisture in the mortar which is important for proper strength gain and it reduces shrinkage of the mortar.

6.4.2 Foundation and Floor Slab Tests

Non-destructive testing was used on the foundation and floor slab in order to determine their compressive strengths. A Schmidt Hammer was used at random points to gauge the 28 day strengths. Figure 6.19 shows the Schmidt Hammer used in the testing of the concrete.



Figure 6.19 – The Schmidt Hammer

Readings were taken off the hammer and compared to the literature provided by the manufacturer in order to find the compressive strength of the concrete. Figure 6.20 is taken from the manufacturer's literature. Upper, lower and middle bound solutions are given in the graph. The average (middle bound) results were used to determine the compressive strengths of the foundation and floor slab.

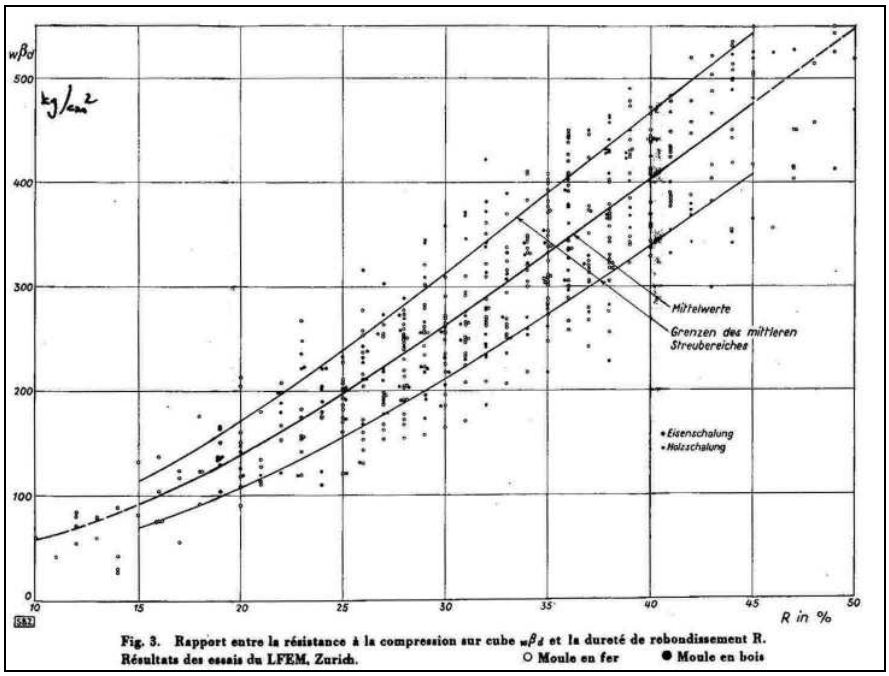

Figure 6.20 – Schmidt Hammer Results (Schmidt, 1950)

The results of the Schmidt Hammer tests are summarized below in table 6.3.

Foundation		Floor Slab	
Hammer Reading	**Compressive Strength [MPa]**	**Hammer Reading**	**Compressive Strength [MPa]**
25	19.1	25	19.1
21	14.7	23	16.7
22	15.7	24	18.1
21	14.7	21	14.7
24	18.1	21	14.7
21	14.7	22	15.7
22	15.7	24	18.1
25	19.1	21	14.7
20	13.7	22	15.7
Average	**16.2 (2 350psi)**	**Average**	**16.4 (2 380psi)**

Table 6.3 – Foundation and Floor Slab Compressive Strengths

The concrete strength required was 15 MPa (2 180 psi) (for low-cost housing). The above results show that this strength was achieved. According to the design calculations this strength was sufficient.

6.5 Cost Analysis

In this section the cost of the prototype 28m^2 (301 ft^2) dome is compared to previous low-cost housing projects. Due to the constantly fluctuating prices of building materials it is difficult to estimate an accurate present value for these projects. Assumptions were made in order to simplify the calculation of the present value costs of low-cost housing. These were:

- An average inflation rate from the year 2000 to 2005 was taken. This amounted to 5.1 % (www.sanlam.co.za).
- Two of the projects presented below were built in foreign countries (Mozambique & Haiti) and the prices for these projects were given in US Dollars. An exchange rate to South African Rands was found at the time of construction of these projects (www.reservebank.co.za). This exchange rate was applied at the time of construction and the present value of these projects was found using the South African average inflation figure of 5.1 % (2000-2005).
- The Subsidy information presented in table 4.4 was obtained from the Department of Housing. The subsidy of R23 100 (US$3 500) represents the subsidy given to the lowest income bracket (R0 – R1500 / month (US$230).

Company	Project	Cost/ Unit	Present Value Cost/ Unit	Subsidy (Lowest Income Bracket)	PV Cost - Subsidy	Floor Area [m^2]	Services (electricity/plumbing)
Kantey-Templar	Mpopomheni	R18 400 (2000)	R23 596 ($3 600)	R23 100 ($3 500)	R 496 ($75)	+/- 30	Yes
	Kokstad	R18 400 (2000)	R23 596	R23 100	R 496	+/- 30	Yes
	Van Reenen	R18 400 (2000)	R23 596	R23 100	R 496	+/- 30	Yes
	Ezakheni	R18 400 (2000)	R23 596	R23 100	R 496	+/- 30	Yes
Monolitic™	EcoShell, Haiti	$1 200 (2004)	R 8777 ($1 350)	R23 100	-	28	No
Wits University	Mozambique Dome	$1 500 (2003)	R14 770 ($2 250)	R23 100	-	27	No
Wits Prototype	Wits 28m^2 Dome	R44 072 (2005)	R44 072 ($6 700)	R23 100	R20 972 ($3 200)	28	No
Estimated Cost	Mass Housing	R30 000 (2005)	R30 000 ($4 550)	R23 100	R6 900 ($1 050)	28	Yes

Table 6.4 – Cost Comparisons of Low-Cost Housing Schemes

Table 6.4 shows that dome structures can be competitive with regards to cost when compared to other low-cost housing schemes. The EcoShell solution proved to be the cheapest solution in this comparison. However, there were no services included in the cost of this dome. The EcoShell is a concrete dome that uses an inflatable formwork to construct it. The initial cost of equipment for a concrete dome is quite high. Therefore this solution would only be viable if it were applied on a mass scale.

The dome built in Mozambique (Magaia, 2003) was built out of earth bricks and the Nubian technique (tracing arm) was used to construct this dome. This technique reduced the cost as expensive formwork and equipment were not needed. The cost of the structure did not include services. However, with services included the cost of the structure would still be competitive.

The dome constructed in this report was the most expensive solution. However, it produced the best structure with regard to the architectural

concerns such as lighting, useable space and overall aesthetics. The dome built for Wits University was a once off project and savings are envisaged for mass housing schemes (table 4.4). The cost of the structure included services and finishes (plaster, paint etc.) as well as labour costs. The labour costs could be reduced if the inhabitants of the houses are involved in the construction of their homes.

Dome structures use the least material to cover a particular floor area. This makes them very economical with regard to material use. However, labour costs are critical with regard to domes as the building technique is different from conventional construction techniques. The cost of labour and supervision for the Wits prototype dome made up 26 % of the domes cost. In conclusion, the key areas which need to be addressed with regards to cost are:

- Building Techniques (Nubian technique/concrete domes possibly cheaper)
- Labour Costs (agreements with communities could reduce these costs)
- Construction Materials (brick/concrete)

7. Conclusions & Recommendations

The objectives of this investigation were to identify the optimal shaped dome structure that can be used in low cost housing; to identify the important design criteria with regard to masonry domes; to utilize affordable materials (compressed earth blocks) that can be acquired in remote areas in the design of the dome; to investigate different methods of dome construction and to construct a durable, architecturally and structurally efficient low cost dome home. The following conclusions are broken down into sub-headings which reflect the objectives mentioned above.

Optimal Dome Shape

In order to determine the optimal dome shape using a circular floor plan; two issues need to be considered. The first issue is structural efficiency, which was defined as the minimizing of tension in the structure. The second issue is architectural efficiency, which was based on useable space within the structure.

In the shape investigation, it was found that the most structurally efficient shaped structures were the catenary and parabola structures with Y/L ratios greater than 0.5 (structure type A – dome from ground level). The sectioned hemisphere with $0.24 < Y/L < 0.32$ was found to be the most efficient shape for structure type C – a dome supported by a ring beam on a cylinder wall. This shape could also be used from ground level. However, for this project the floor area was limited and this range of Y/L values would have resulted in structures with very low roofs. The structure chosen for construction was a compromise between the two issues mentioned above. Structurally, the hemisphere is the most efficient shape to build onto a cylinder wall as it meets the wall vertically (transferring its thrust vertically into the wall). However, tension still exists in this type of structure. The useable space in the structure (structure type B) is excellent.

For the three different types of structures the following shapes and Y/L ratios are recommended:

- Structure Type A – Catenary – $Y/L > 0.5$
- Structure Type B – Hemisphere
- Structure Type C – Sectioned Hemisphere – $0.24 < Y/L < 0.32$

Important Design Criteria for Masonry Domes

In the analysis section of this report it was found that the most critical areas in domes are around the window openings. In these regions, high tension forces and moments occur in both meridian and hoop directions. In masonry structures tension is critical and should be minimized or avoided if possible. From the analysis it was found that the inclusion of arches in window and door openings reduces the tension in these regions. The arches stiffen the structure. However, under temperature loading, it was found that some form of reinforcing (in both meridian and hoop directions) was required in these regions.

In the prototype structure that was built another critical region was recognized. This was the bottom third of the hemisphere (measured from the intersection of the dome with the cylinder wall). Significant hoop tension exists in this region and reinforcing (wire mesh) is recommended.

The most critical load cases were 1.5DL (for compression resistance), 0.9DL + 1.3 WL (suction side – for hoop tension in the dome) and 0.9DL + 1.2 TL (for tension around the openings).

Wind Loading

The hoop tension in the dome (centre section) was critical for this load case. However, the 1.5DL load case produced very similar results to this load case and it can be assumed that wind load has a small effect on the structure. This

structural efficiency under wind loading is one of the major benefits of dome structures.

Temperature Loading

The fixity of the base of a dome is important when temperature load is being considered. If the base is fixed and there is a temperature differential between the dome and the foundation, large hoop forces and moments (hoop & meridian) will occur towards the base of the dome. In this investigation, a DPC was provided at this interface providing a slip plane. This plane is important if reinforcing in this region is to be avoided.

It is recommended that when a structural analysis is done on a dome structure particular attention should be given to the openings within the structure as well as temperature loading on the structure. The openings should be rounded to reduce stress concentrations and arches should be built within the openings to stiffen the structure.

Materials Investigated for Dome Construction

The materials investigated for use in the dome were cement stabilized earth blocks, wire mesh, wire wrapping (stitching around openings) and fibre reinforced plaster.

Materials Resisting Compression

The cement stabilized earth blocks proved to be a good alternative to standard clay or concrete bricks. Their thermal properties are more favorable than standard bricks and they can be made on site in the most rural areas of Southern Africa.

Materials Resisting Tension (Cracking)

The wire mesh and fibre plaster were investigated for their potential to resist tension and stop any cracking of the structure. The fibre plaster was not used because the discontinuous nature of the fibres, which allows cracks to spread once they have started. The wire mesh, on the other hand, intersects the crack and prevents it from spreading..

Wire wrapping around highly stressed regions (openings) was used in order to resist tension in these regions. The wire wrapping was placed perpendicular to potential cracks observed in previously built dome structures, which matched the high stress regions shown by the finite element analysis. This type of reinforcing allows the tension regions to be targeted and it minimizes the wastage of expensive tension resisting materials.

It is recommended that wire mesh be used on the inside and outside faces of the dome structure in order to resist the small tensile forces within the structure as well as to prevent plaster cracking (Williams-Ellis, 1947). The effectiveness of the wire wrapping around the openings in the structure is still being observed but this method of reinforcing could possibly replace the inefficient use of Brickforce in the structure. It is important to note that no cracking has occurred on the prototype structure to date.

Methods of Construction

Two viable methods of construction of the dome were identified in this report. The first method was the Nubian (tracing arm) method of construction and the second was the construction of the dome using an inflatable formwork. The inflatable formwork and its associated equipment may be difficult to use in rural areas for small projects and for these types of projects it is advisable that the Nubian technique be used. This technique may be more time consuming than the inflatable formwork method but it has been proven successful in India

at the Auroville Institute and could be used by rural communities to build their own homes.

The inflatable formwork method of construction is an efficient method which saves time and can be effectively used on a mass scale as the cost of the equipment is spread over many houses. A greater amount of skill and supervision is needed for this method of construction.

The dome structure has proved to be a cost effective structure in Mozambique and the United States. The dome built in this project was not as competitive as these structures with regard to cost (high labour costs). However, in the cost analysis this structure was the only dome structure to make provision for services and the quality of the structure was very good. Further studies into construction techniques are recommended. Dome and vault roof structures built on square floor plans could also be investigated as these structures would provide a greater amount of useable space than circular floor plans.

Appendix A (Selected Abaqus^{TM} Output)

The results of the analysis done on the prototype 28m^2 (301 ft^2) dome are presented in tabular format below. The results are presented along the centre section as seen in figure 4.7. The load cases that were critical for this cross-section were the 1.5DL and 0.9DL+1.3WL load cases. For localized results around the window and door openings see sections 4.4.2 and 5.2.1.

1.5DL

X	Y	Hoop Force [kN/m]	Meridian Moment [kNm/m]	Meridian Force [kN/m]	Hoop Moment [kNm/m
0.205	3.762	-5.915	-0.009	-5.759	-0.011
0.306	3.753	-6.070	-0.009	-5.478	-0.012
0.406	3.740	-6.000	-0.008	-5.440	-0.012
0.506	3.723	-5.930	-0.008	-5.417	-0.012
0.605	3.703	-5.862	-0.008	-5.388	-0.012
0.703	3.679	-5.795	-0.008	-5.351	-0.012
0.800	3.652	-5.724	-0.008	-5.306	-0.012
0.897	3.621	-5.649	-0.008	-5.256	-0.012
0.992	3.586	-5.569	-0.007	-5.200	-0.012
1.085	3.548	-5.480	-0.007	-5.140	-0.011
1.178	3.507	-5.383	-0.007	-5.078	-0.011
1.268	3.463	-5.276	-0.007	-5.014	-0.010
1.357	3.415	-5.157	-0.008	-4.950	-0.009
1.445	3.363	-5.025	-0.008	-4.888	-0.009
1.530	3.309	-4.876	-0.009	-4.828	-0.008
1.613	3.252	-4.709	-0.010	-4.774	-0.007
1.694	3.191	-4.519	-0.011	-4.726	-0.006
1.773	3.128	-4.304	-0.012	-4.687	-0.004
1.850	3.062	-4.060	-0.014	-4.659	-0.004
1.924	2.993	-3.783	-0.016	-4.643	-0.003
1.995	2.922	-3.469	-0.017	-4.642	-0.002
2.064	2.847	-3.116	-0.018	-4.656	-0.002
2.130	2.771	-2.719	-0.019	-4.689	-0.002
2.193	2.692	-2.276	-0.020	-4.741	-0.002
2.253	2.611	-1.784	-0.019	-4.817	-0.003
2.311	2.527	-1.242	-0.018	-4.917	-0.004
2.365	2.442	-0.649	-0.015	-5.047	-0.005
2.416	2.355	-0.006	-0.011	-5.211	-0.006
2.464	2.266	0.683	-0.006	-5.411	-0.008
2.508	2.175	1.411	0.001	-5.654	-0.009
2.550	2.083	2.165	0.010	-5.942	-0.009
2.587	1.989	2.928	0.020	-6.278	-0.009

X	Y	Hoop Force [kN/m]	Meridian Moment [kNm/m]	Meridian Force [kN/m]	Hoop Moment [kNm/m
2.622	1.894	3.673	0.032	-6.664	-0.007
2.653	1.798	4.367	0.045	-7.098	-0.006
2.680	1.700	4.968	0.058	-7.579	-0.002
2.704	1.602	5.431	0.071	-8.098	0.001
2.724	1.503	5.708	0.081	-8.650	0.005
2.741	1.403	5.756	0.088	-9.226	0.008
2.753	1.303	5.544	0.086	-9.818	0.011
2.763	1.202	5.070	0.072	-10.419	0.011
2.768	1.101	4.363	0.043	-11.021	0.008
2.770	1.000	9.878	-0.012	-11.619	0.001
2.77	0.900	7.839	-0.067	-12.572	-0.006
2.77	0.800	5.962	-0.098	-13.564	-0.007
2.77	0.700	4.263	-0.107	-14.593	-0.005
2.77	0.600	2.736	-0.100	-15.652	-0.001
2.77	0.500	1.358	-0.082	-16.731	0.003
2.77	0.400	0.098	-0.058	-17.825	0.006
2.77	0.300	-1.080	-0.032	-18.926	0.008
2.77	0.200	-2.211	-0.010	-20.031	0.009
2.77	0.100	-3.326	0.004	-21.136	0.008
2.77	0.000	-4.447	0.002	-22.239	0.008

Table A1 – 1.5DL – Centre Section Results

0.9DL+1.3WL (Suction Side)

X	Y	Hoop Force [kN/m]	Meridian Moment [kNm/m]	Meridian Force [kN/m]	Hoop Moment [kNm/m
0.205	3.762	-3.559	-0.005	-3.364	-0.008
0.317	3.752	-3.512	-0.005	-2.986	-0.008
0.429	3.737	-3.421	-0.005	-2.917	-0.008
0.540	3.717	-3.309	-0.004	-2.859	-0.008
0.647	3.693	-3.191	-0.004	-2.776	-0.007
0.752	3.666	-3.082	-0.004	-2.694	-0.007
0.856	3.634	-2.972	-0.004	-2.608	-0.008
0.959	3.599	-2.862	-0.005	-2.518	-0.007
1.060	3.559	-2.744	-0.004	-2.424	-0.007
1.160	3.516	-2.623	-0.004	-2.330	-0.006
1.258	3.468	-2.497	-0.004	-2.237	-0.006
1.353	3.417	-2.364	-0.005	-2.146	-0.005
1.447	3.362	-2.223	-0.006	-2.056	-0.005
1.539	3.303	-2.067	-0.006	-1.968	-0.004
1.628	3.241	-1.900	-0.006	-1.887	-0.003
1.715	3.175	-1.717	-0.008	-1.812	-0.002
1.799	3.106	-1.516	-0.009	-1.746	-0.001
1.880	3.034	-1.294	-0.010	-1.690	-0.001

X	Y	Hoop Force [kN/m]	Meridian Moment [kNm/m]	Meridian Force [kN/m]	Hoop Moment [kNm/m
1.959	2.959	-1.044	-0.011	-1.644	0.000
2.034	2.880	-0.769	-0.012	-1.612	0.000
2.106	2.799	-0.463	-0.012	-1.594	0.000
2.175	2.715	-0.126	-0.013	-1.593	-0.001
2.241	2.628	0.245	-0.012	-1.612	-0.002
2.303	2.539	0.656	-0.011	-1.650	-0.003
2.362	2.447	1.103	-0.008	-1.717	-0.004
2.417	2.353	1.588	-0.005	-1.811	-0.006
2.468	2.258	2.108	0.000	-1.941	-0.007
2.516	2.160	2.661	0.005	-2.112	-0.009
2.559	2.060	3.233	0.012	-2.321	-0.009
2.599	1.959	3.814	0.020	-2.584	-0.008
2.634	1.856	4.375	0.029	-2.890	-0.007
2.666	1.752	4.893	0.039	-3.245	-0.005
2.693	1.647	5.328	0.048	-3.642	-0.002
2.717	1.540	5.618	0.057	-4.075	0.002
2.736	1.433	5.775	0.063	-4.551	0.006
2.751	1.326	5.720	0.065	-5.049	0.010
2.761	1.217	5.446	0.059	-5.569	0.012
2.768	1.109	4.974	0.043	-6.103	0.010
2.770	1.000	10.540	0.008	-6.643	0.040
2.770	0.900	8.800	-0.025	-7.376	0.032
2.770	0.800	7.196	-0.040	-8.159	0.033
2.770	0.700	5.731	-0.038	-8.984	0.034
2.770	0.600	4.382	-0.026	-9.842	0.036
2.770	0.500	3.120	-0.007	-10.724	0.036
2.770	0.400	1.910	0.012	-11.622	0.035
2.770	0.300	0.716	0.029	-12.530	0.032
2.770	0.200	-0.494	0.038	-13.442	0.026
2.770	0.100	-1.744	0.032	-14.353	0.019
2.770	0.000	-3.047	0.003	-15.259	0.014

Table A2 – 0.9DL+1.3WL (Suction side) – Centre Section Results

Appendix B (Alternative Structure)

The alternative structure, presented below (figure B1), is a sectioned hemisphere with a Y/L ratio of 0.3. Structurally and architecturally this structure was more efficient than the dome constructed. However, the projected cost of this structure was greater than the one built.

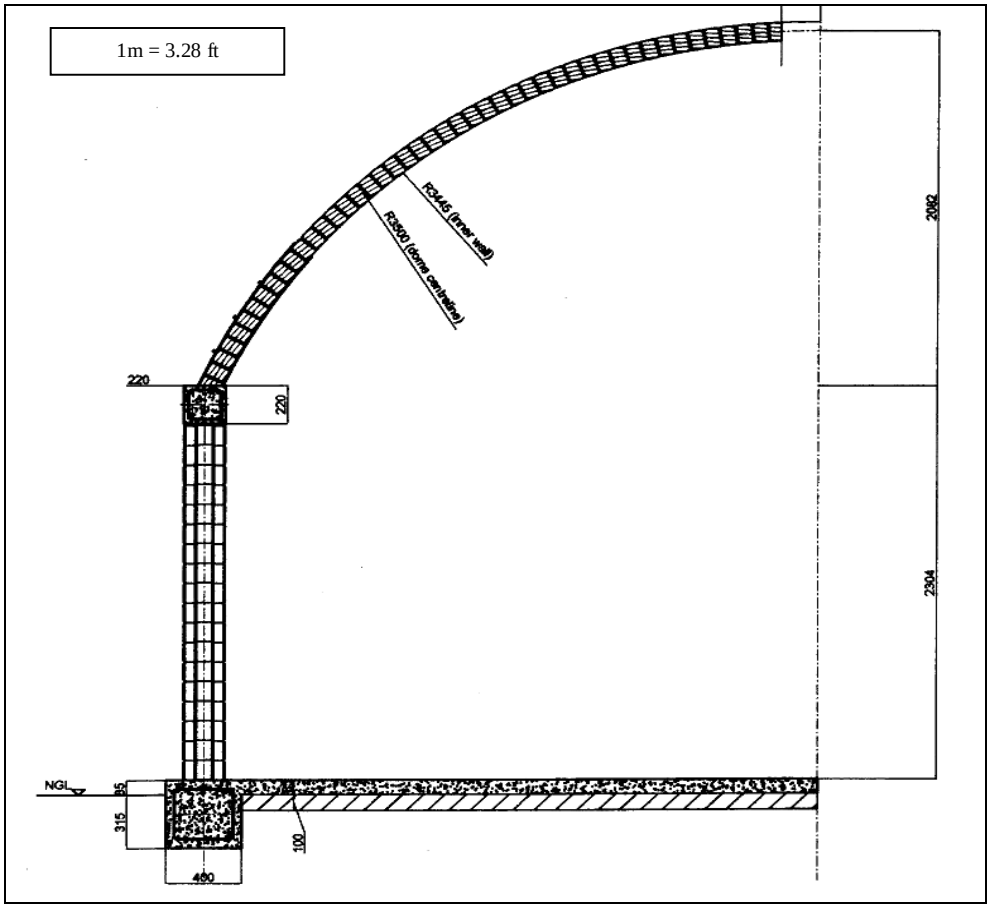

Figure B1 – Alternative Structure – Structure Type C

The forces and moments in the dome and cylinder wall are presented in the following figures.

The Dome Results

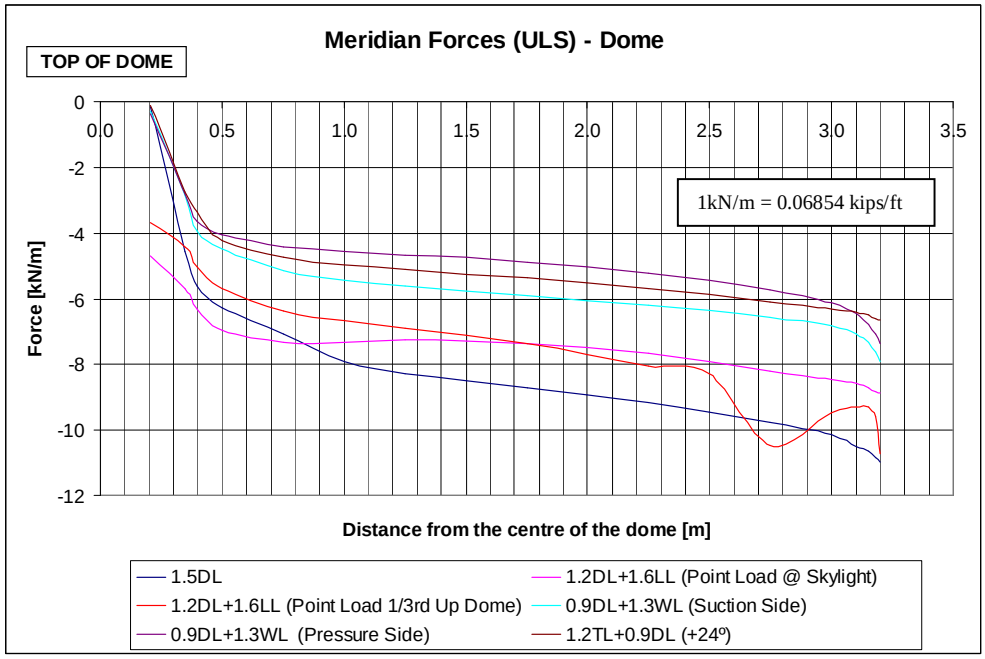

Figure B2 – Meridian Forces (Dome) – Structure Type C

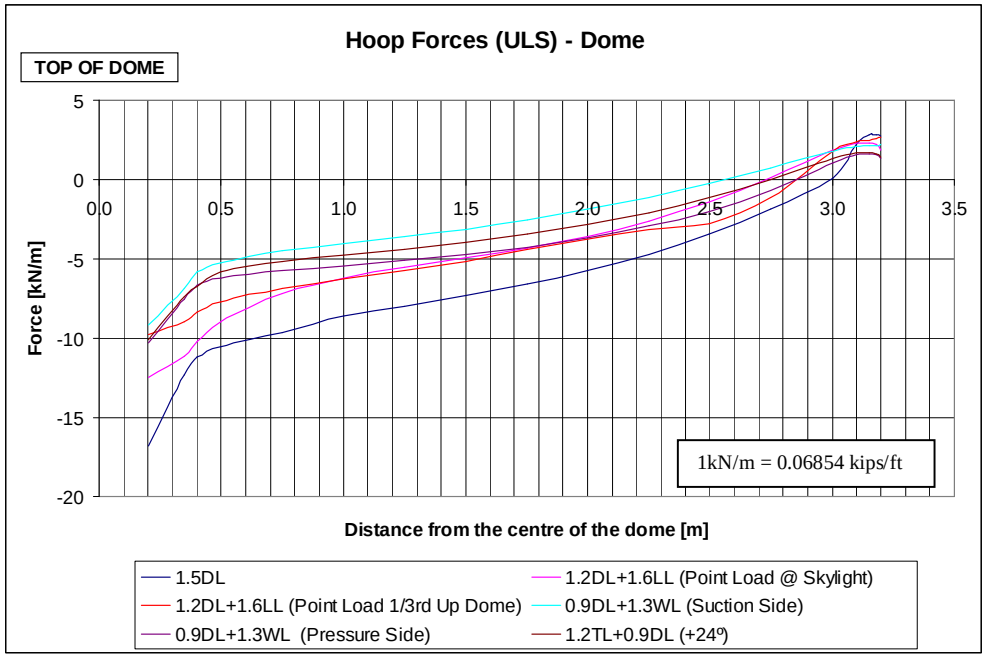

Figure B3 – Hoop Forces (Dome) - Structure Type C

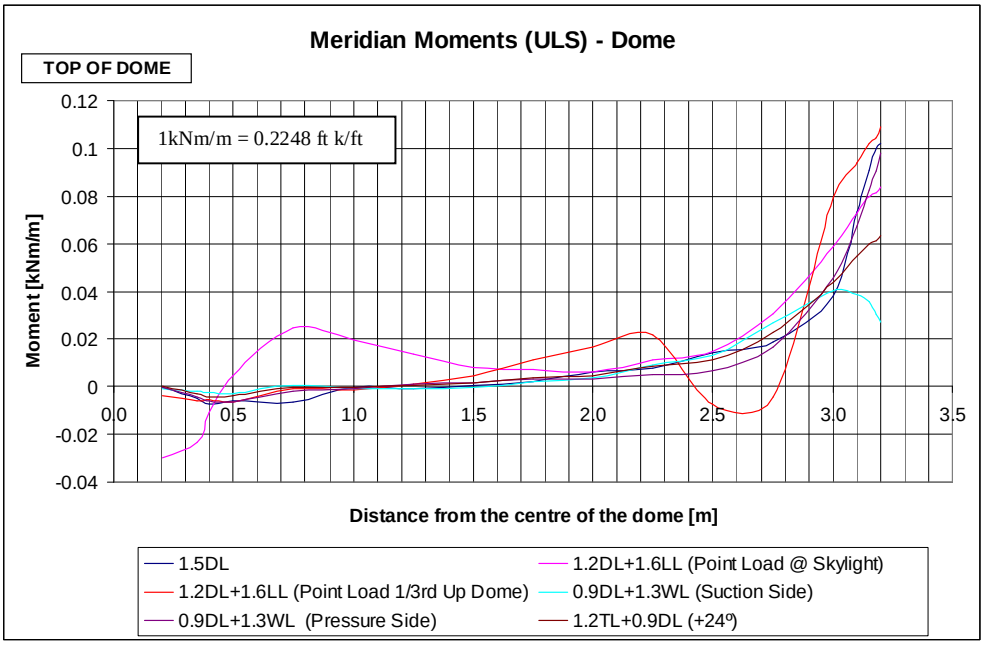

Figure B4 – Meridian Moments (Dome) – Structure Type C

The Cylinder Wall Results

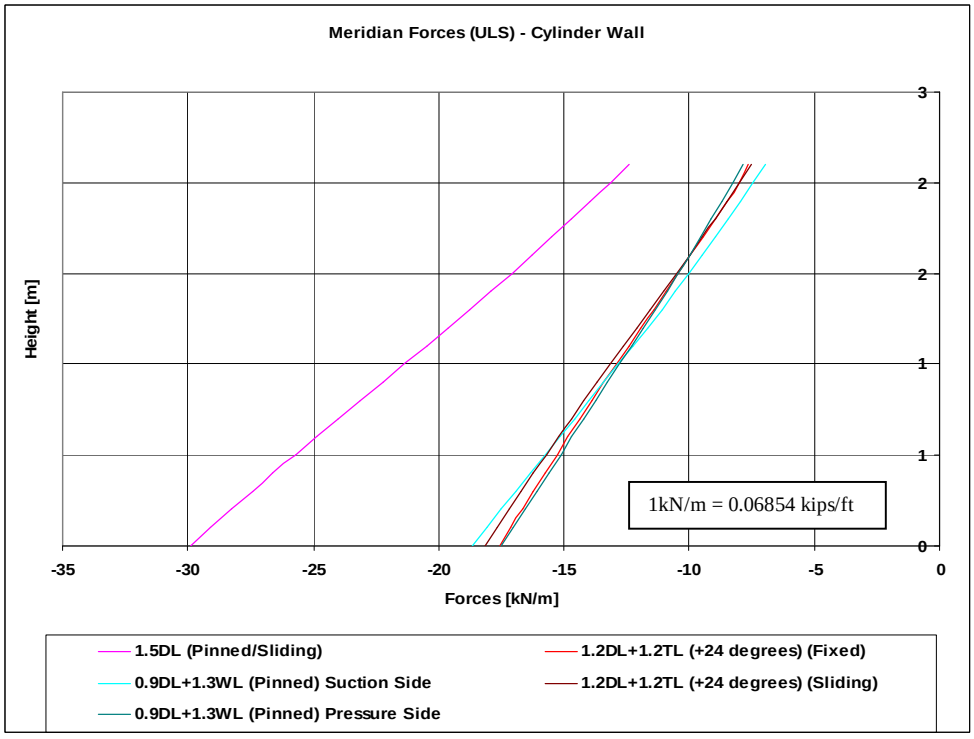

Figure B5 – Meridian Forces (Cylinder) – Structure Type C

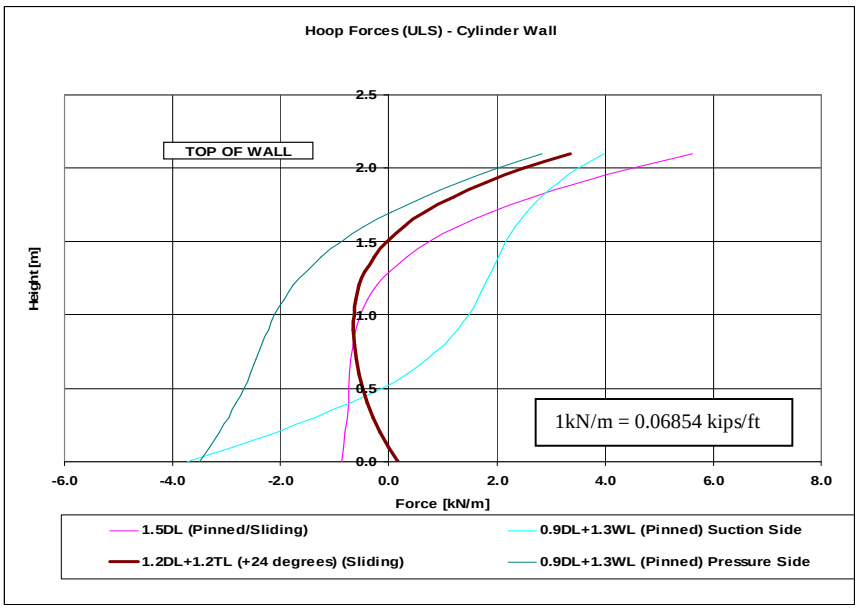

Figure B6 – Hoop Forces (Cylinder) – Structure Type C

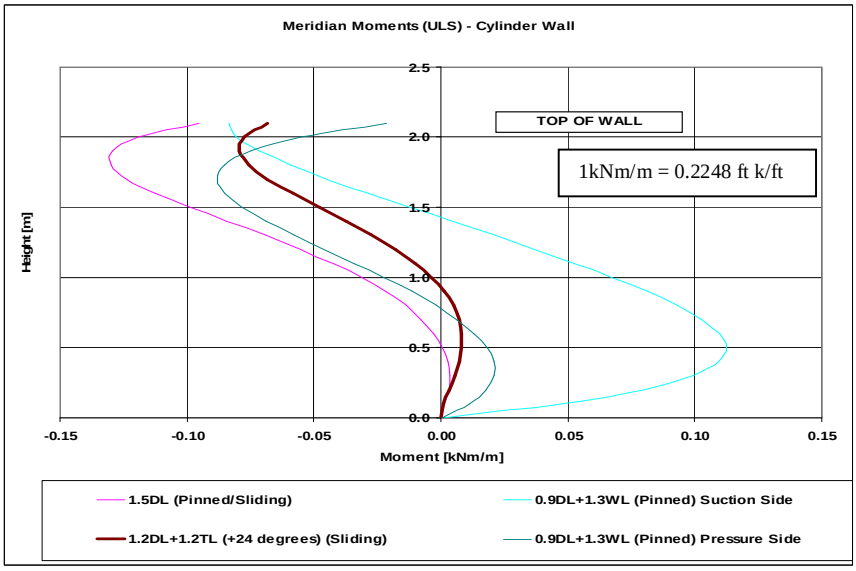

Figure B7 – Meridian Moments (Cylinder) – Structure Type C

These forces and moments were well within the allowable stress zone of an uncracked masonry analysis. The absence of openings in the dome (except for the skylight) improved the efficiency of the dome. The ring beam at the base of the dome roof acts like a lintel for the window openings in the cylinder wall. A similar design to this was used at the Thholego Eco-Village.

References

Addis, B. et al (2001) **Fulton's Concrete Technology: Fibre Reinforced Concrete**, Cement and Concrete Institute, Midrand, South Africa.

Agrément Certificate 96/237 **HydraForm Building System**, Agrément South Africa, Pretoria.

Bath, K.J. (1982) **Finite Element Procedures in Engineering Analysis,** Prentice-Hall Inc., Engelwood Cliffs, USA.

Billington, D.P. (1982) **Thin Shell Concrete Structures 2nd Ed**, New York:McGraw-Hill Book Company.

British Standards Institution (1992) **BS 5628:Part1- 1992: Structural Use of Unreinforced Masonry**, London.

British Standards Institution (1975) **BS 4618 Section 5.6- 1975: Guide to Sliding Friction**, London.

Crofts, F.S. and Lane, J.W. (2000) **Structural Concrete Masonry: A Design Guide**, Concrete Manufacturers Association, Midrand, South Africa.

Curtin, W.G. et al (1982) **Structural Masonry Designers' Manual**, London: Granada

Doat, P. et al (1991) **Building with Earth**, The Mud Village Society, New Delhi.

Fernandez, R (2003) **Fibre Reinforced Soil Crete Blocks for the Construction of Low-Cost Housing**, MSc Dissertation, University of the Witwatersrand, Johannesburg.

Gardi, R. (1973) **Indigenous African Architecture,** Van Nostrand Reinhold, London

Garrison, K. (2004) **Helping the Poorest of the Poor – EcoShells in Haiti**. INTERNET. http://www.monolithic.com. Cited 3 March 2005.

Gohnert, M. and Magaia, S.J. (2004) **Design and Construction of an Earth Brick Dome used for Low-Cost Housing**, Journal of South African Institute of Civil Engineering, vol.46, no.2, pp. 9-14.

Houben, H. and Guillaud, H. (1994) **Earth Construction: A Comprehensive Guide**, Intermediate Technology Publications, London.

HydraForm™ (2004) **HydraForm Training Manual rev.1**, HydraForm South Africa.

Kantey and Templar (2000) **Low-Cost Housing Project Summary Sheets**. INTERNET, http://www.kanteys.co.za. Cited 10 October 2005.

Kirchner, M. (1988) **Technical Evaluation of Dome Type Construction and its Potential as a Housing Form**, Discourse, University of the Witwatersrand.

Kohler, T.H. (1982) **A Technical Guide to Good House Construction**, National Building Research Institute of the CSIR, Johannesburg

Lamb, J.K. (1998) **An Investigation into the Thermal Capacity of Earthblocks and their Performance in Buildings**. MSc Dissertation, University of the Witwatersrand, Johannesburg.

Magaia, S.J. (2003) **Domes in Low-Cost Housing**. MSc Dissertation, University of the Witwatersrand, Johannesburg.

Melaragno, M. (1991) **An Introduction to Shell Structures**, The Art and Science of Vaulting, Van Nostrand Reinhold, New York.

Merchant, D.H. (1963) **Formwork for Concrete Shell Structures Technical Report No.21**, Department of Civil Engineering Stanford University, USA.

Monaghan, D.(2003) **FEA Portal @ www.DermotMonaghan.com**, INTERNET, http://www.dermotmonaghan.com, Cited January 2004.

Schmidt, E. (1950) **Le Sclérométre á Béton**, Photocopied Manual, Zurich.

Snow, Sir.F. (1965) **Formwork for Modern Structures**, Chapman and Hall, London.

South African Bureau of Standards (1989) **SABS 0160:1989: The General Procedures and Loadings to be Adopted in the Design of Buildings**, Limit States Design, Pretoria.

South African Bureau of Standards (2000) **SABS 0100-1:2000: The Structural Use of Concrete**, Pretoria.

South African Bureau of Standards (1980) **SABS 0164-1: 1980: Unreinforced Masonry**, Pretoria.

The Joint Structural Division of the SAICE and IStrucE (1996) **Checklist for Structural Design**. SAICE, Midrand, South Africa.

Uzoegbo, H.C. (2003) **Structural Behaviour of Dry-Stack Interlocking Block Walling Systems Subject to In-Plane Loading**, Concrete Beton, Pretoria.

Van de Berg, D. (2002) **Dome Space Resources Study,** INTERNET, http://www.domespace.co.za. Cited 10 October 2005.